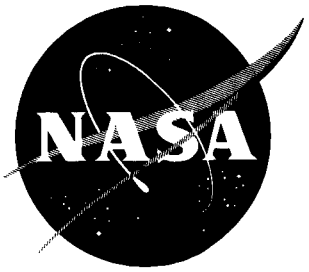

TECHNICAL NOTE
D-44

FORCE-TEST INVESTIGATION OF THE STABILITY AND CONTROL CHARACTERISTICS OF A 1/8-SCALE MODEL OF A TILT-WING VERTICAL-TAKE-OFF-AND-LANDING AIRPLANE

By Louis P. Tosti

Langley Research Center
Langley Field, Va.

NATIONAL AERONAUTICS AND SPACE ADMINISTRATION

WASHINGTON March 1960

NATIONAL AERONAUTICS AND SPACE ADMINISTRATION

TECHNICAL NOTE D-44

FORCE-TEST INVESTIGATION OF THE STABILITY AND CONTROL CHARACTERISTICS OF A 1/8-SCALE MODEL OF A TILT-WING VERTICAL-TAKE-OFF-AND-LANDING AIRPLANE

By Louis P. Tosti

SUMMARY

A force-test investigation has been made to determine the aerodynamic characteristics of a 1/8-scale model of a tilt-wing vertical-take-off-and-landing airplane in the short- and long-wing configurations. The model had two 6-blade dual-rotating propellers that were not interconnected mounted on a wing that could be tilted up to an incidence angle of about 90° for vertical take-off and landing.

The investigation included measurements of both the longitudinal and lateral stability and control characteristics in the normal-forward-flight, transition, and hovering ranges. Tests in the forward-flight and transition conditions were made at various wing incidences and power conditions. Tests in the hovering condition were made in the presence of the ground. The data are presented without analysis.

INTRODUCTION

An investigation has been made of the stability and control characteristics of a 1/8-scale model of the Hiller X-18 vertical-take-off-and-landing (VTOL) airplane. The results of the free-flight tests of the model are reported in reference 1, and the results of the force tests are presented in the present paper.

The force tests included measurements on the model for two wing spans of both longitudinal and lateral stability and control characteristics for the normal-forward-flight, transition, and hovering conditions. The tests in the forward-flight condition were made at wing incidences of 4.5° and 10° for thrust coefficients from -0.15 to 1.08. The tests in the transition-flight condition were made for wing incidences from 20° to 80° with various power settings to represent conditions of steady level flight, 0.25g forward acceleration, and 0.25g deceleration.

The tests in the hovering-flight condition were made at wing incidences of 85°, 90°, and 94.5° for heights above the ground from 0 to 2 propeller diameters. The tail effectiveness was determined by varying the incidence of the complete horizontal tail. The control effectiveness of the aileron, rudder, elevator, and differential propeller pitch controls were determined for the complete flight range. Two different leading-edge slat configurations were also tested for a limited number of conditions.

SYMBOLS

In general, the force-test data of the model are referred to the stability system of axes. Figure 1 shows these axes and the positive directions of the forces, moments, and angular displacements. The body system of axes shown in figure 2 is used to present only the propeller alone data.

The definitions of the symbols used in the present paper are as follows:

b	wing span, ft
c	wing chord, ft
n	rotational speed, rpm
q	free-stream dynamic pressure, lb/sq ft
R	Reynolds number
S	wing area, sq ft
X,Z	body axes
X_S,Y_S,Z_S	stability axes
F_L	lift, lb
F'_D	drag, lb
M_{Y_S}	pitching moment, ft-lb
F_Y	side force, lb
M_{X_S}	rolling moment, ft-lb

M_{Zs} yawing moment, ft-lb

C_L lift coefficient, $\frac{F_L}{qS}$

C_D' drag coefficient, $\frac{F_D'}{qS}$

C_m pitching-moment coefficient, $\frac{\text{Pitching moment}}{qSc}$

C_Y side-force coefficient, $\frac{F_Y}{qS}$

C_l rolling-moment coefficient, $\frac{M_{Xs}}{qSb}$

C_n yawing-moment coefficient, $\frac{M_{Zs}}{qSb}$

C_N normal-force coefficient in body system of axes, perpendicular to propeller axis in -Z direction

C_X axial-force coefficient in body system of axes, positive forward from propellers along propeller axis (in X direction)

T_c' thrust coefficient, $\frac{\text{Thrust}}{qS}$

g acceleration due to gravity

V_a scaled-up airplane velocity, knots

h/d ratio of distance between ground and bottom of wheels to propeller diameter

i_t horizontal-tail incidence, positive trailing edge down, deg

i_w wing incidence, deg

α	angle of attack of fuselage, deg
α_p	angle of attack of propeller, deg
β	angle of sideslip, deg
β_F	blade angle of front propellers measured at 0.75 radius, deg
β_R	blade angle of rear propellers measured at 0.75 radius $(\beta_{LR} = \beta_{RR})$, deg
β_{LR}	blade angle of left rear propeller measured at 0.75 radius, deg
β_{RR}	blade angle of right rear propeller measured at 0.75 radius, deg
$\delta_a{}'_L$	deflection of left aileron (both inboard and outboard portions), positive trailing edge down, deg
$\delta_a{}'_R$	deflection of right aileron (both inboard and outboard portions), positive trailing edge down, deg
δ_a	differential aileron control deflection, $\delta_a{}'_R - \delta_a{}'_L$, deg
δ_e	deflection of elevator, positive trailing edge down, deg
δ_r	deflection of rudder, positive trailing edge left, deg
ϕ	angle of roll, deg

MODEL

The model used in the investigation was the 1/8-scale flying model of the Hiller X-18 airplane which was used in the flight-test investigation of reference 1. A photograph of the model is shown in figure 3, and a three-view sketch showing some of the more important dimensions is shown in figure 4. Table I presents the geometric characteristics scaled up to the full-size-airplane values. The model had two 6-blade dual-rotating propellers powered by a 5-horsepower electric motor in each nacelle. The propellers on the right and left wings were not interconnected. The speeds of the motors were changed together to vary the thrust of the propellers. The propeller blades were designed for the hovering condition and their geometric characteristics are shown in figure 5.

The wing was pivoted at the 34.8-percent-chord station and could be rotated to provide incidence angles from 4.5° to 94.5°. Most of the tests were made on the model with a wing span of 6 feet, which scaled up to 48 feet on the full-scale airplane and is called the short-wing configuration in this report. A large number of tests were also made on the model with tip extensions added to the wing to form a wing with a span of 7.5 feet, which scaled up to 60 feet and is called the long-wing configuration in this report. The model had conventional aileron, rudder, and elevator controls for forward flight. For hovering flight the ailerons provided yaw control, an air jet at the tail provided pitch control, and differential total pitch of the rear elements of the propellers provided roll control.

TESTS

The tests were made in the Langley full-scale tunnel with the model support strut mounted near the lower edge of the entrance cone and about 6 feet above the ground board. Electric strain-gage balances were used to measure the forces and moments on the model, and electric tachometers were used to indicate the various model propeller speeds needed in the tests. Although during some of the tests another model was left in the tunnel approximately 10 feet behind and slightly to the left of the present model, no corrections for flow angularity or blockage due to the presence of the models have been applied to the data, since the blockage and interference effects were believed to be small.

For the forward-flight condition at a wing incidence of 4.5°, force tests were made to determine the longitudinal and lateral stability and control characteristics of the short-wing configuration at various thrust coefficients. Similar tests were made for the long-wing configuration except that the longitudinal-control tests were not made. The effects of two configurations of leading-edge slats, one high and one low as shown in figure 6, were studied at various values of thrust coefficient. At a wing incidence of 10°, force tests were made to determine the longitudinal stability and control characteristics of the short- and long-wing configurations at various thrust coefficients.

For the transition-flight conditions at wing incidences from 20° to 80°, tests were made to determine the longitudinal and lateral stability and control characteristics of the short- and long-wing configurations at conditions of zero and 0.25g forward acceleration and 0.25g deceleration. The longitudinal runs for both the long- and short-wing configuration at the various accelerations were made to simulate transitions with the fuselage attitude level, 7° nose down, and 10° nose up.

For the hovering-flight condition, only the short-wing configuration was tested. The longitudinal stability characteristics at wing incidences of 85°, 90°, and 94.5° and the lateral control characteristics at a wing incidence of 90° were determined in proximity to the ground for a range of heights from 0 to 2 propeller diameters from the ground. The characteristics of the model in a side wind were studied with the model at 90° to the air flow for angles of roll from 16° to -16° for a wing incidence of 94.5°.

In order to represent actual flight conditions more closely, the pitch angles of the propellers were set high in the forward-flight condition and lower in transition and hovering flight. The propeller pitch settings were all measured at the 0.75-radius station. In the forward-flight condition at wing incidences of 4.5° and 10°, the pitch of the front elements of the dual-rotating propellers was set at 30° and that of the rear elements was set at $28\frac{1}{2}^{\circ}$. In the transition- and hovering-flight conditions, all the propeller elements were generally set at 10°.

L 6 1 8

All the data of the force-test investigation have been referred to the center-of-gravity locations of the full-scale airplane for the particular angle of wing incidence involved as shown in figure 7 except for the propeller-alone data in which the data are referred to a point on the shaft axis midway between the front and rear elements of the dual-rotating propellers as shown in figure 2.

The tests at wing incidences of 4.5° and 10° were made at an airspeed of about 22 knots, which gave an effective Reynolds number based on the wing chord and free-stream velocity of about 330,000. In order to represent the power conditions of the full-scale airplane at higher angles of wing incidence, it was necessary to reduce the tunnel airspeed below 22 knots to avoid exceeding the motor limitations of the model. In all the tail-off lateral or longitudinal tests, both the vertical and horizontal tails were removed as a unit.

PRESENTATION OF RESULTS

The results are presented in figures 8 to 39. The data for the normal-forward-flight tests (i_w = 4.5° and 10°) are presented in coefficient form, but since the coefficients approach infinity and become essentially meaningless as the velocity approaches zero, the data for the transition- and hovering-flight tests (wing incidence above 20°) have been scaled up to the weight of the full-scale airplane of 27,278 pounds. It should be noted that although the data have been scaled up to correspond to the weight of 27,278 pounds, for tests made

at power settings that gave zero net drag, 0.25g acceleration, or 0.25g deceleration, at $\alpha = -7^\circ$, 0°, and 10°, the data can be interpolated and rescaled in terms of other conditions such as climb or glide or trim at other angles of attack. If the data are rescaled, all forces, moments, and velocities are simply multiplied by the proper factors required to make the lift equal to the desired value for the desired condition. This scaling is done in a manner similar to the method that was used for scaling up the original data, as shown in the appendix.

Arrangement of the figures presenting the test data and the details of the test conditions are given in tables II and III. Table II(a) covers the longitudinal tests of the forward-flight configuration at wing-incidence angles of 4.5° and 10° (figs. 8 to 17) and table II(b) covers the longitudinal tests of the transition and hovering configurations at wing-incidence angles between 20° and 94.5° (figs. 18 to 28). Table III covers all the lateral tests at wing-incidence angles from 4.5° to 94.5° (figs. 29 to 39).

CONCLUDING REMARKS

Data have been presented for a 1/8-scale model of a vertical-take-off-and-landing airplane in the short- and long-wing configurations with either wing capable of being tilted from an incidence of 4.5° for forward flight to an incidence of 94.5° for hovering flight. Included are longitudinal and lateral stability and control data in the normal-forward-flight, transition, and hovering ranges.

Langley Research Center,
National Aeronautics and Space Administration,
Langley Field, Va., June 19, 1959.

APPENDIX

METHOD OF SCALING UP DATA

The force, moment, and velocity data of the model were scaled up by means of the following equations:

$$F_A = F_M \frac{W}{L_o}$$

$$M_A = M_M \frac{W}{L_o} N$$

$$V_A = \frac{V_T}{N} \sqrt{\frac{W}{L_o}}$$

where

F_A scaled-up airplane force

F_M measured model force (lift, drag, or side force)

L_o measured model lift at trim condition (at $\alpha = -7^\circ$, 0°, or 10°)

M_A scaled-up airplane moment

M_M measured model moment (rolling, yawing, or pitching moment)

N scale factor, 8

V_A scaled-up airplane velocity

V_T measured tunnel velocity

W weight of airplane, 27,278 lb

REFERENCE

1. Tosti, Louis P.: Flight Investigation of Stability and Control Characteristics of a 1/8-Scale Model of a Tilt-Wing Vertical-Take-Off-and-Landing Airplane. NASA TN D-45, 1960.

TABLE I.- SCALED-UP GEOMETRIC CHARACTERISTICS OF THE MODEL

Propellers (6 blades each):	
Diameter, ft	16
Chord, ft	1.43
Total solidity	0.286
Wing:	
Area, sq ft	528 and 660
Span, ft	48 and 60
Chord, ft	11.0
Aspect ratio	4.36 and 5.45
Taper ratio	1.0
Airfoil section	NACA 23015
Pivot station, percent chord	34.8
Sweepback (leading edge), deg	0
Dihedral angle, deg	0
Incidence relative to propeller axis, deg	4.5
Ailerons (each):	
Chord, ft	2.20
Span, ft:	
Outboard portion	6.46
Inboard portion	8.41
Hinge line, percent chord	0.80
Vertical tail:	
Area, sq ft	118.2
Span, ft	14.33
Tip chord, ft	4.42
Root chord, ft	12.08
Aspect ratio	1.19
Taper ratio	0.273
Airfoil section	NACA 0009
Sweepback (leading edge), deg	22.15
Rudder (hinge line perpendicular to fuselage center line):	
Tip chord (behind hinge line), ft	1.0
Root chord (behind hinge line), ft	2.87
Span, ft	16.75
Horizontal tail:	
Area, (projected), sq ft	197.75
Span (projected), ft	28.21
Tip chord, ft	4.00
Root chord, ft	10.02
Aspect ratio	4.03
Taper ratio	0.399
Airfoil section	NACA 0011
Sweepback (leading edge), deg	15.94
Dihedral angle, deg	15
Elevator (hinge line perpendicular to fuselage center line):	
Tip chord (behind hinge line), ft	1.33
Root chord (behind hinge line), ft	3.25
Span (each), ft	13.84
Overall length, ft	62.67

TABLE II.- LONGITUDINAL TESTS

(a) Forward-flight configuration (i_w = 4.5° and 10°); $\delta_a'_R = \delta_r = \beta = 0°$

Figure	i_w, deg	Wing span	Type or object of test	T_c'	α, deg	i_t, deg	δ_e, deg	$\delta_a'_L$, deg	β_F, deg (a)
8	4.5	Short	Reynolds number effect		-6 to 35	Off	Off	0	Off
9(a) 9(b) 9(c)	4.5	Short	Fuselage alone Fuselage and tails alone Tail effectiveness	0	-6 to 24	0.6 to 20	0	0	30
10(a) 10(b) 10(c)	(b) 4.5	Short	Wing alone - stability at various T_c' Complete model - stability at various T_c'	-0.12 to 0.62 -.15 to .77	(b) -6 to 24	0.6 20	0	0	30
11(a) 11(b) 11(c) 11(d) 11(e) 11(f) 11(g)	4.5	Short	Elevator effectiveness	-0.15 .06 .24 .51 .77 1.08	-6 to 35 -6 to 24	0.6 .6, Off	-20 to 10 -20 to 0, off	0	Off 30
12(a) 12(b)	4.5	Short	Longitudinal effects of ailerons	-0.15 to 0.77	0 9, 18	0.6	0	0 to 40	30
13(a) 13(b) 13(c) 13(d)	4.5	Short	Low slat effects Low and high slat effects	-0.15 .24 .77	-6 to 35 -6 to 24	0.6	0	0	Off 30
14(a) 14(b)	4.5	Long	Stability at various T_c' (tails off) (tails on)	-0.07 to 0.84 -.07 to .57	-6 to 24	Off 0.6	Off 0	0	30
15(a) 15(b) 15(c) 15(d) 15(e) 15(f) 15(g)	10	Short	Propellers off Elevator effectiveness	-0.15 .06 .24 .51 .77 1.08	-9 to 21	0.6 .6, Off	0 -20 to 10, Off -10 to 10, Off -20 to 10, Off	0	Off 30
16(a) 16(b) 16(c) 16(d) 16(e) 16(f) 16(g)	10	Long	Stability at various T_c' (tails off) Elevator effectiveness at various T_c' Tail effectiveness at various T_c'	-0.04 to 0.77 -.04 to .53	-6 to 24	Off 0.6 5 10 20	Off 0 10 20 0	0	30
17	10	Long	Elevator effectiveness at various T_c'	-0.04 to 0.77	0	0.6	-20 to 20	0	30

[a] When $\beta_F = 30°$, $\beta_R = 28.5°$.

[b] Wing-alone test made through an angle-of-attack range of -6° to 24°.

TABLE II.- LONGITUDINAL TESTS - Concluded

(b) Transition and hovering configurations (i_w = 20° to 94.5°); $\delta_e = \delta_a = \beta = 0°$

Figure	i_w, deg	Wing span	Type or object of test	Power conditions	α, deg	i_t, deg	β_F, deg (a)
Transition							
18(a) 18(b)			Propellers alone; V_a = 22 knots; α_p = -10° to 90°	Windmilling to 1,340 rpm Windmilling to 2,733 rpm			30 10
19	20, 35	Short	Stability at various α (tails on)		-9 to 18	0.6	Off
20(a) 20(b) 20(c) 20(d) 20(e)	20 35 50 65 80	Short	Power set for α = 0°	0 acceleration	-10 to 20	0.6, 10, Off 0.6, 20, Off 0.6, 10, Off	10
21(a) 21(b) 21(c) 21(d)	20 35 50 65	Short	Power set for α = 0°	0.25g acceleration	-10 to 20	0.6, 10, Off 0.6, Off	10
22(a) 22(b) 22(c) 22(d) 22(e) 22(f)	20 35 50 65 80 90	Short	Power set for α = 0°	0.25g deceleration	-10 to 20	0.6, 10, Off 0.6, Off 0.6, 10, Off 0.6, Off	10
23(a) 23(b) 23(c) 23(d)	24.5 39.5 54.4 69.5	Short	Power set for α = -7°	0 and 0.25g acceleration, 0.25g deceleration	-13 to 17 -10 to 20 -13 to 17	0.6	10
24(a) 24(b) 24(c) 24(d)	20 35 50 65	Short	Power set for α = 10°	0 and 0.25g acceleration, 0.25g deceleration 0 and 0.25g deceleration	4 to 34	0.6	10
25(a) 25(b) 25(c) 25(d)	20 35 50 65	Long	Power set for α = 0°	0 and 0.25g acceleration, 0.25g deceleration	-6 to 24	0.6	10
26(a) 26(b) 26(c) 26(d)	24.5 39.5 54.4 69.5	Long	Power set for α = -7°	0 and 0.25g acceleration, 0.25g deceleration	-13 to 17	0.6	10
27(a) 27(b) 27(c) 27(d)	20 35 50 65	Long	Power set for α = 10°	0 and 0.25g acceleration, 0.25g deceleration 0 and 0.25g deceleration	4 to 34	0.6	10
Hovering							
28(a) 28(b) 28(c)	85, 90, 94.5 85 94.5	Short	Ground proximity (h/d = 0 to 2)	Power on	0 -9, 0, 9	0.6	10

[a]When β_F = 30°, β_R = 28.5°; when β_F = 10°, β_R = 10°.

TABLE III.- LATERAL TESTS

Forward-Flight, Transition, and Hovering Configurations (i_w = 4.5° to 94.5°); $\delta_{a'R}$ = 0°

Figure	i_w, deg	Wing span	Type or object of test	Power condition or T_c'	α, deg	i_t, deg	δ_e, deg	$\delta_{a'L}$, deg	δ_r, deg	β, deg	β_F, deg (a)
Forward flight											
29(a) 29(b) 29(c) 29(d) 29(e) 29(f)	4.5	Short	Stability at various α (tails off)	Propellers off -0.15 .06 .24 .51 .77	-6 to 18	Off	Off	0	Off	-20 to 20	Off 30
30(a) 30(b) 30(c) 30(d) 30(e) 30(f)	4.5	Short	Stability at various α (tails on)	Propellers off -0.15 .06 .24 .51 .77	-6 to 18 6, 12, 18 12, 18	0.6	0	0	0	-20 to 20	Off 30
31(a) 31(b) 31(c)	4.5	Short	Aileron control at various α Aileron control at various T_c' Rudder control at various α	Propellers off 0.24, 0.77 -.15	0, 9, 18 0 0, 9, 18	0.6	0	-30 to 30 0	0 -30 to 30	0	Off 30, Off 30
32(a) 32(b)	4.5	Long	Stability at various T_c'	-0.07 to 0.57	0	Off 0.6	Off 0	0	Off 0	-20 to 20	30, Off
33(a) 33(b)	4.5	Long	Aileron control at various T_c' Rudder control at various α	0.11, 0.57 -.15	0 0, 9, 18	0.6	0	-30 to 30 0	0 -30 to 30	0	30, Off
Transition											
34	20 to 80	Short	Stability of short wing	Zero acceleration	0	0.6	0	0	0	-20 to 20	10
35(a) 35(b) 35(c)	20 to 80 20, 35 20 to 80	Short	Aileron control effectiveness Rudder control effectiveness Propeller control effectiveness	Zero acceleration	0	0.6	0	-30 to 30 0	0 -30 to 30 0	0	10 (b)
36	20 to 65	Long	Stability of long wing	Zero acceleration	0	0.6	0	0	0	-20 to 20	10
37(a) 37(b)	20 to 65 20 to 50	Long	Aileron control effectiveness Rudder control effectiveness	Zero acceleration	0	0.6	0	-30 to 30 0	0 -30 to 30	0	10
Hovering											
38(a) 38(b)	90	Short	Aileron control (h/d = 0 to 2) Propeller control (h/d = 0 to 2)	Power on	0	0.6	0	-30 to 30 0	0	0	16 (c)
39	94.5	Short	Rolling stability in sidewise flow (ϕ = -16° to 16°; V_a = 9, 19, 37 knots)	Power on	0	0.6	0	0	0	270	10

[a] In all cases, except as noted, when β_F = 30°, β_R = 28.5°; when β_F = 16°, β_R = 14.5°; and when β_F = 10°, β_R = 10°.

[b] β_F = 10°; β_{RR} = 10°; β_{LR} varies between 9° and 12°.

[c] β_F = 16°; β_{RR} = 14.5°; β_{LR} = 14°, 15.5°, and 16.5°.

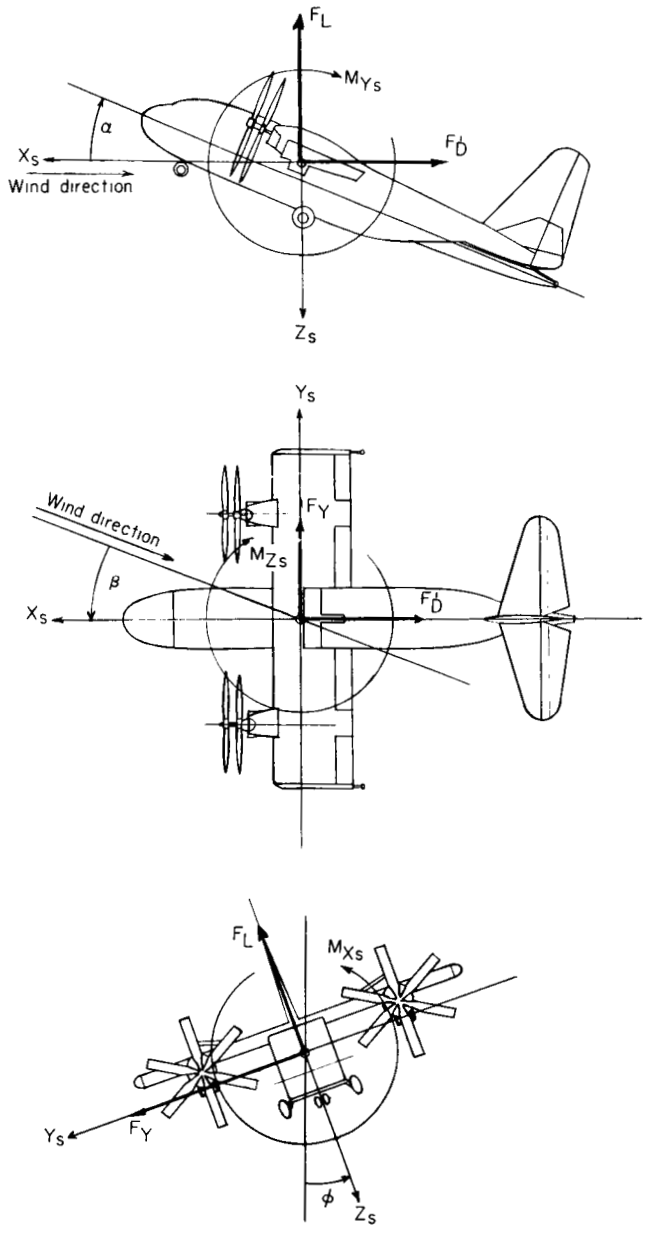

Figure 1.- Stability system of axes. Arrows indicate positive directions of moments, forces, and angular displacements. This system of axes is defined as an orthogonal system having the origin at the center of gravity and in which the Z-axis is in the plane of symmetry and perpendicular to the relative wind, the X-axis is in the plane of symmetry and perpendicular to the Z-axis, and the Y-axis is perpendicular to the plane of symmetry.

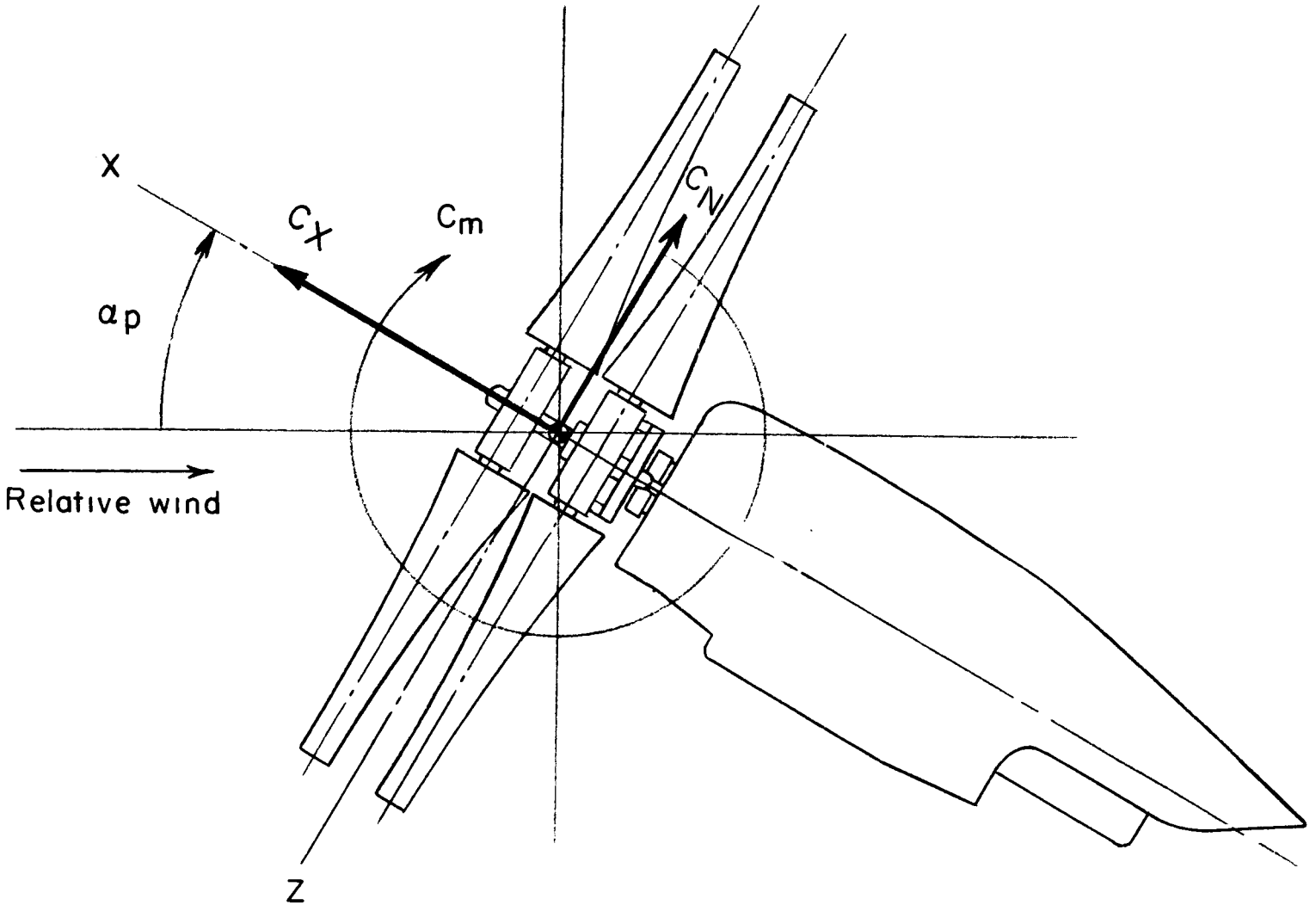

Figure 2.- Body system of axes for propellers-alone force tests. Direction of the forces and moment coefficients are positive.

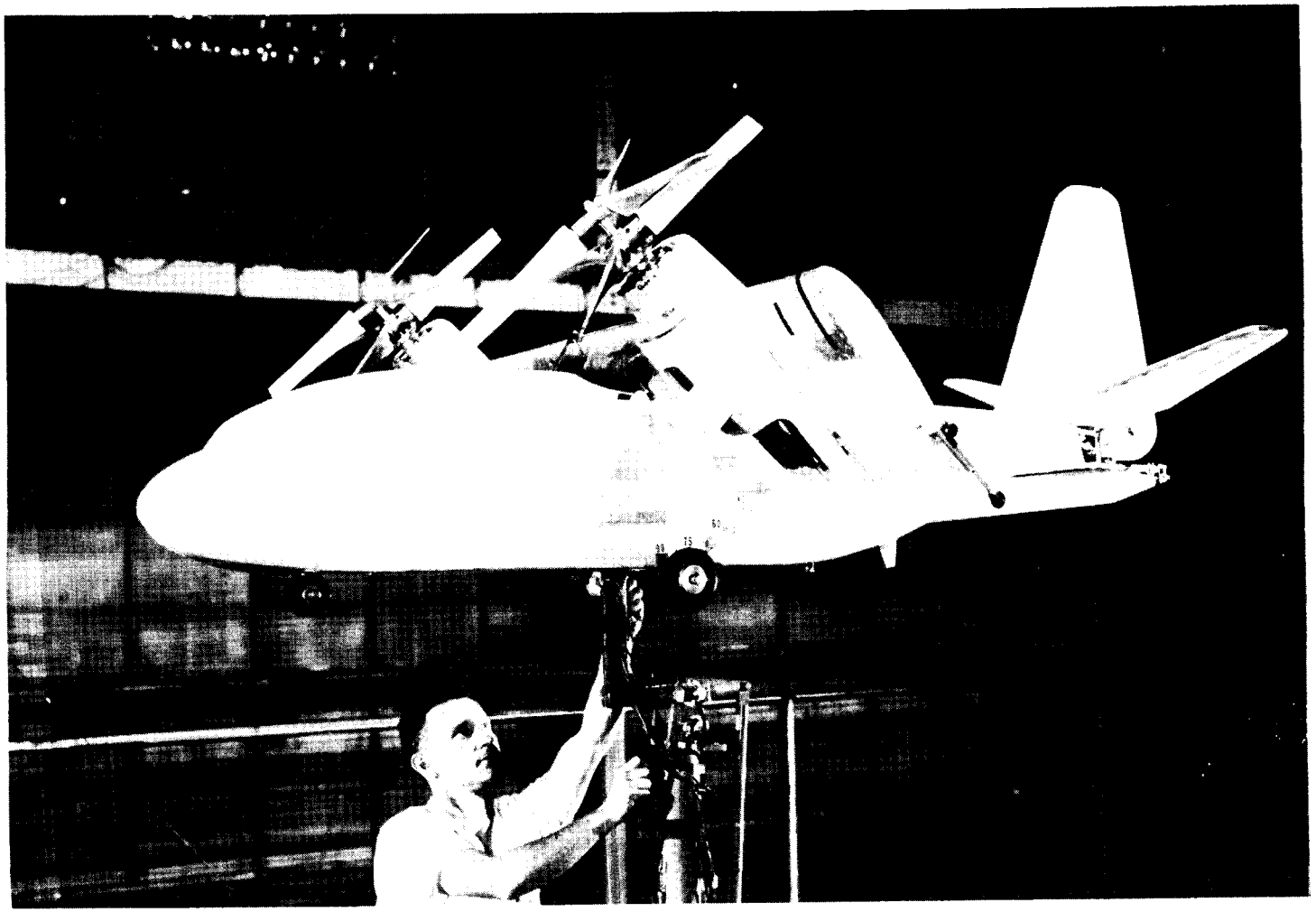

L-57-2151

Figure 3.- Photograph of 1/8-scale model of the Hiller X-18 airplane in the Langley full-scale tunnel.

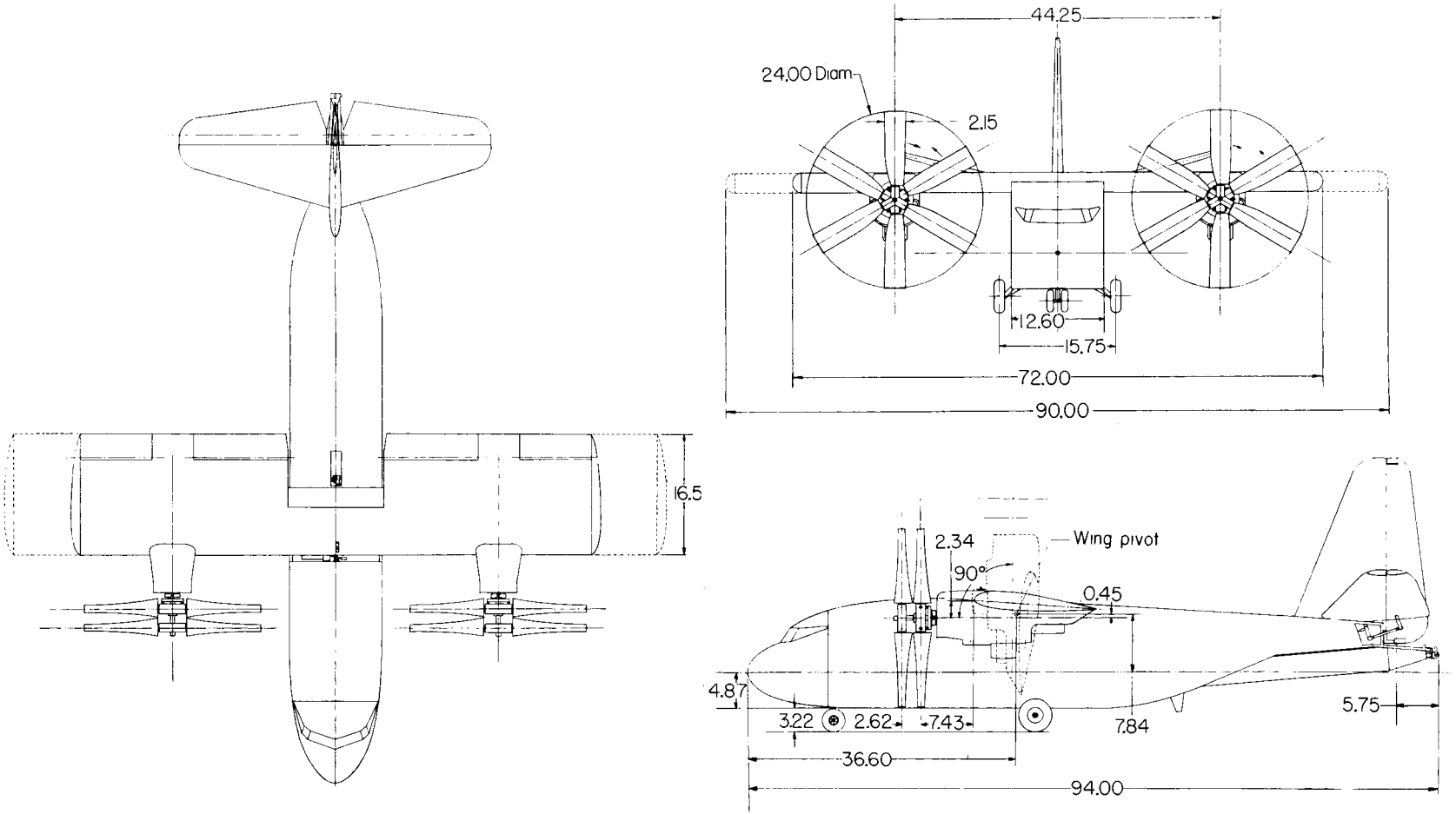

Figure 4.- Three-view sketch of model. All dimensions are in inches.

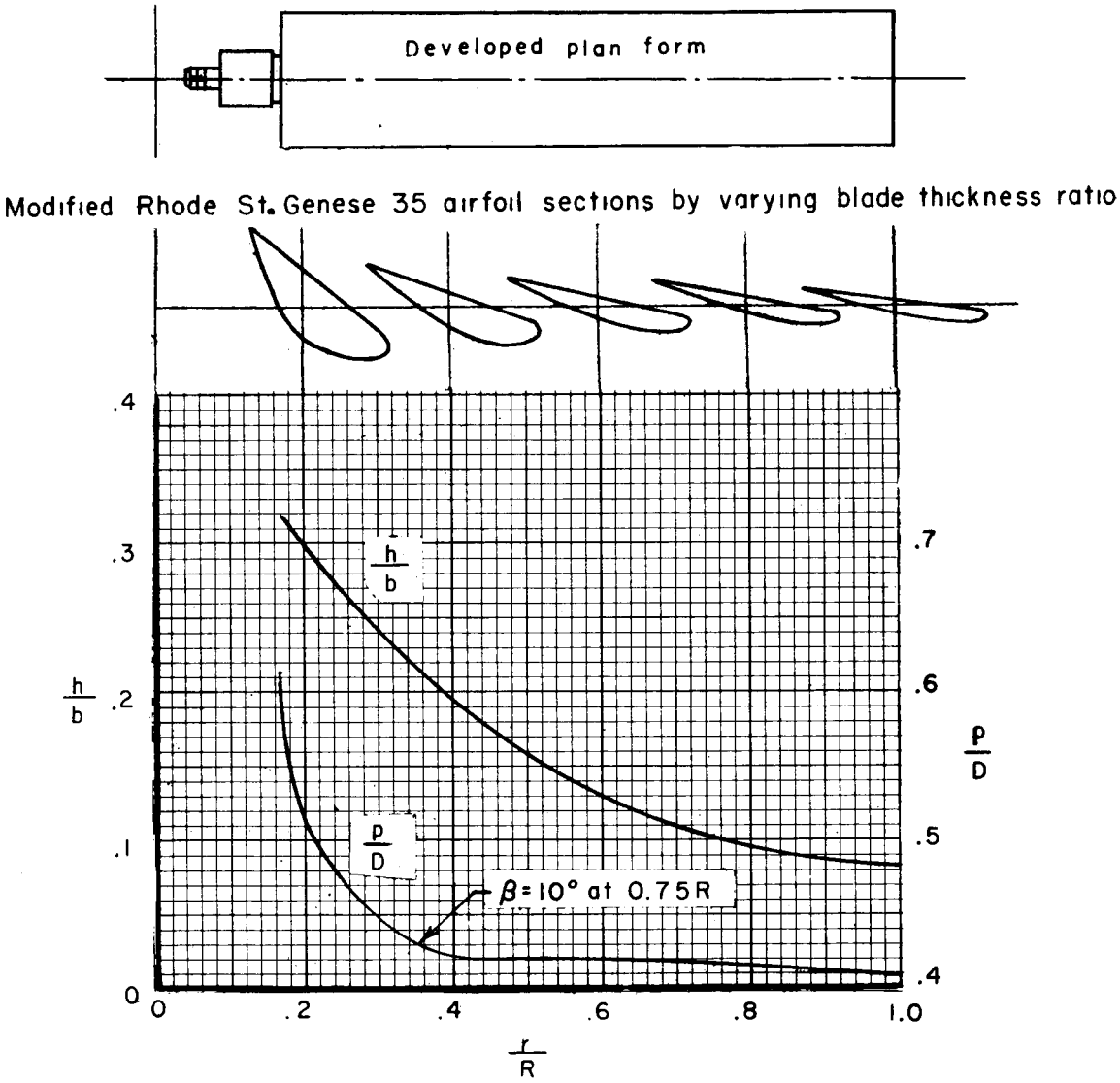

Figure 5.- Blade form curves. In this figure, symbols are as follows: D, diameter (D = 24 inches); R, radius; r, station radius; b, section chord (b = 2.15 inches); h, section thickness; p, geometric pitch ($p = 2\pi r \tan \beta$); β, section blade angle.

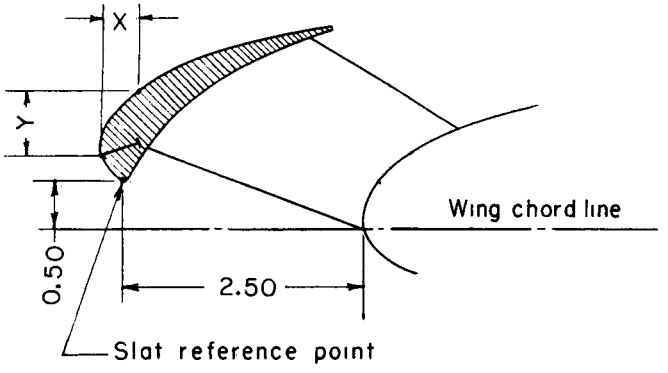

High slat

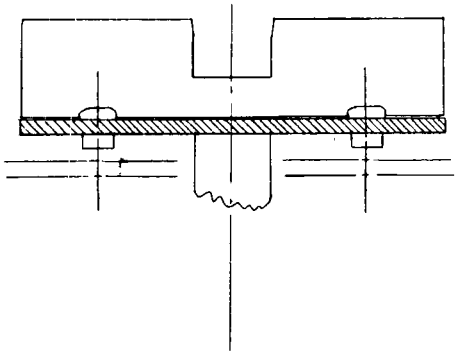

Slat Ordinates		
Station(X)	Upper(Y) surface	Lower(Y) surface
0	--	0
0.206	0.551	-0.231[a]
0.330	--	-0.135
0.412	0.732	0.000
0.825	0.971	0.515
1.238	1.139	0.856
1.650	1.260	1.098
2.310	1.388	1.378
Leading-edge radius 0.409		
Slope of radius through leading edge 0.305		
[a] This point is defined as the "slat reference point"		

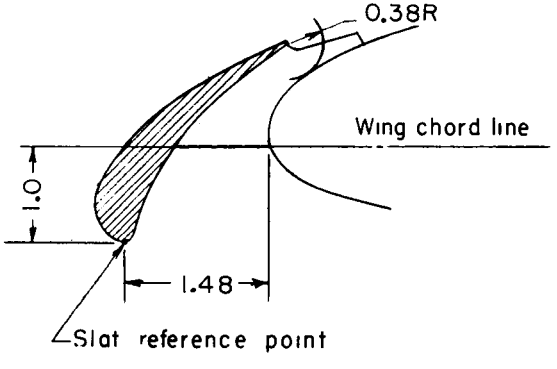

Low slat

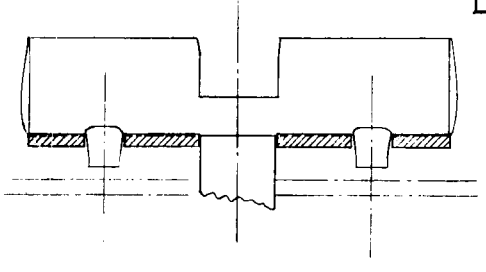

Figure 6.- High and low leading-edge slat configurations tested on short-wing configuration only. All dimensions are in inches.

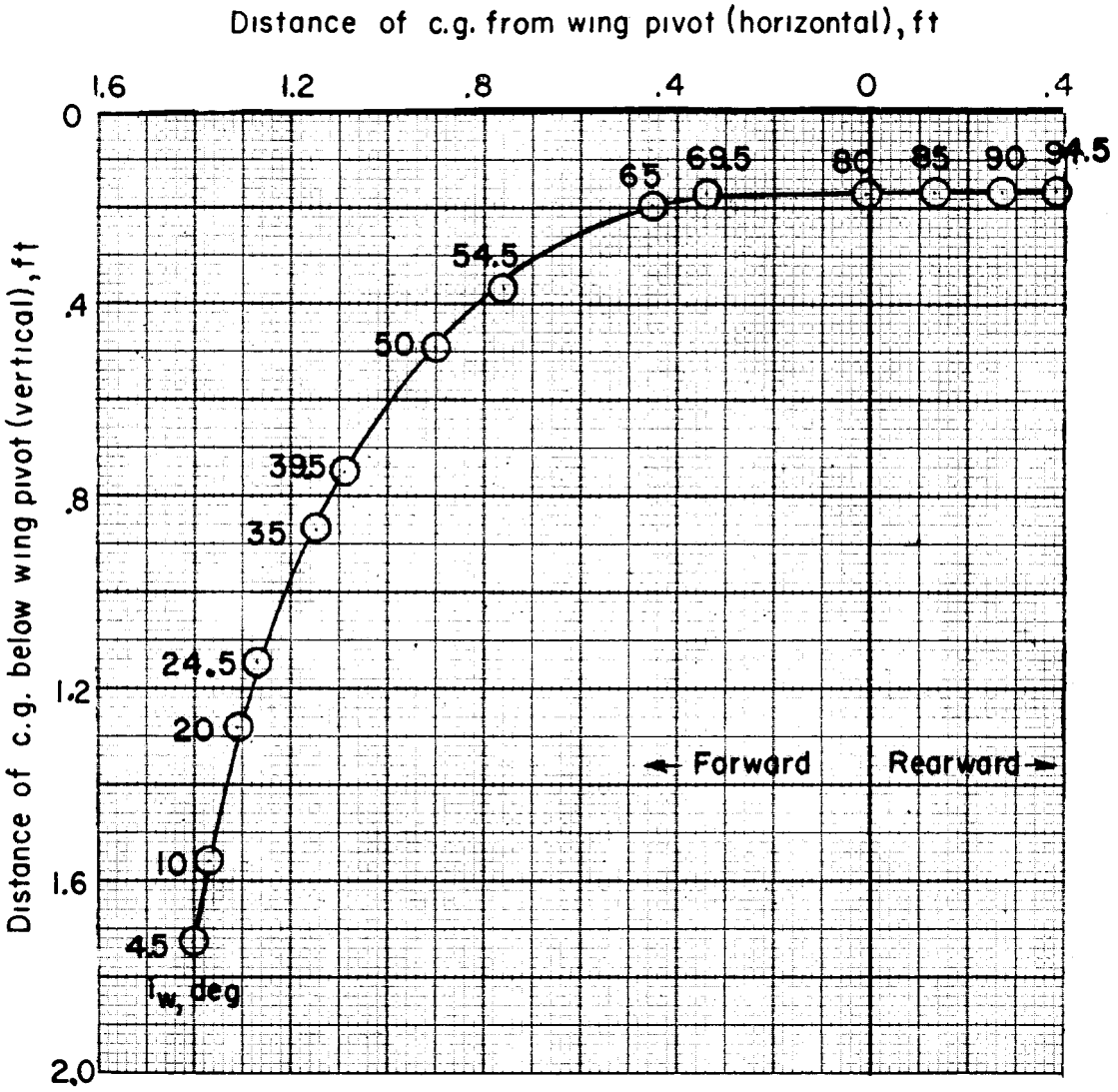

Figure 7.- Center-of-gravity locations of full-scale airplane at a weight of 27,278 pounds for various wing-incidence angles.

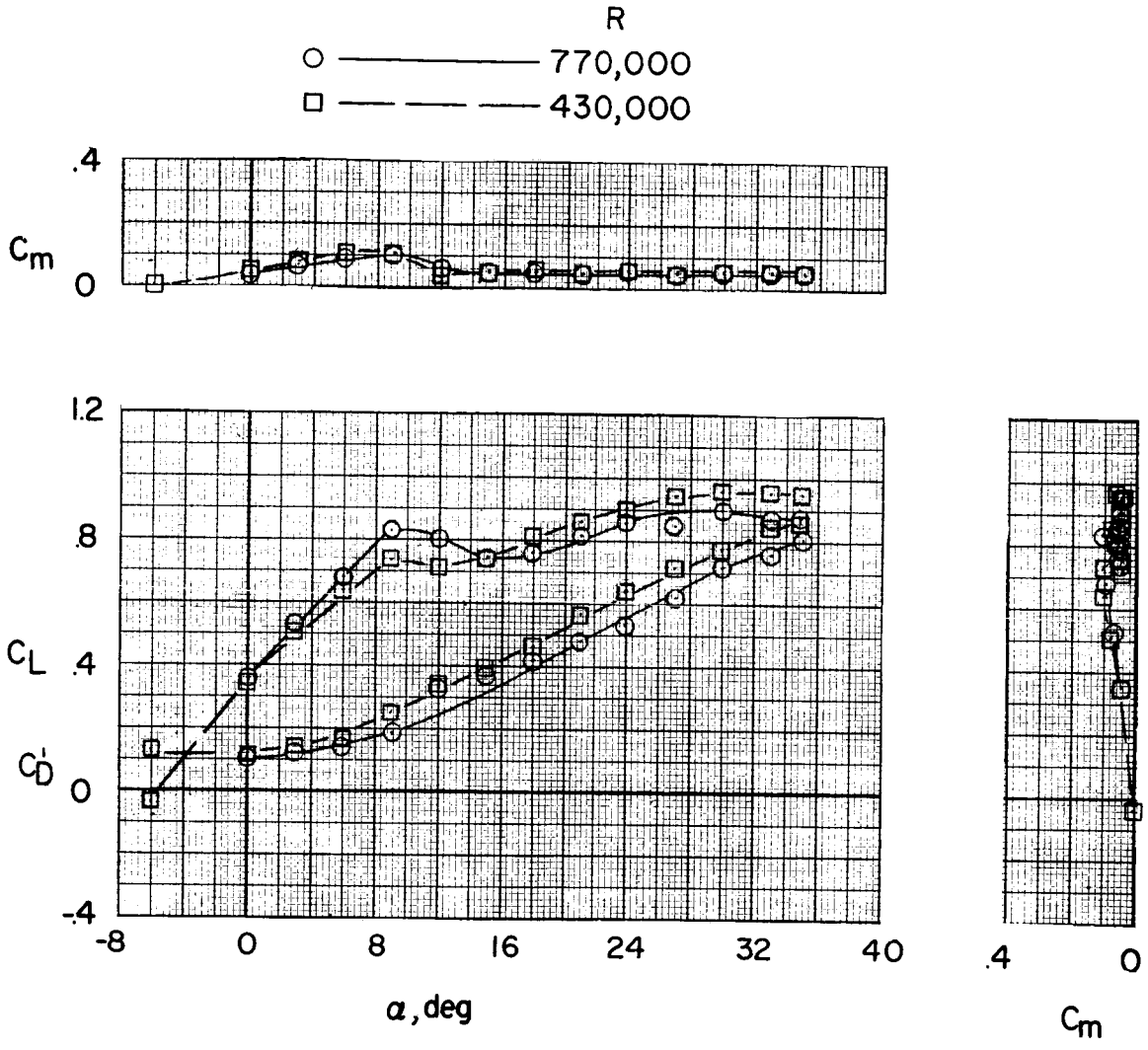

Figure 8.- Longitudinal stability characteristics to show Reynolds number effect. $i_w = 4.5^\circ$; short wing; tails and propellers off; $\beta = 0^\circ$.

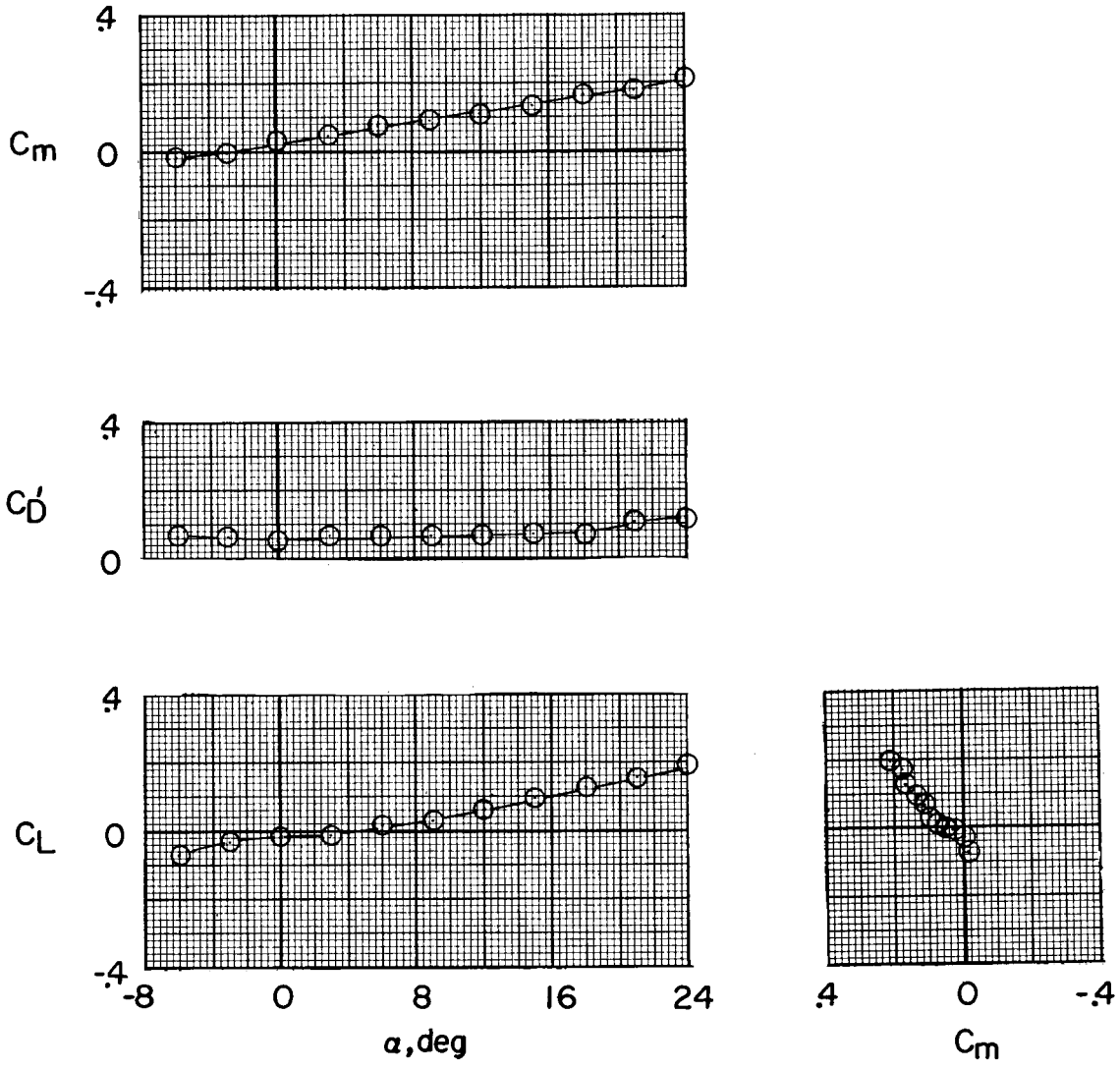

(a) Fuselage alone.

Figure 9.- Longitudinal stability and control characteristics in normal forward flight. $\beta = 0^{\circ}$.

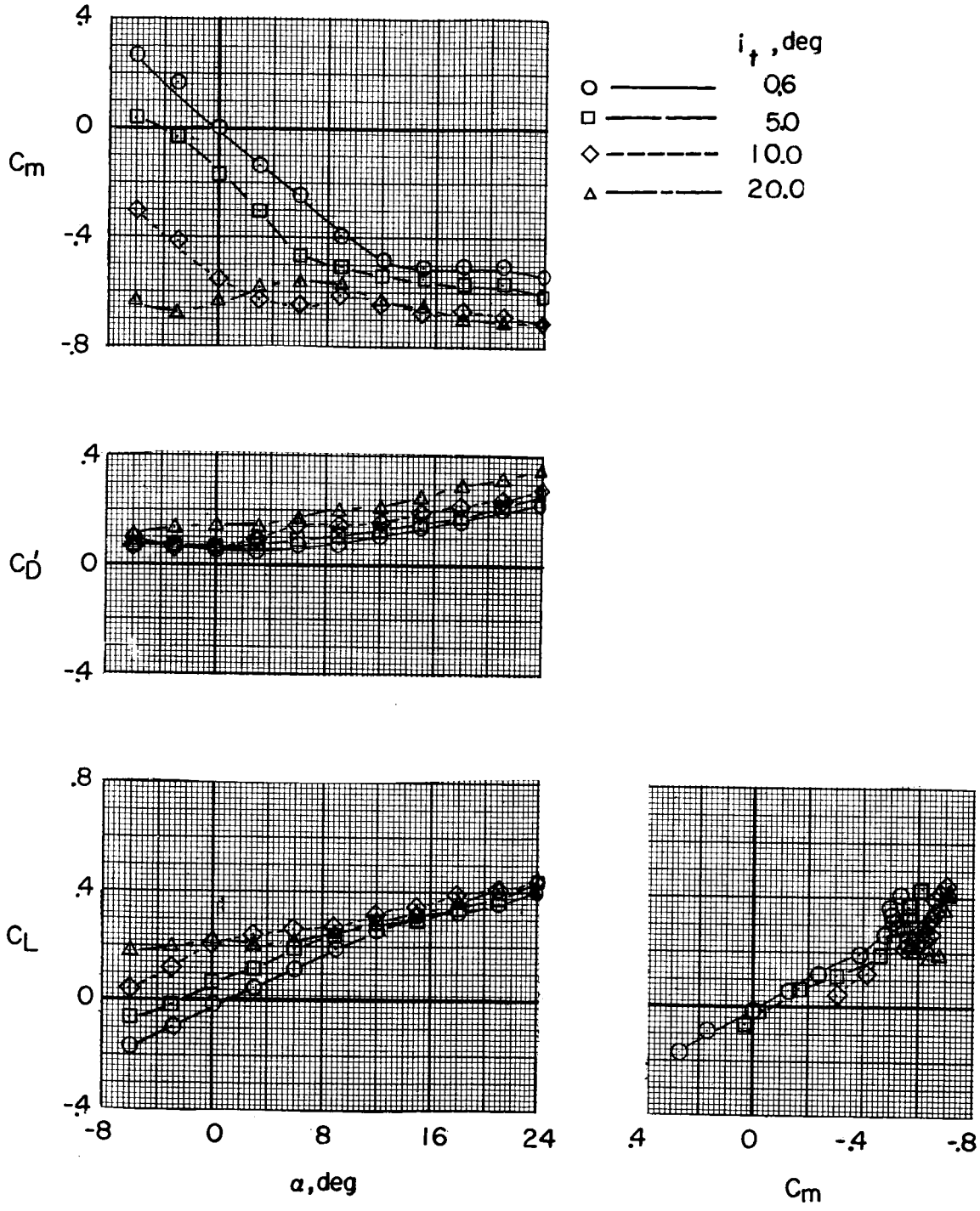

(b) Fuselage and tails. $\delta_e = 0^\circ$.

Figure 9.- Continued.

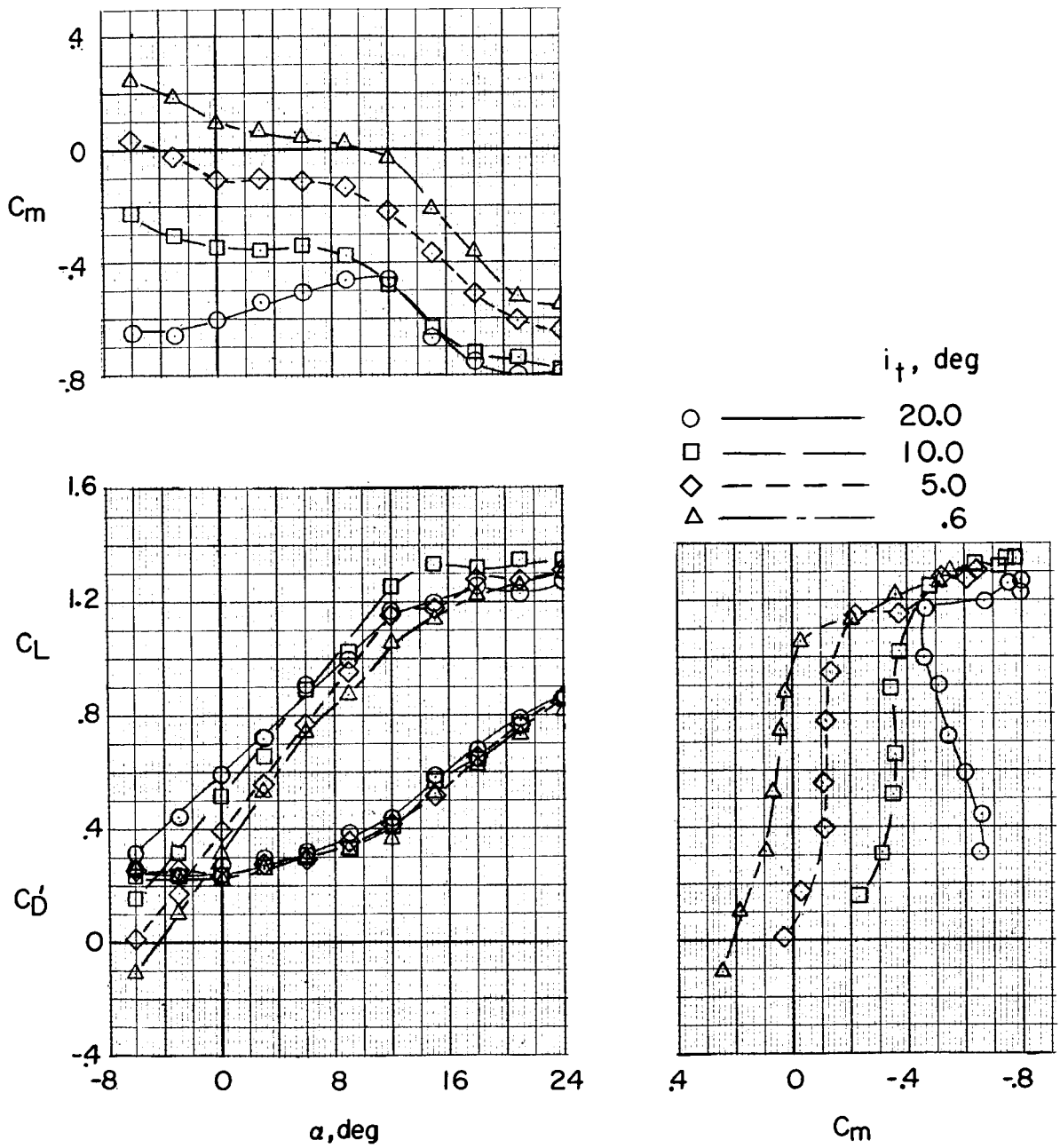

(c) Complete model. $i_w = 4.5^\circ$; short wing; $\delta_e = 0^\circ$; $\beta_F = 30^\circ$; $T_c' = 0$.

Figure 9.- Concluded.

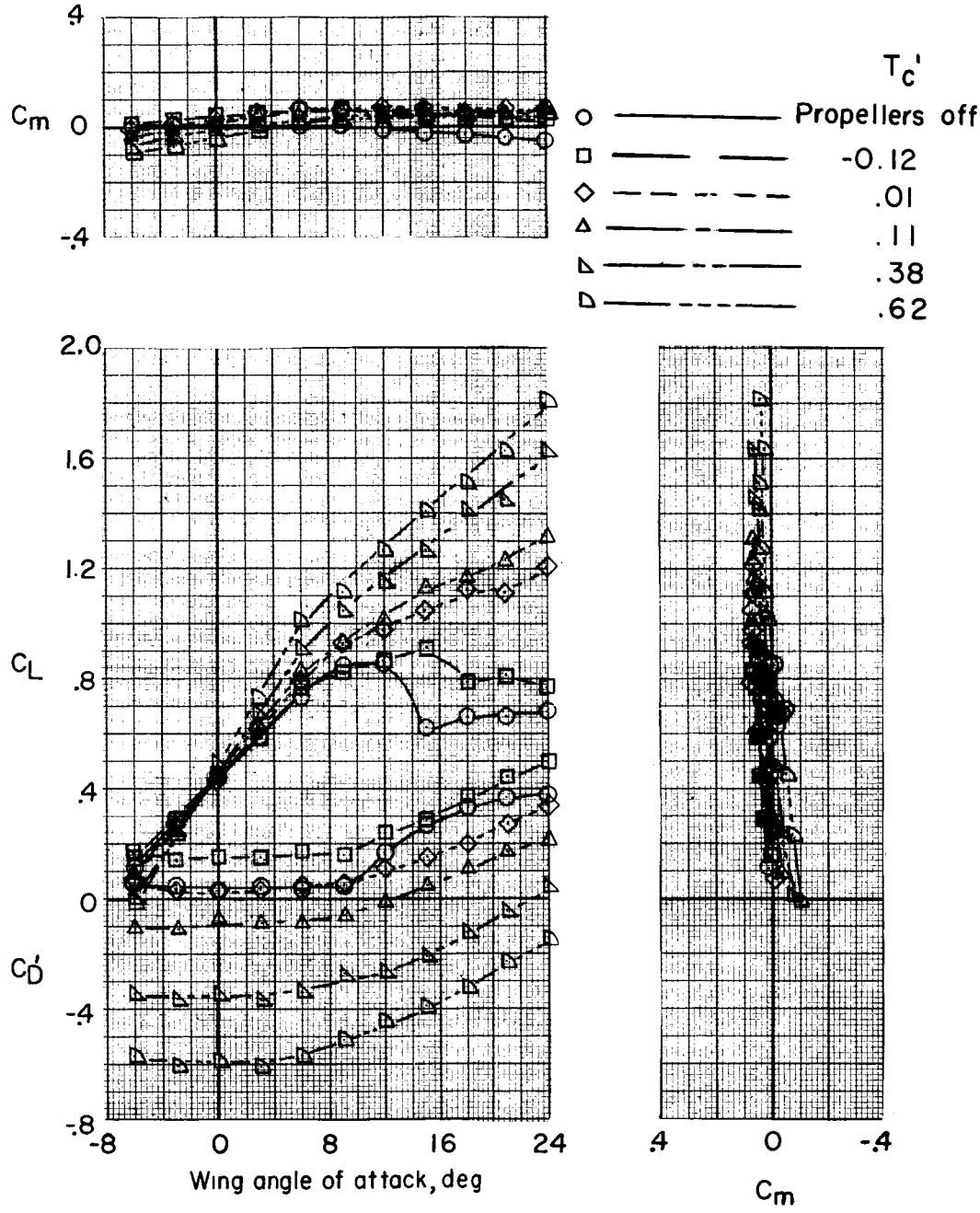

(a) Wing alone.

Figure 10.- Longitudinal stability characteristics at various thrust coefficients. Short wing.

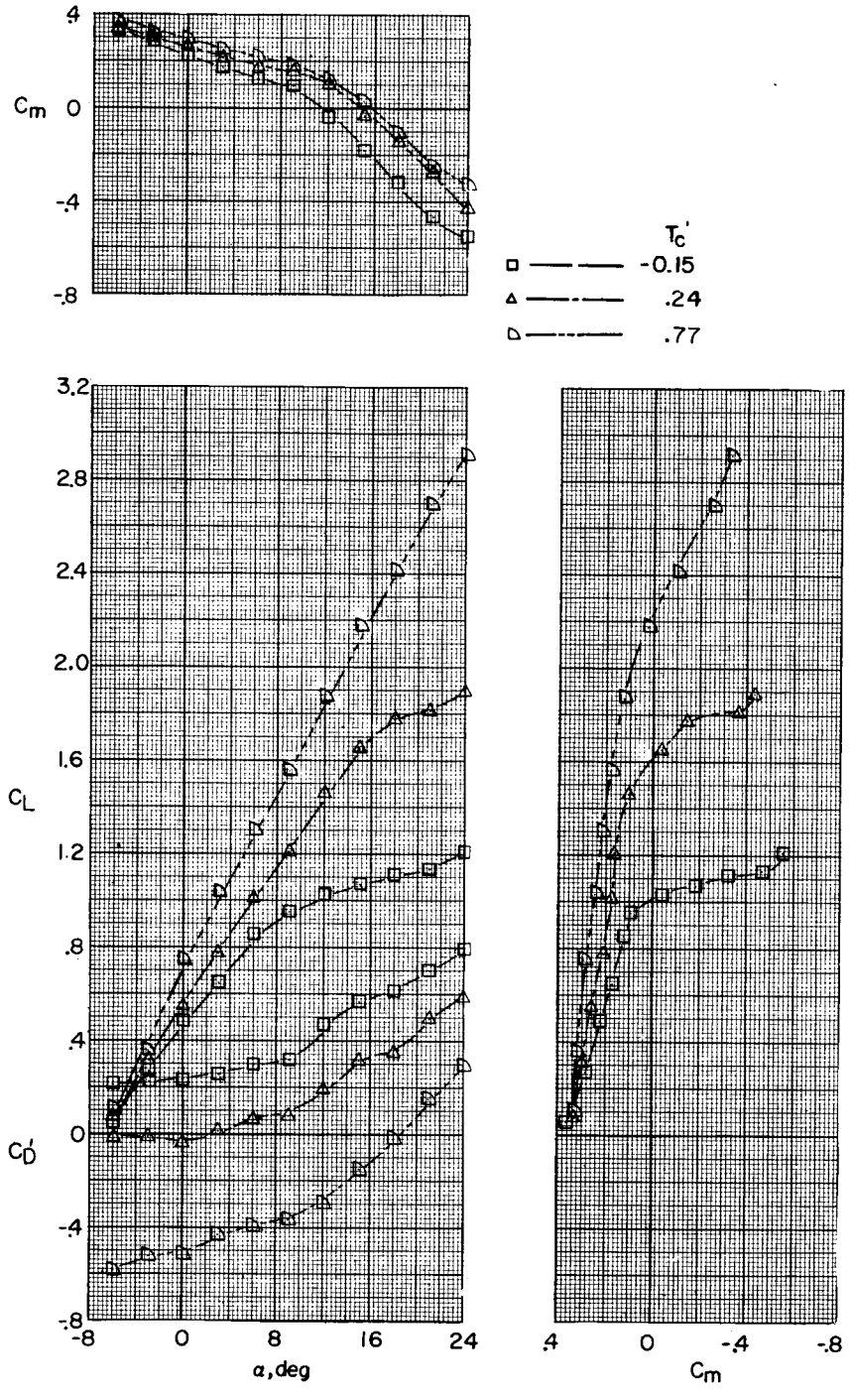

(b) Complete model. $i_w = 4.5°$; $i_t = 0.6°$; $\delta_e = 0°$; $\beta_F = 30°$.

Figure 10.- Continued.

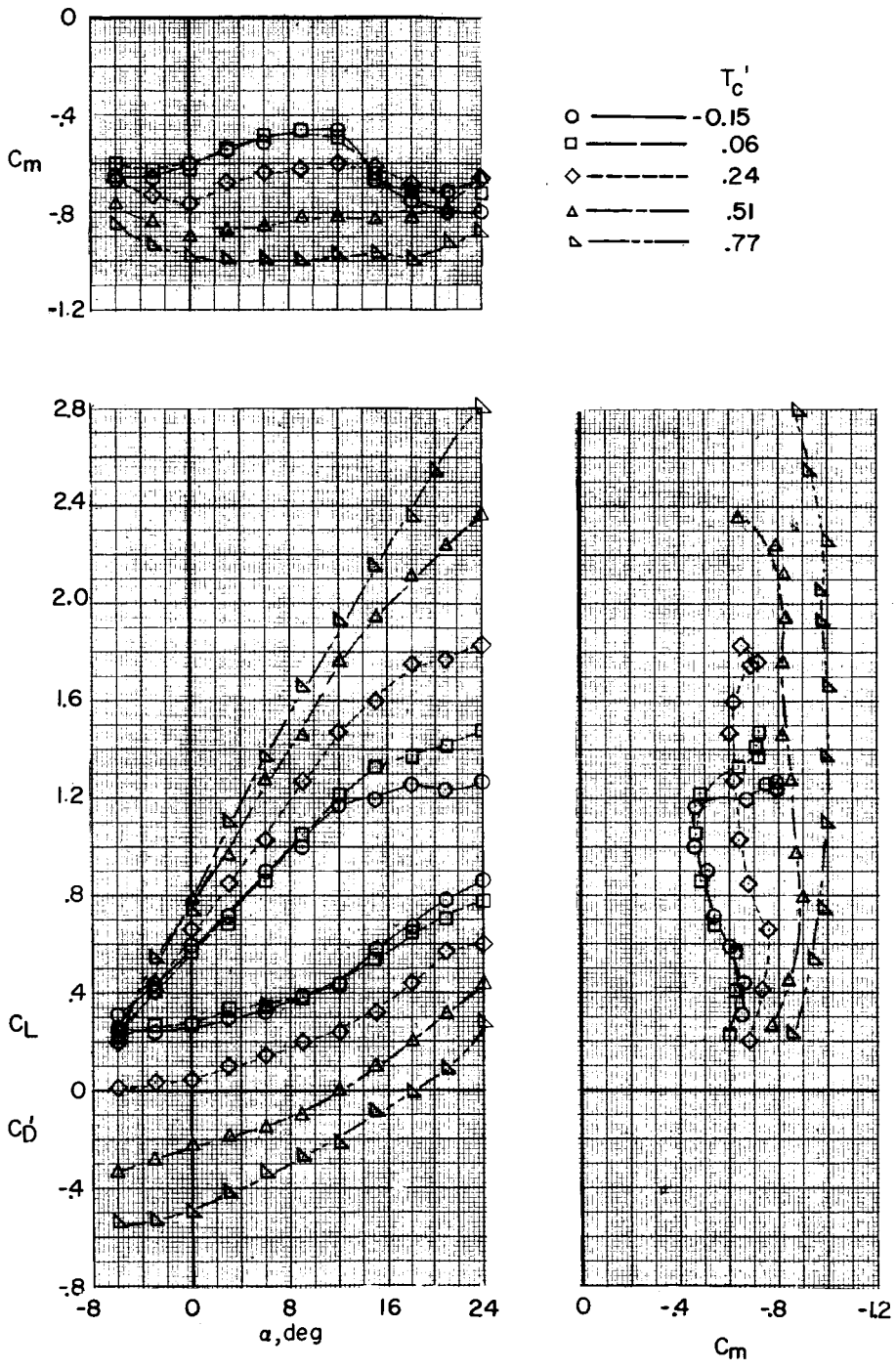

(c) Complete model. $i_W = 4.5^\circ$; $i_t = 20^\circ$; $\delta_e = 0^\circ$; $\beta_F = 30^\circ$.

Figure 10.- Concluded.

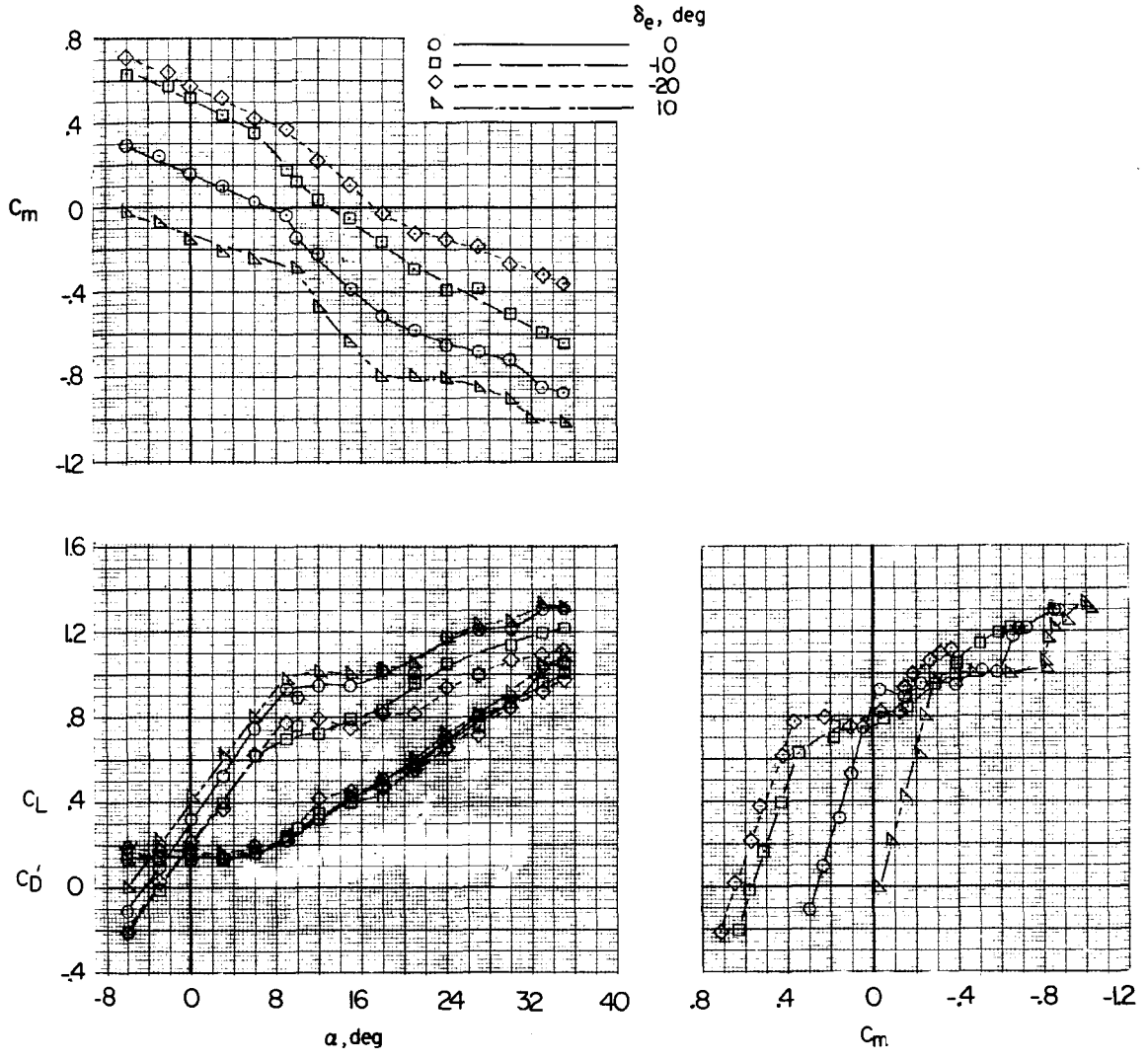

(a) Propellers off.

Figure 11.- Longitudinal stability and control characteristics in normal forward flight for various thrust coefficients and elevator positions. $i_w = 4.5^\circ$; short wing; $i_t = 0.6^\circ$; $\beta_F = 30^\circ$.

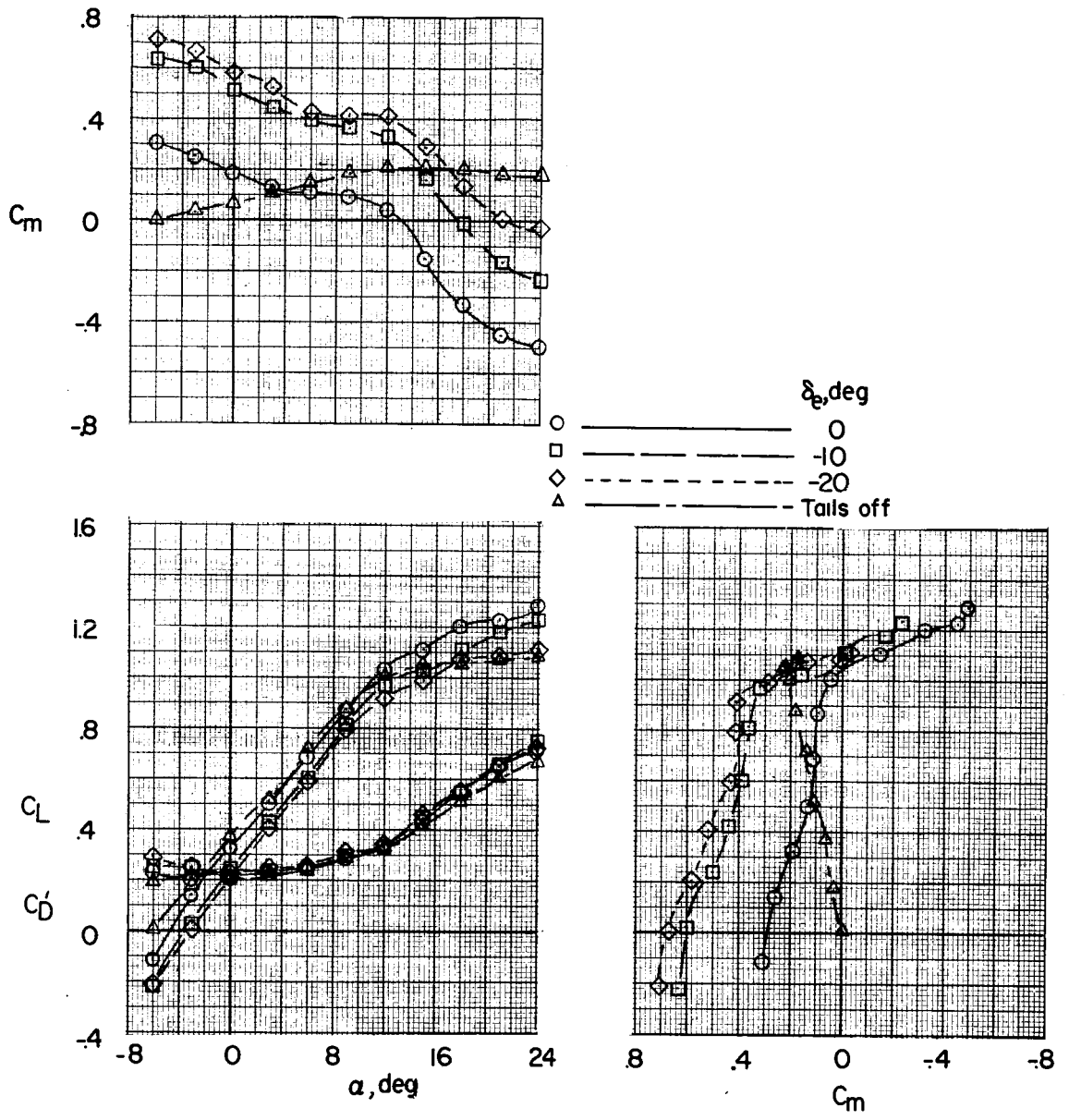

(b) $T_c' = -0.15$.

Figure 11.- Continued.

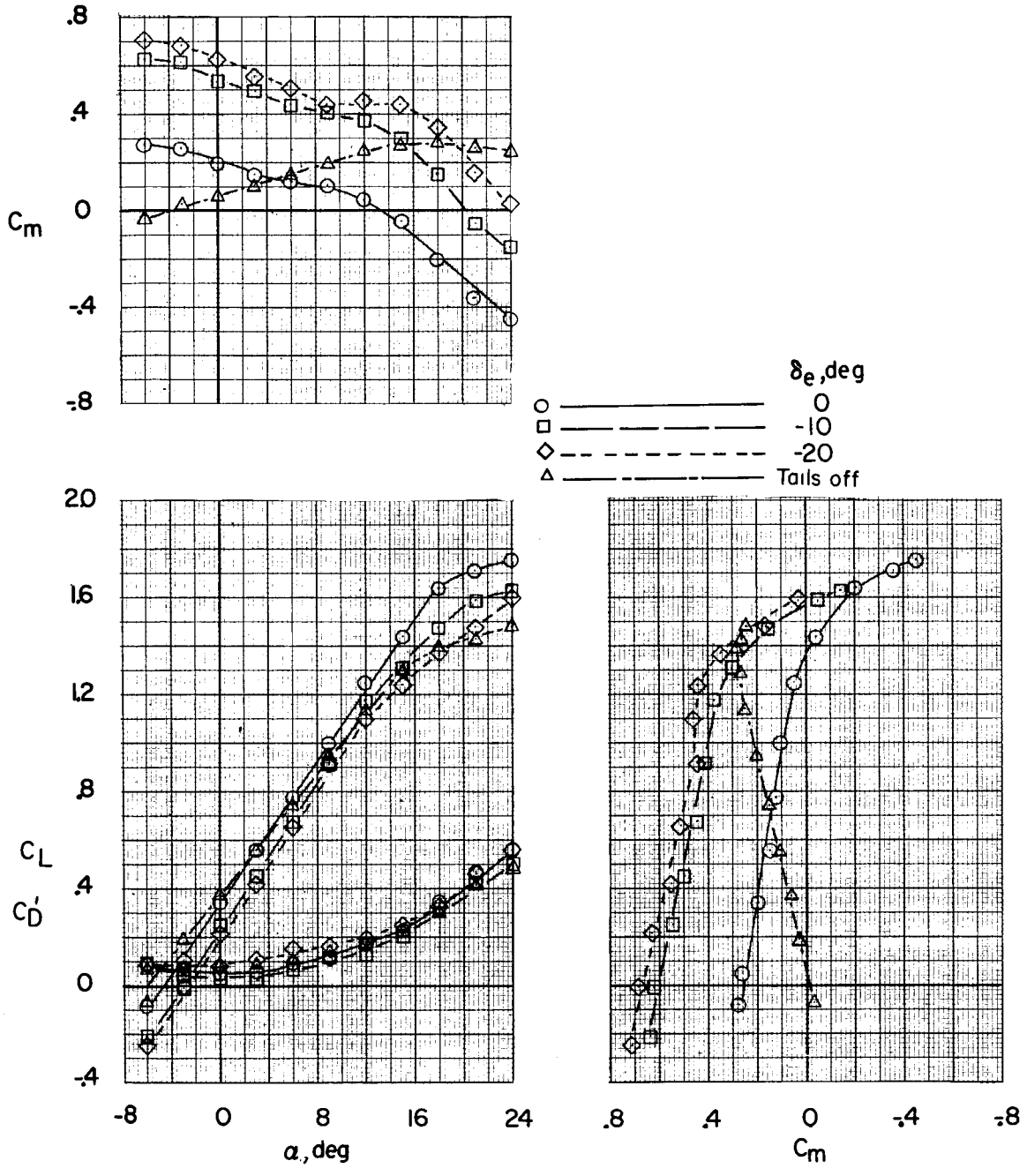

(c) $T_c' = 0.06$.

Figure 11.- Continued.

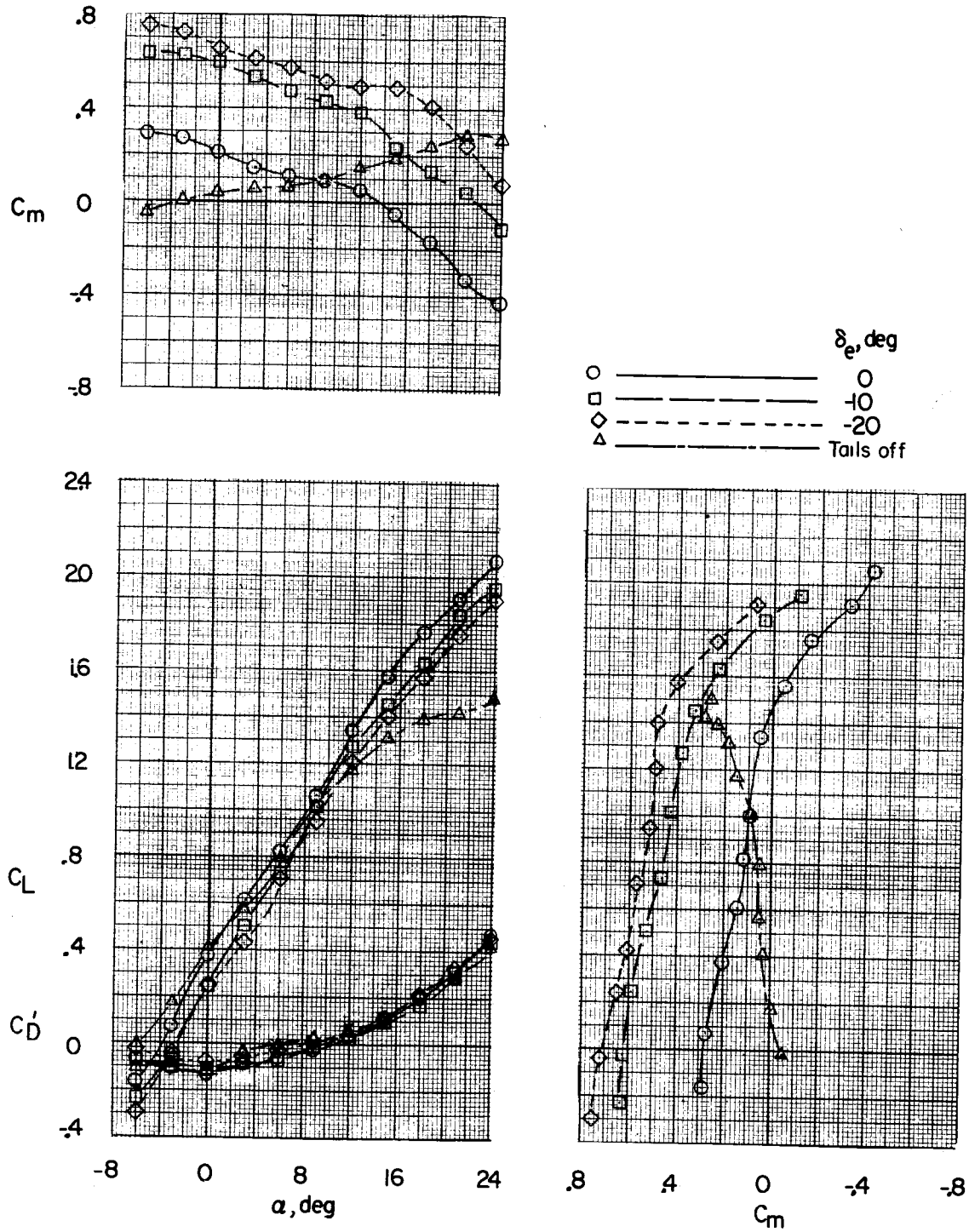

(d) $T_c' = 0.24$.

Figure 11.- Continued.

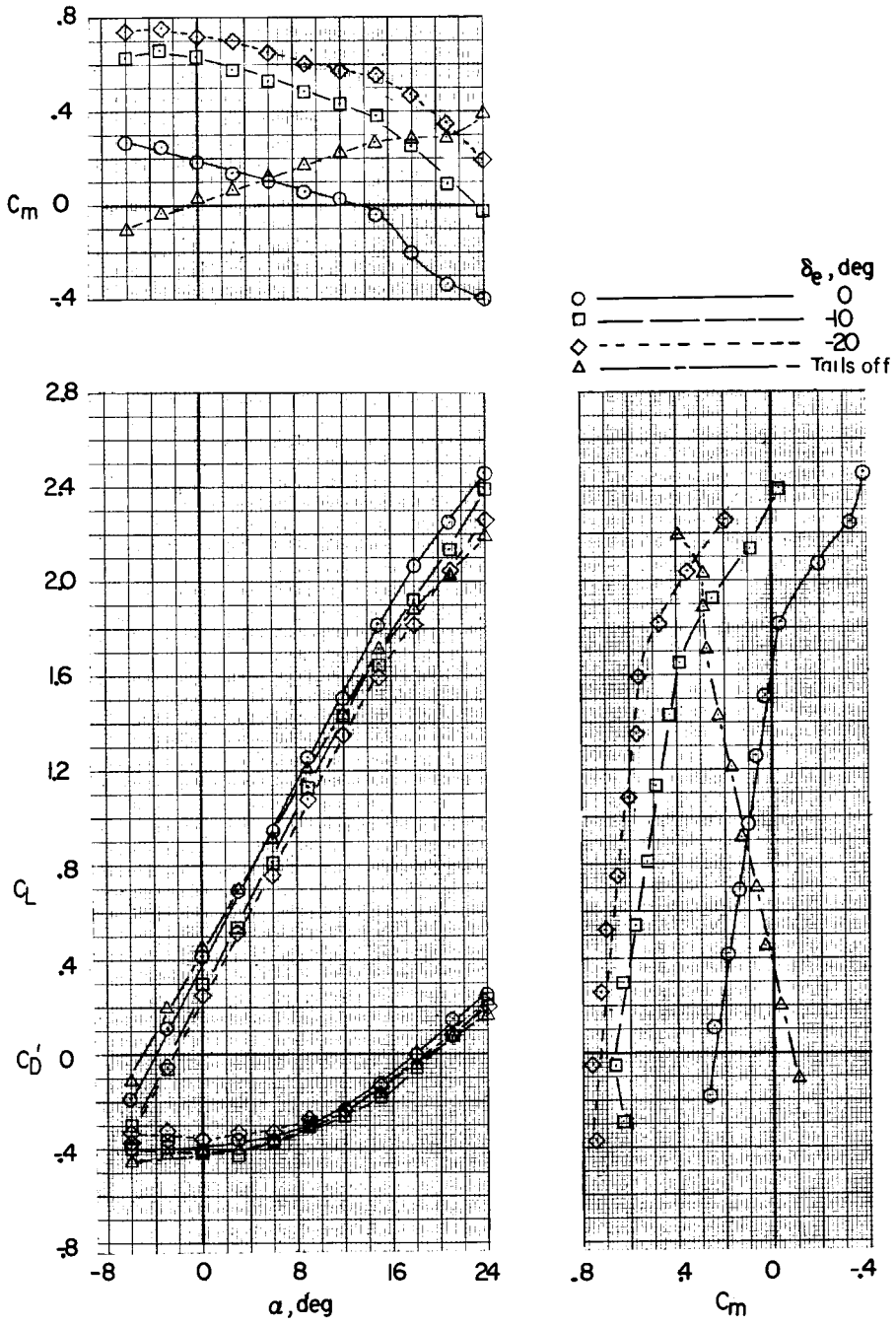

(e) $T_c' = 0.51$.

Figure 11.- Continued.

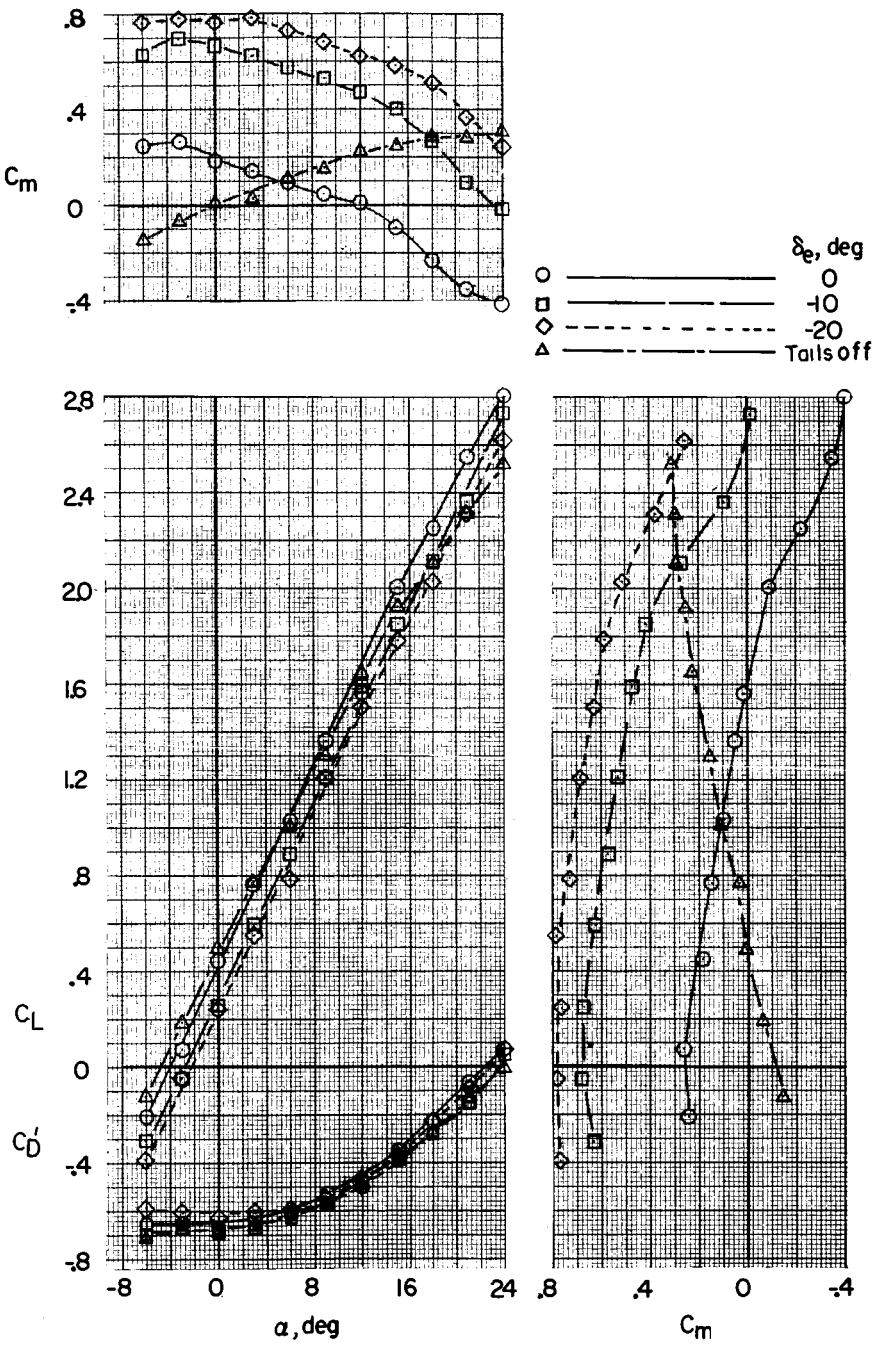

(f) $T_c' = 0.77$.

Figure 11.- Continued.

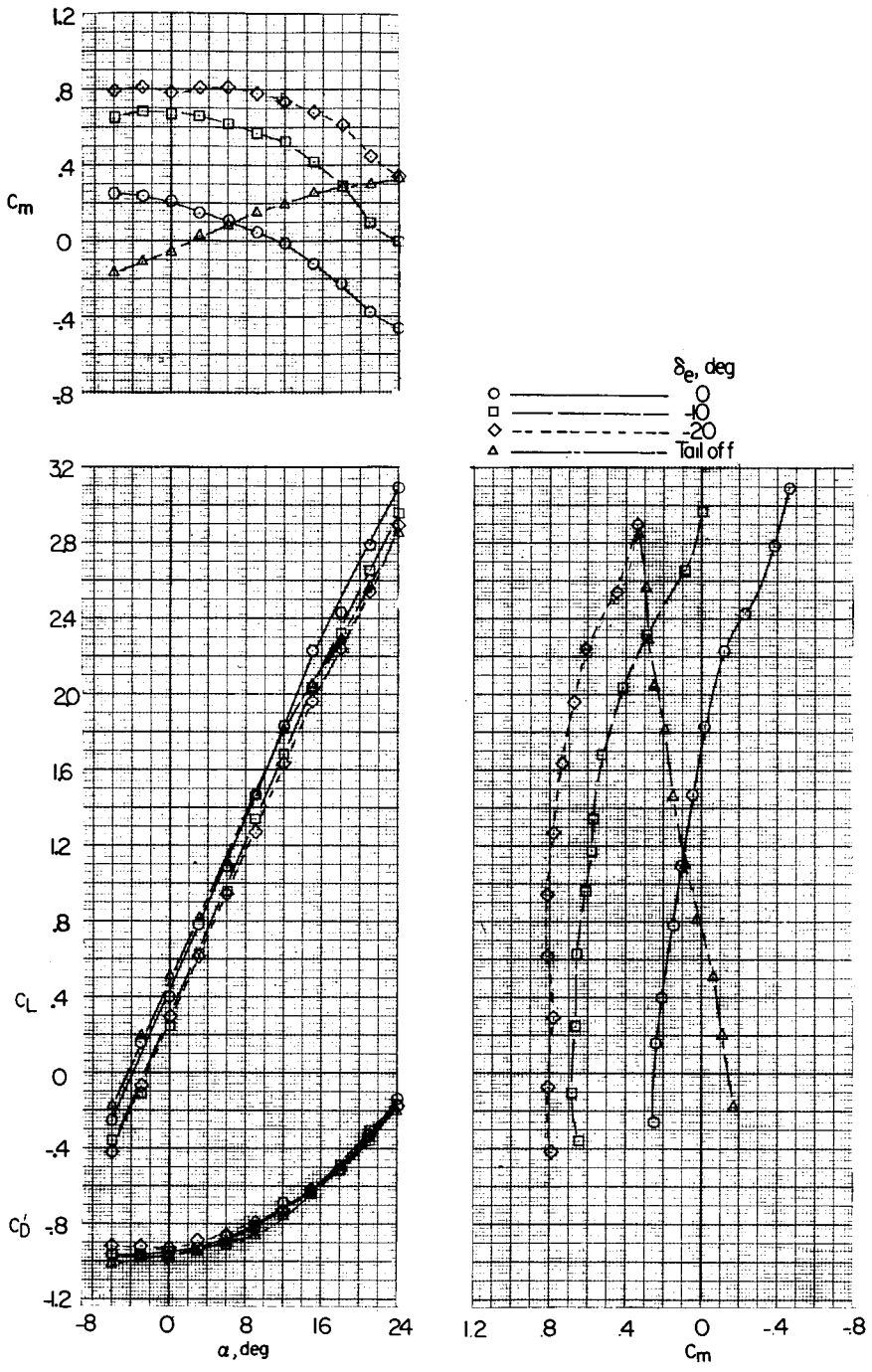

(g) $T_c' = 1.08$.

Figure 11.- Concluded.

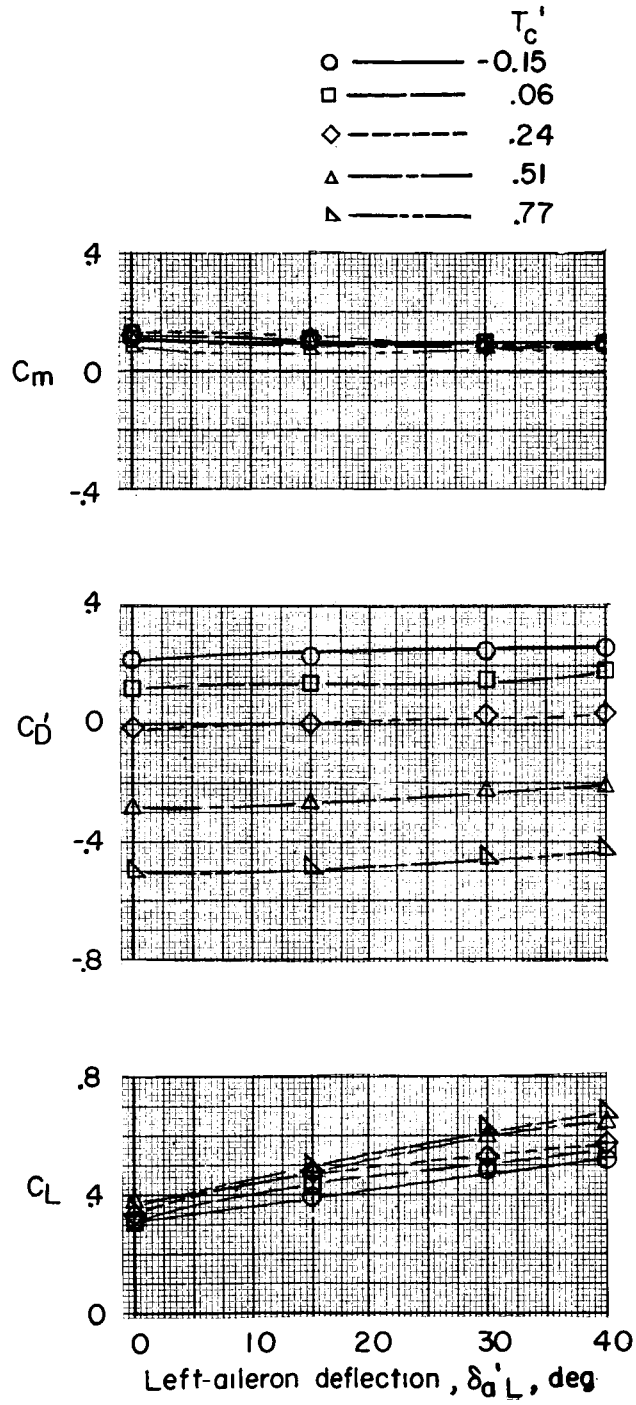

(a) $\alpha = 0^\circ$.

Figure 12.- Longitudinal effects of aileron control in normal forward flight. $i_w = 4.5^\circ$; short wing; $i_t = 0.6^\circ$; $\delta_e = \delta_{a'R} = 0$; $\beta_F = 30^\circ$.

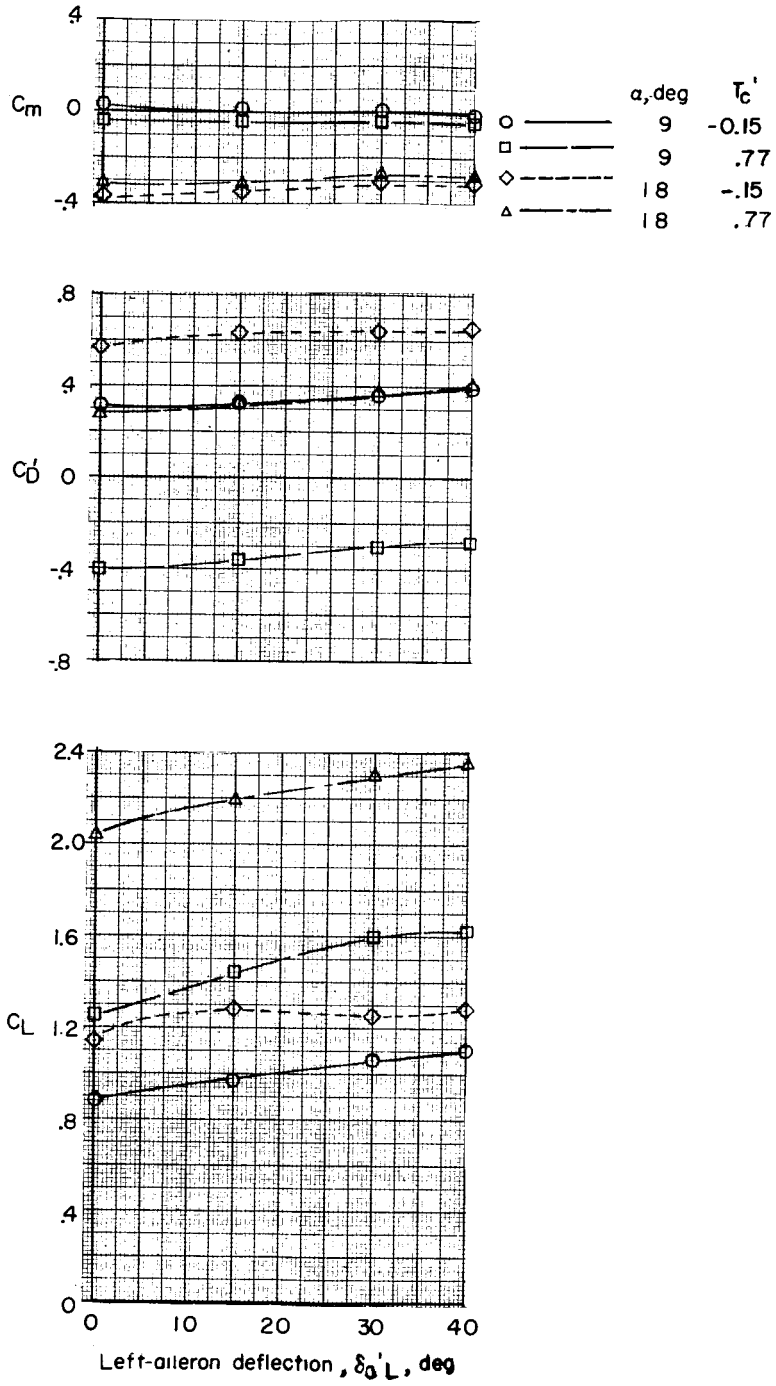

(b) $\alpha = 9^\circ$ or 18°.

Figure 12.- Concluded.

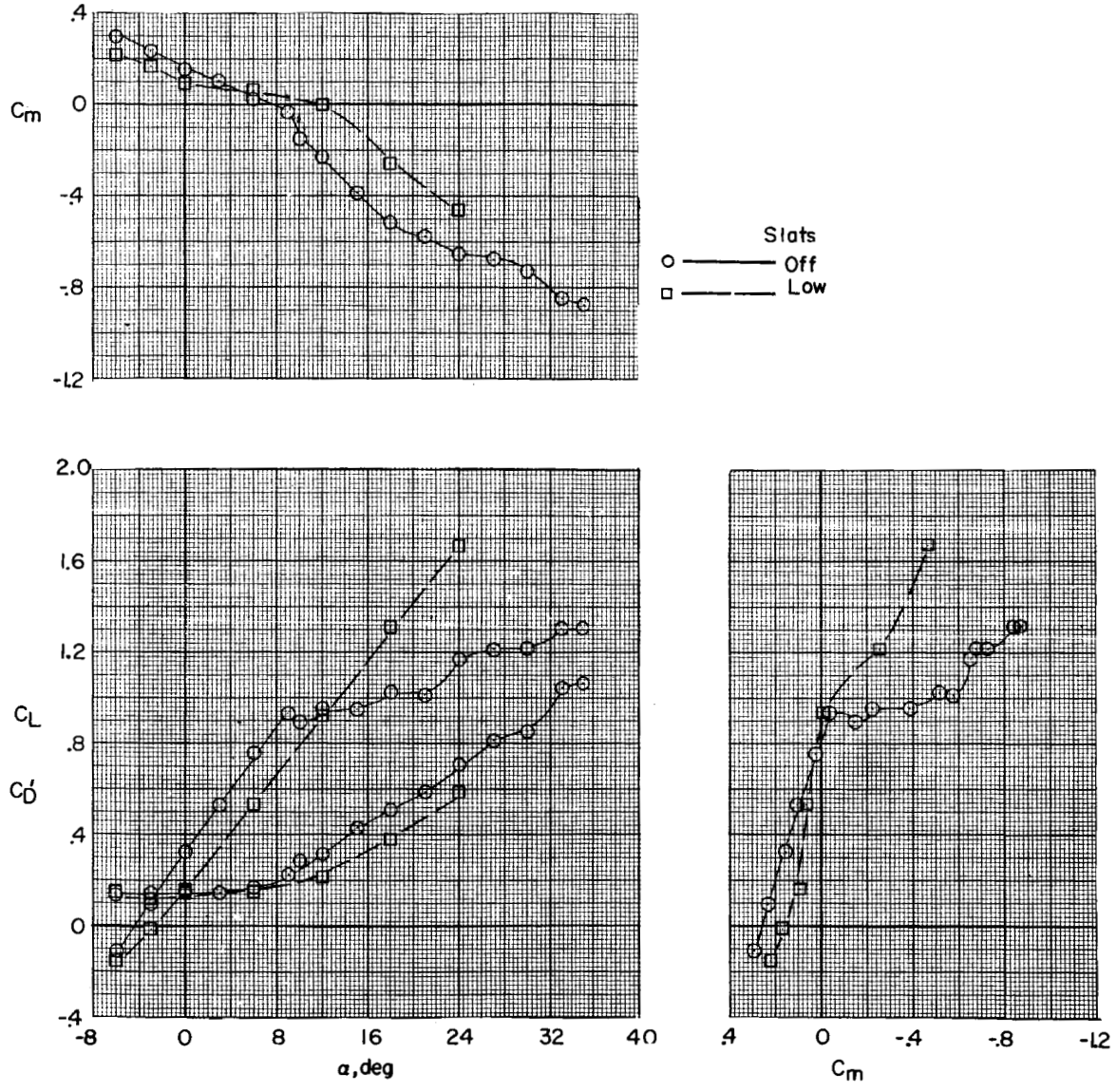

(a) Propellers off.

Figure 13.- Longitudinal effects of wing leading-edge slats in normal forward flight. $i_w = 4.5^\circ$; short wing; $i_t = 0.6^\circ$; $\delta_e = 0^\circ$.

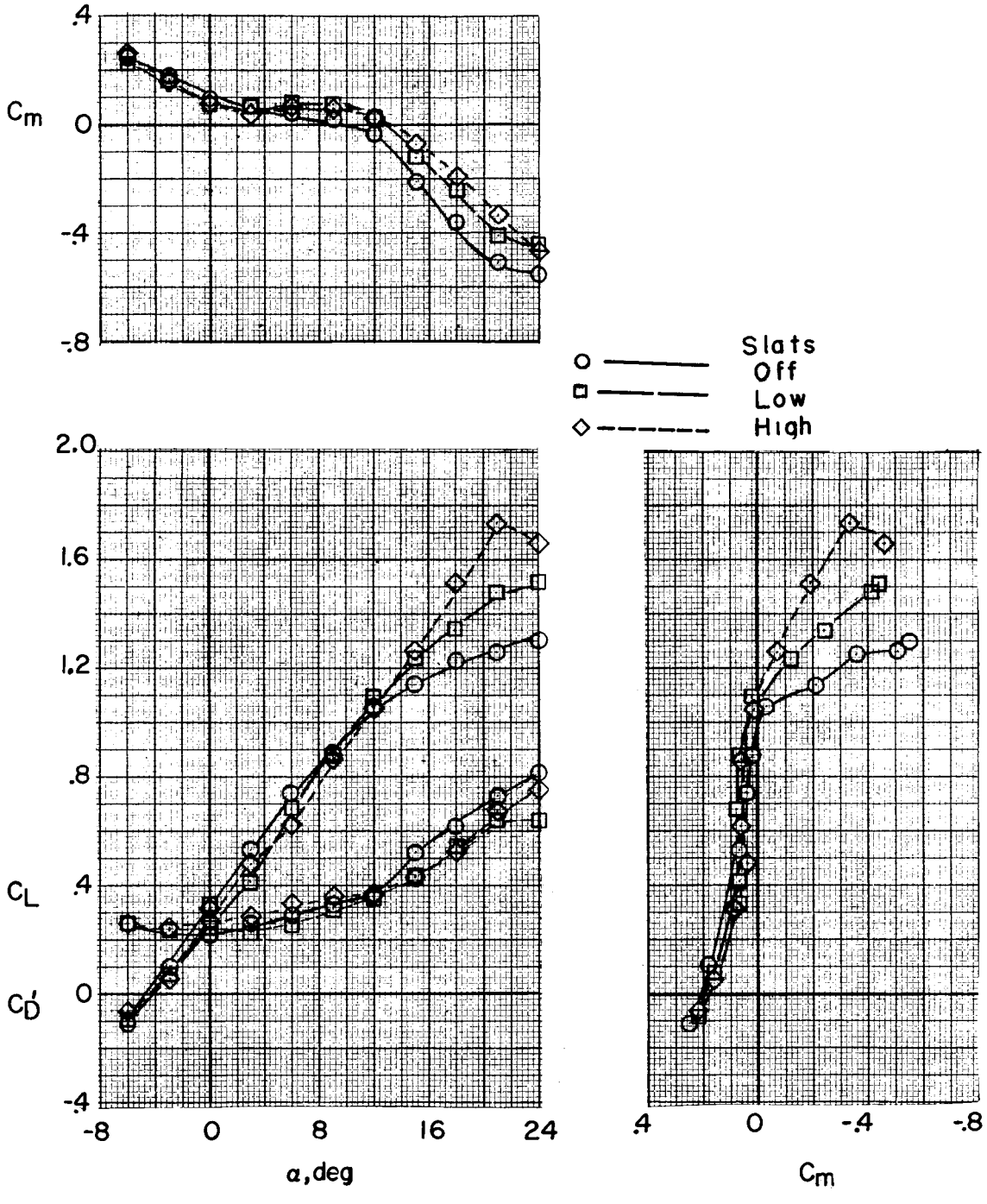

(b) $T_c' = -0.15$; $\beta_F = 30^\circ$.

Figure 13.- Continued.

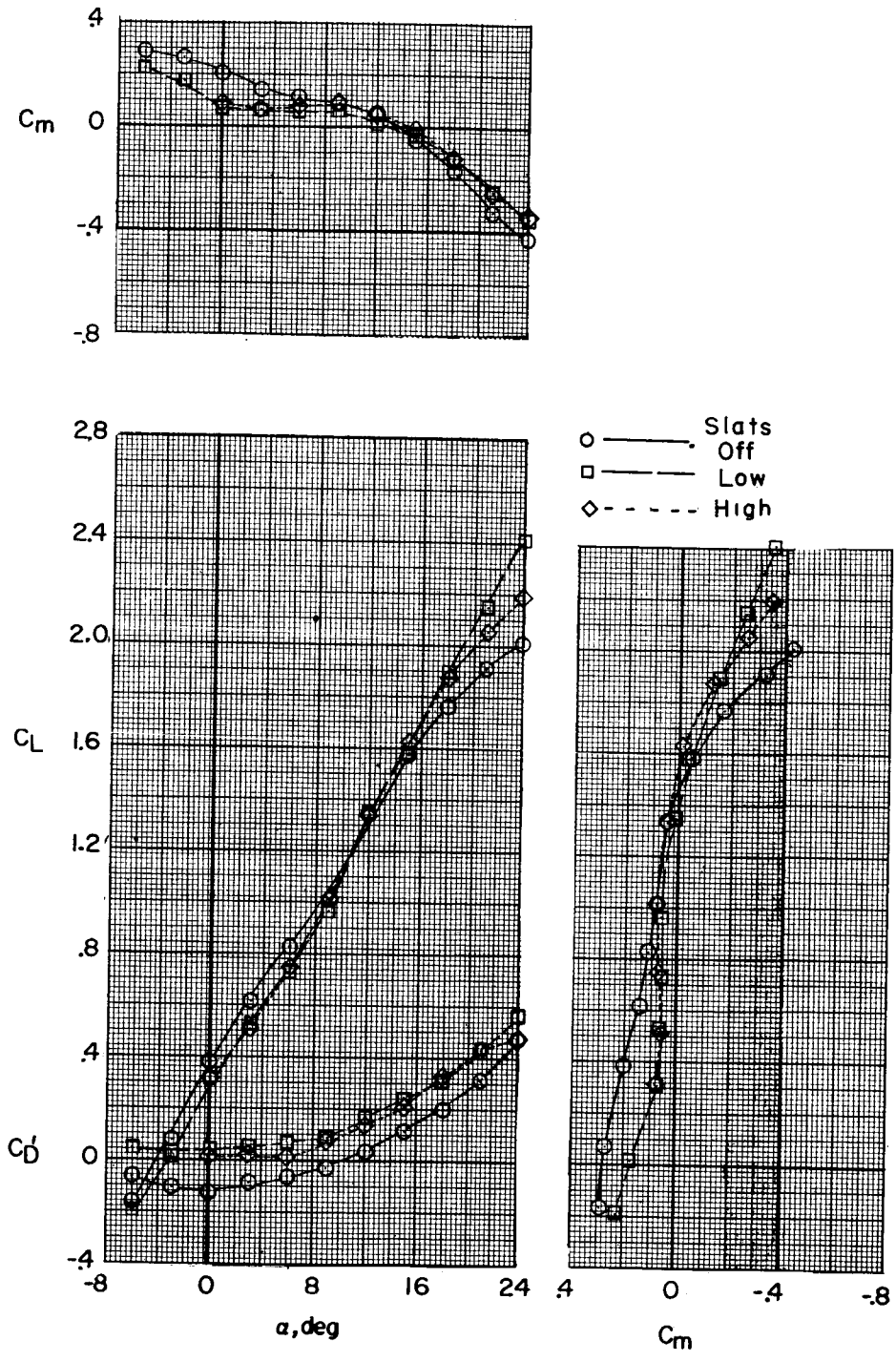

(c) $T_c' = 0.24$; $\beta_F = 30^\circ$.

Figure 13.- Continued.

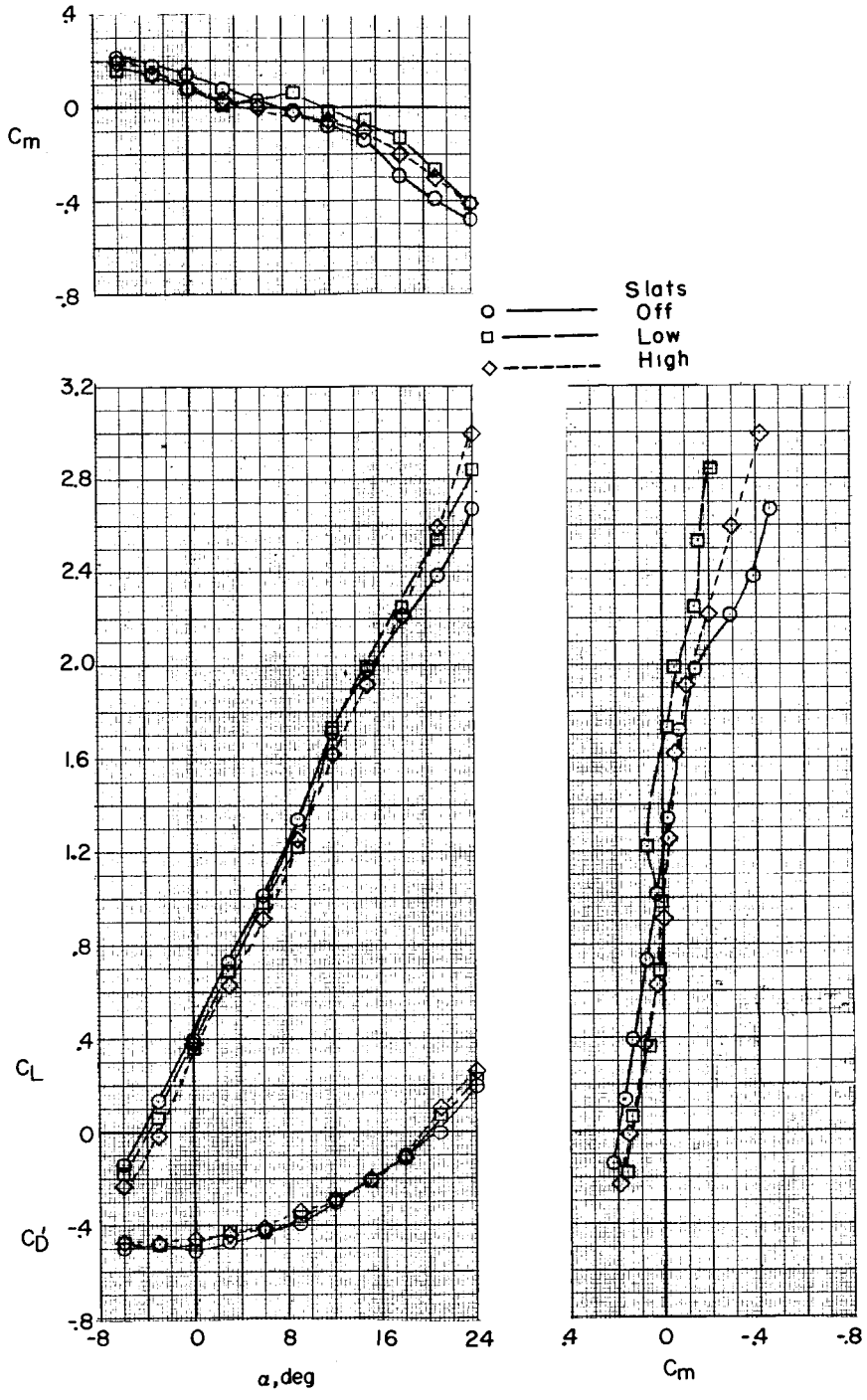

(d) $T_c' = 0.77$; $\beta_F = 30^\circ$.

Figure 13.- Concluded.

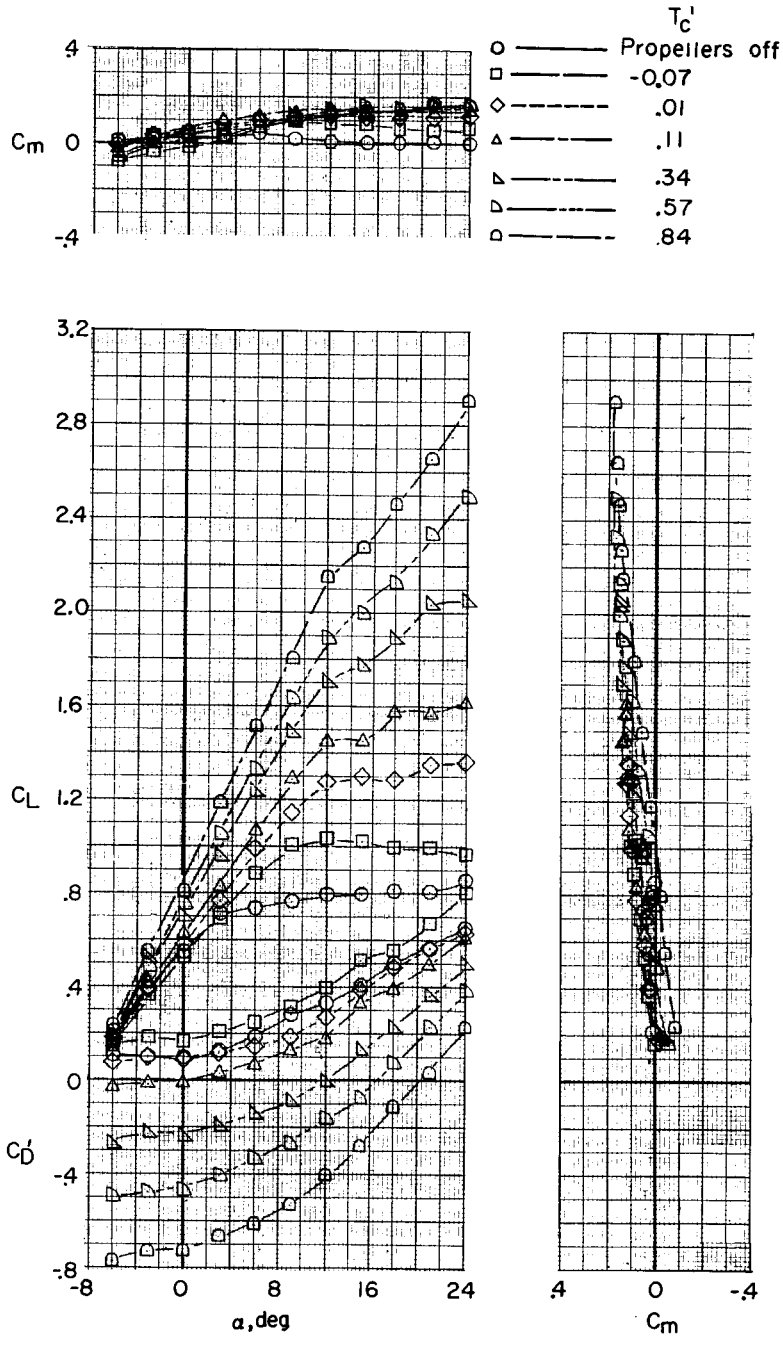

(a) Tails off.

Figure 14.- Longitudinal stability characteristics of long-wing configuration at various thrust coefficients. $i_w = 4.5^\circ$; $\beta_F = 30^\circ$.

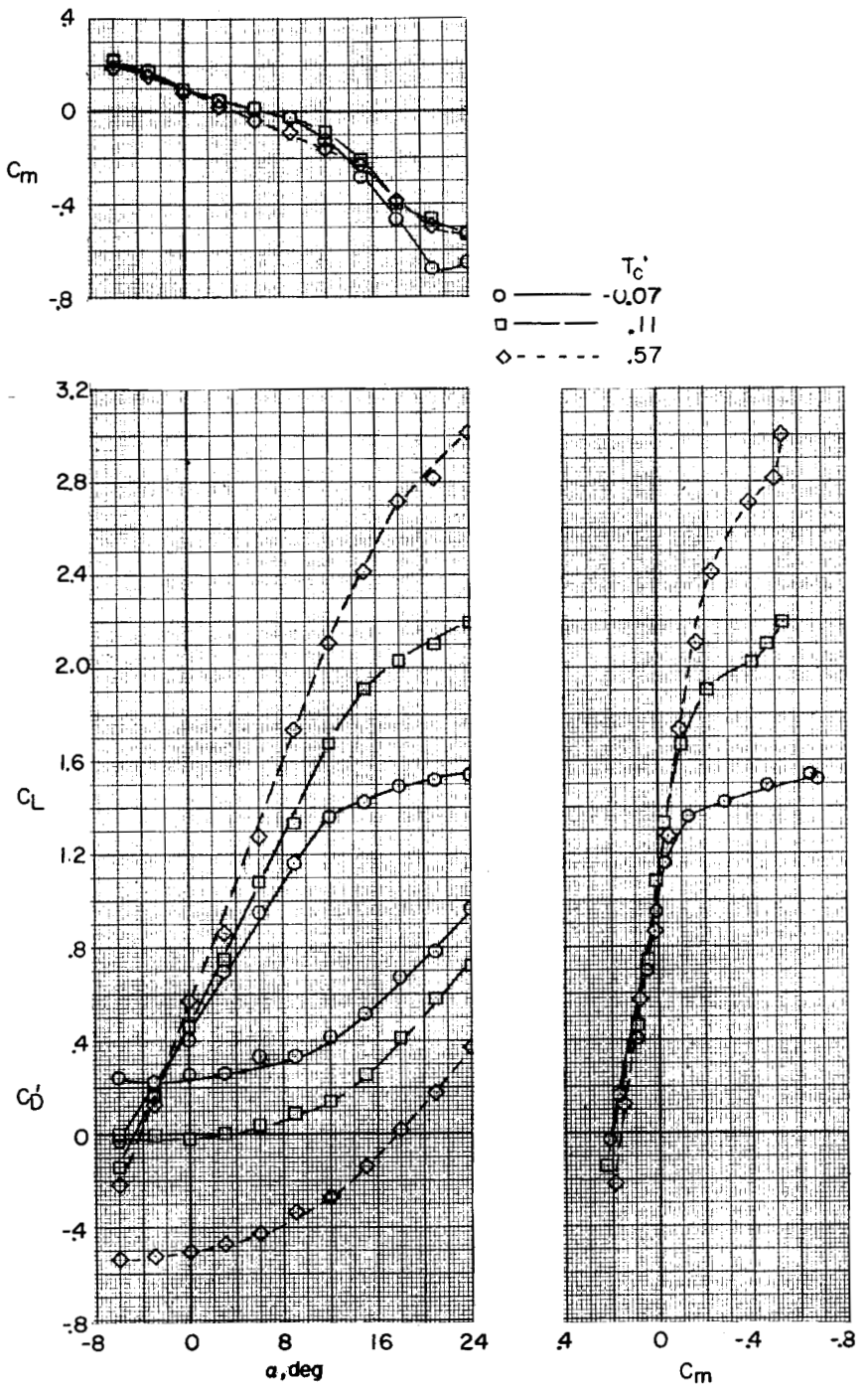

(b) Complete model. $i_t = 0.6^\circ$; $\delta_e = 0^\circ$.

Figure 14.- Concluded.

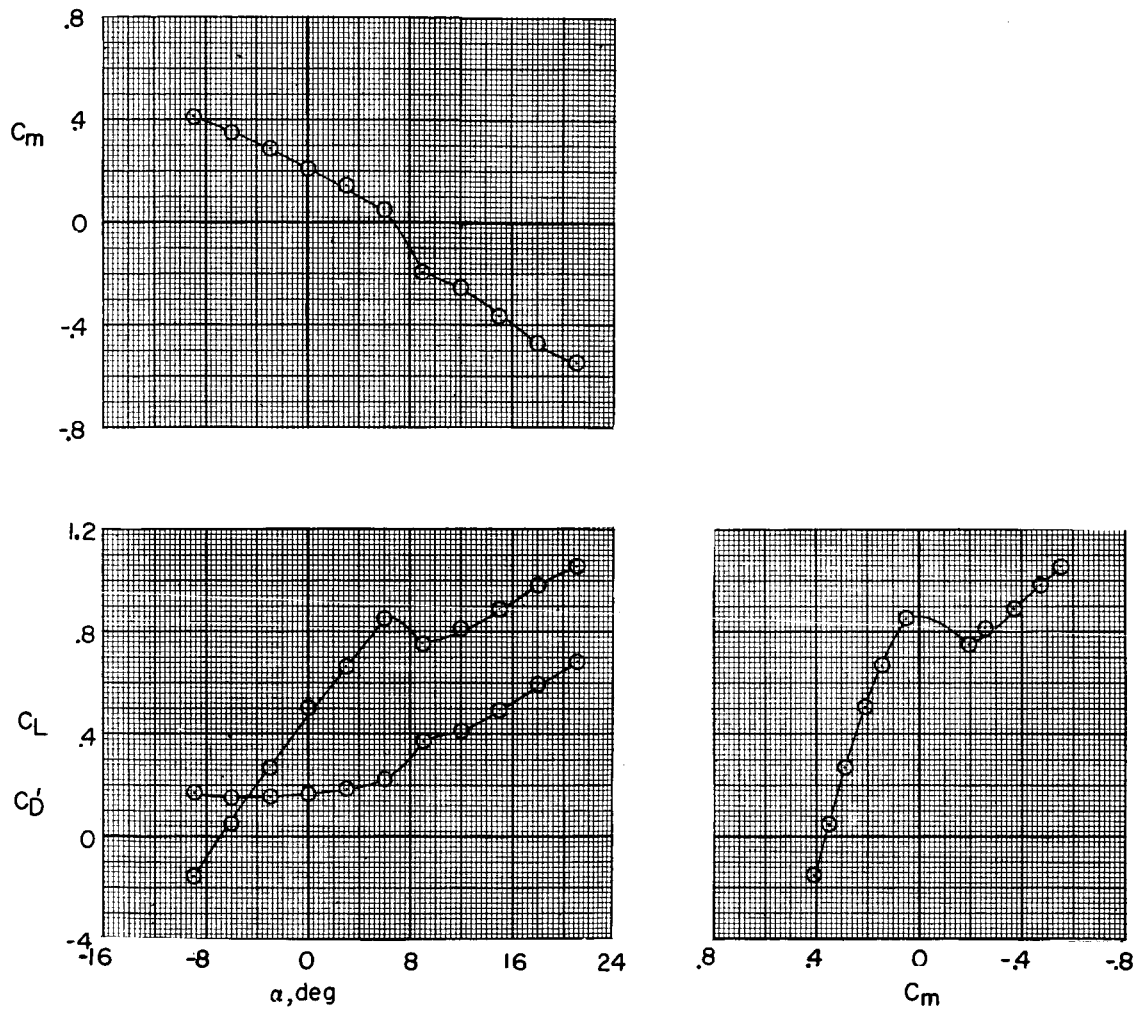

(a) Propellers off.

Figure 15.- Longitudinal stability and control characteristics in normal forward flight for various thrust coefficients and elevator positions. $i_w = 10^\circ$; short wing; $i_t = 0.6^\circ$; $\beta_F = 30^\circ$.

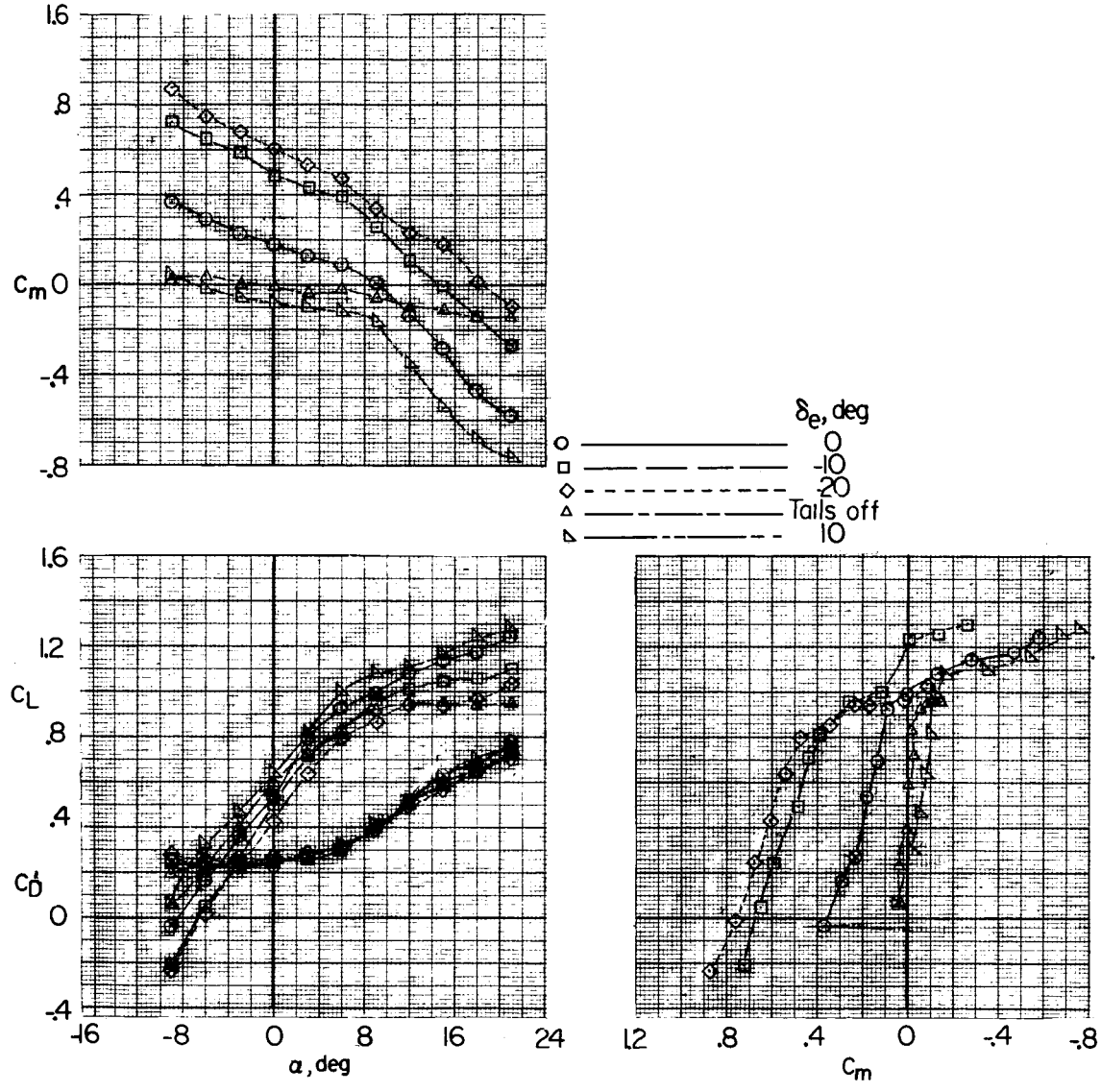

(b) $T_c' = -0.15$.

Figure 15.- Continued.

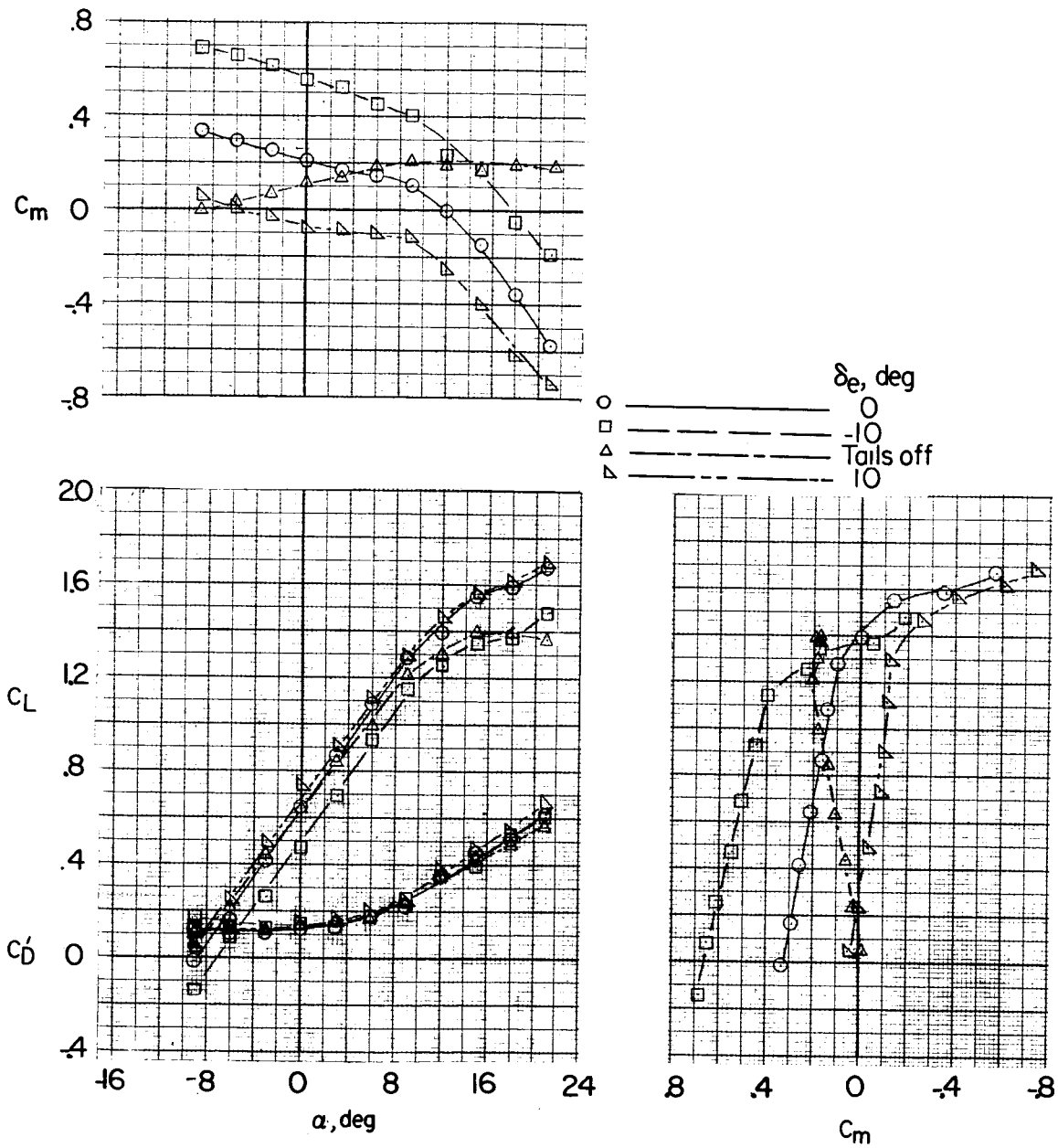

(c) $T_c' = 0.06$.

Figure 15.- Continued.

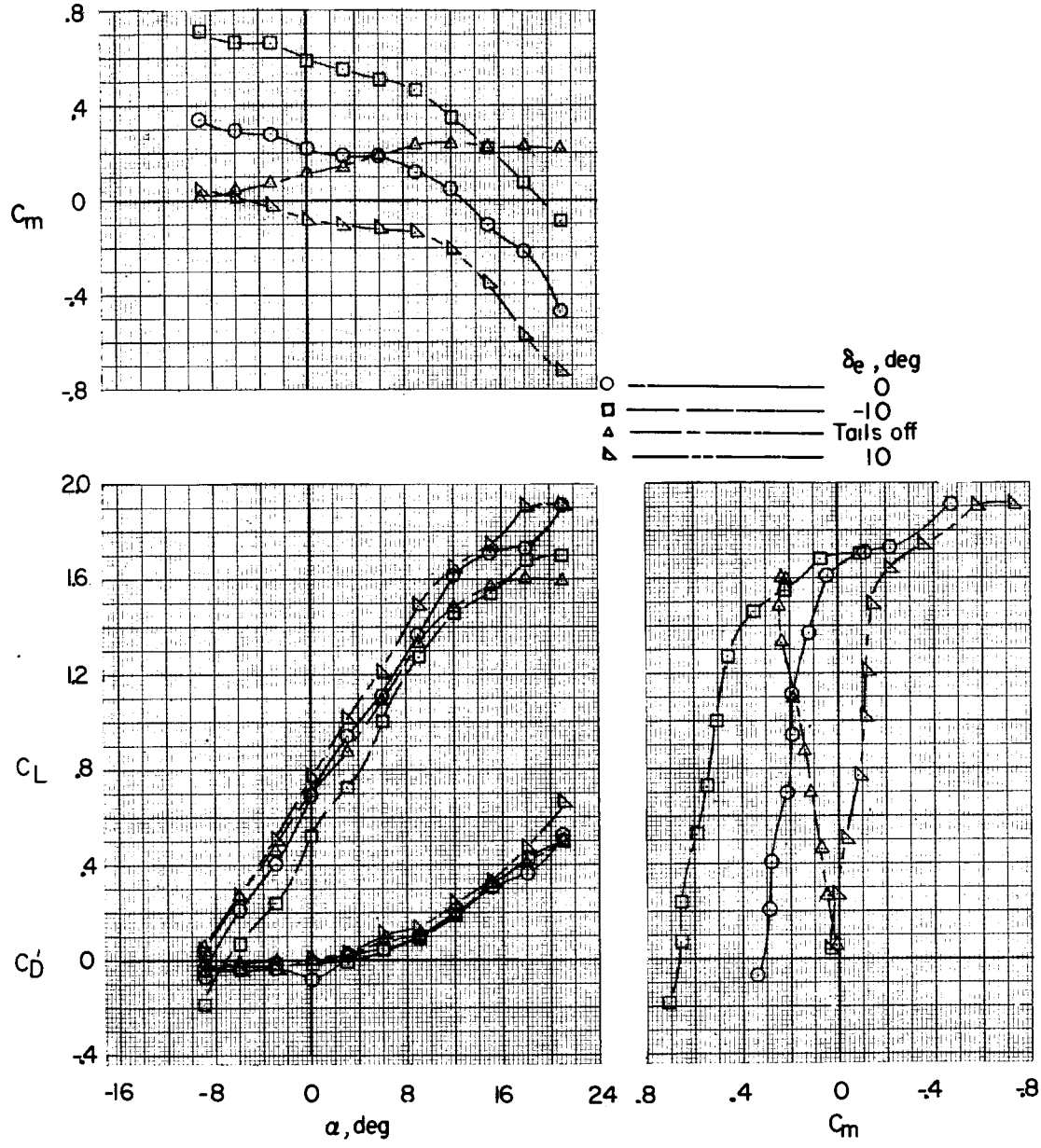

(d) $T_c' = 0.24$.

Figure 15.- Continued.

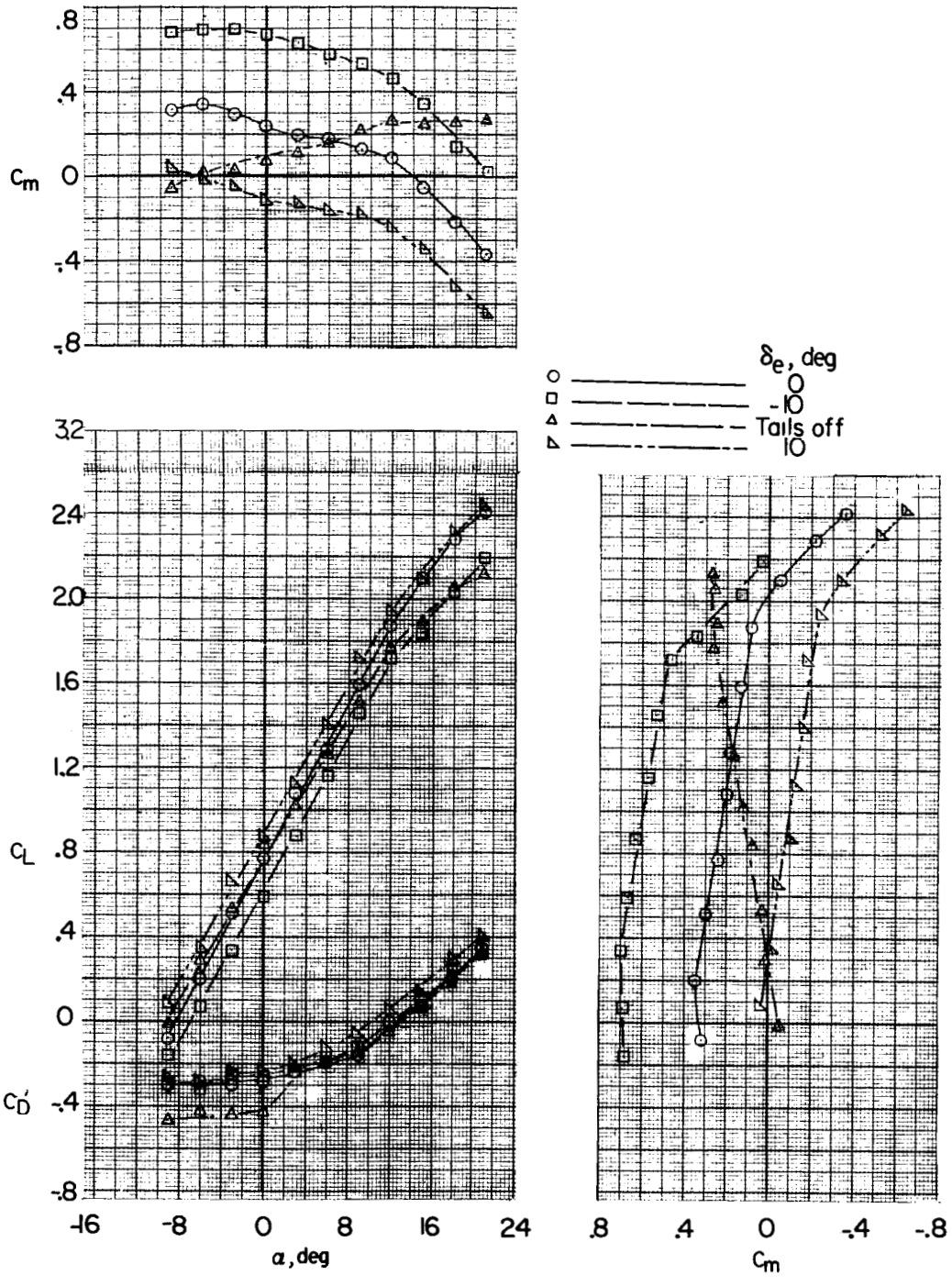

(e) $T_c' = 0.51$.

Figure 15.- Continued.

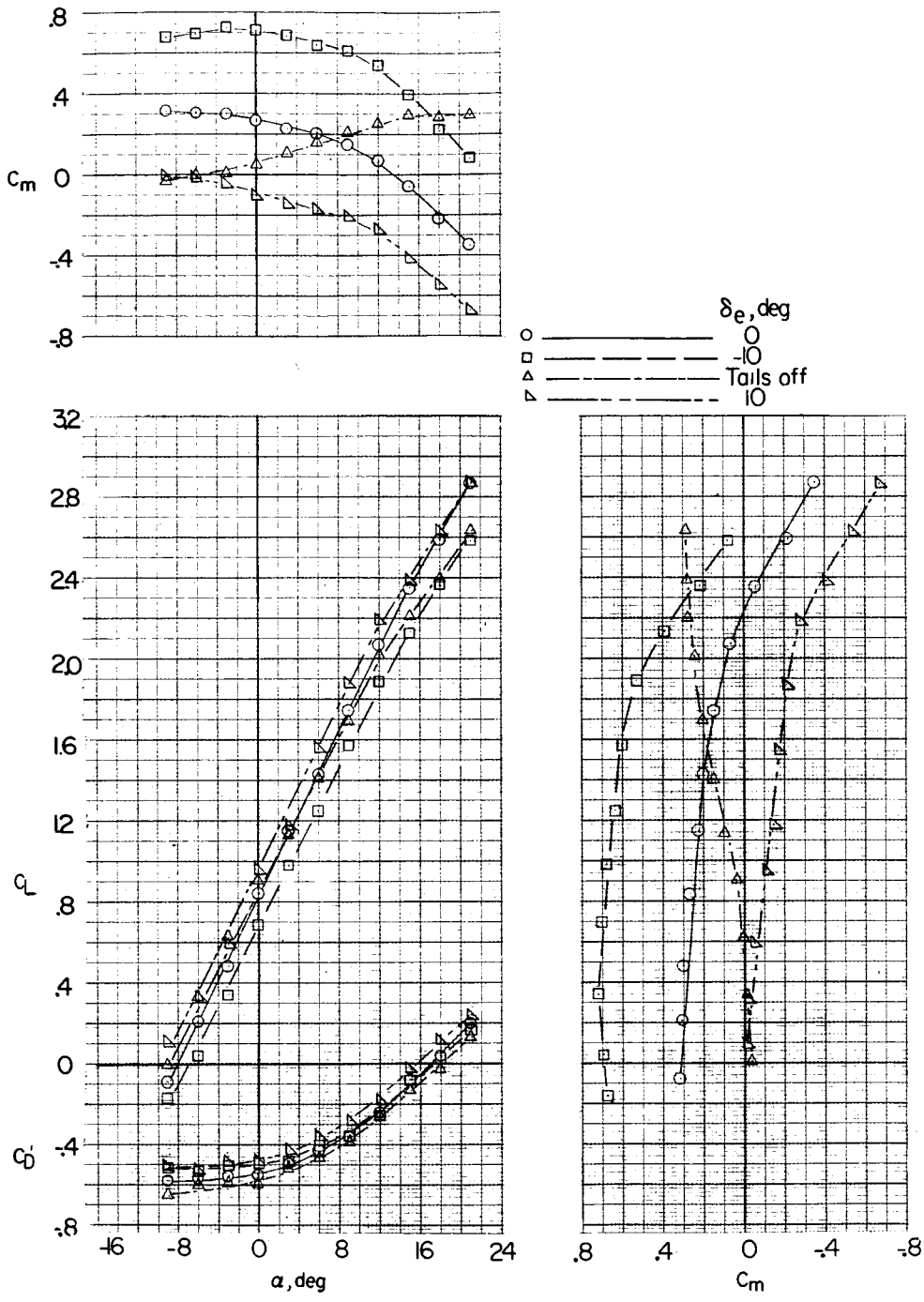

(f) $T_c' = 0.77$.

Figure 15.- Continued.

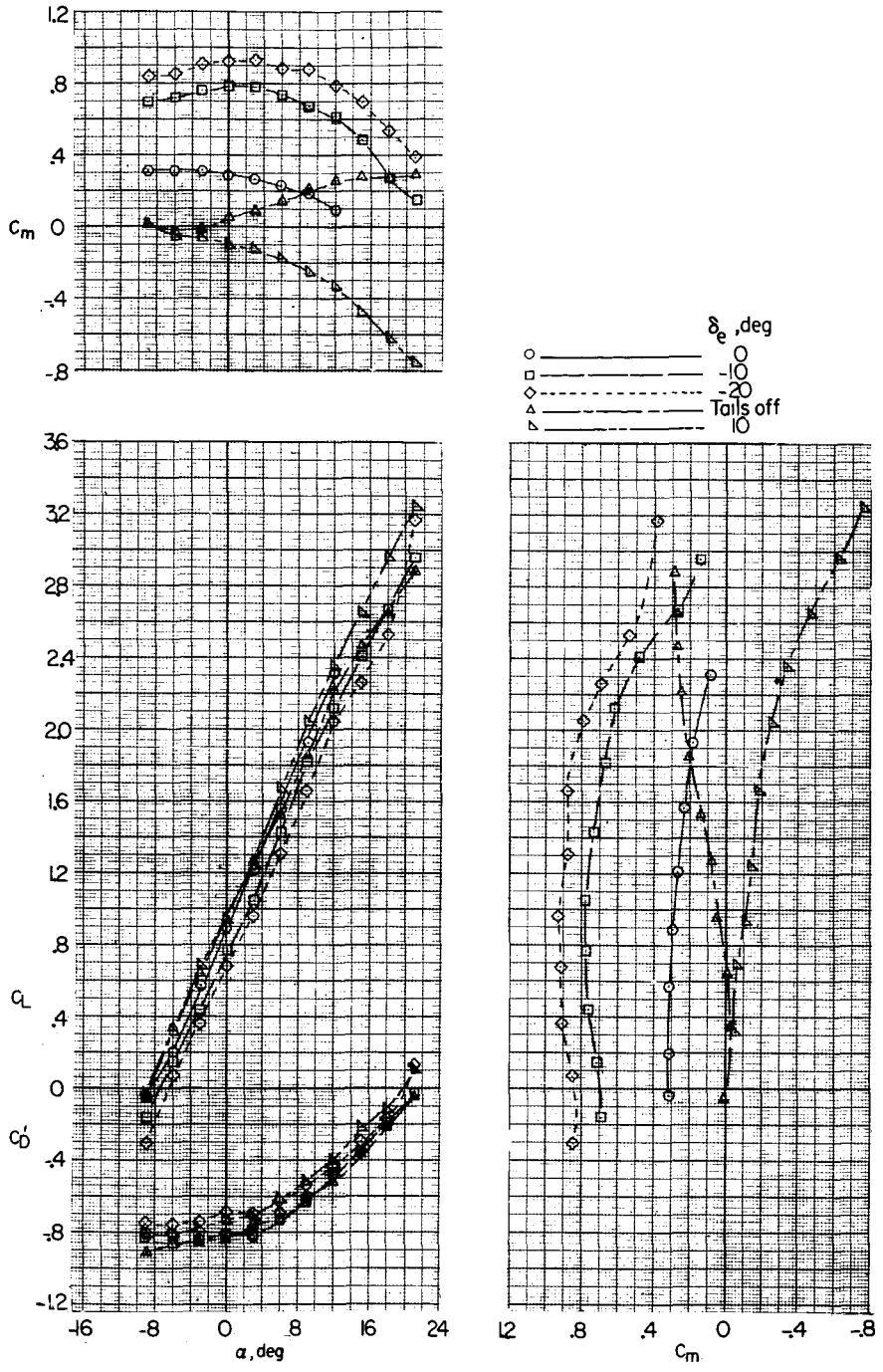

(g) $T_c' = 1.08$.

Figure 15.- Concluded.

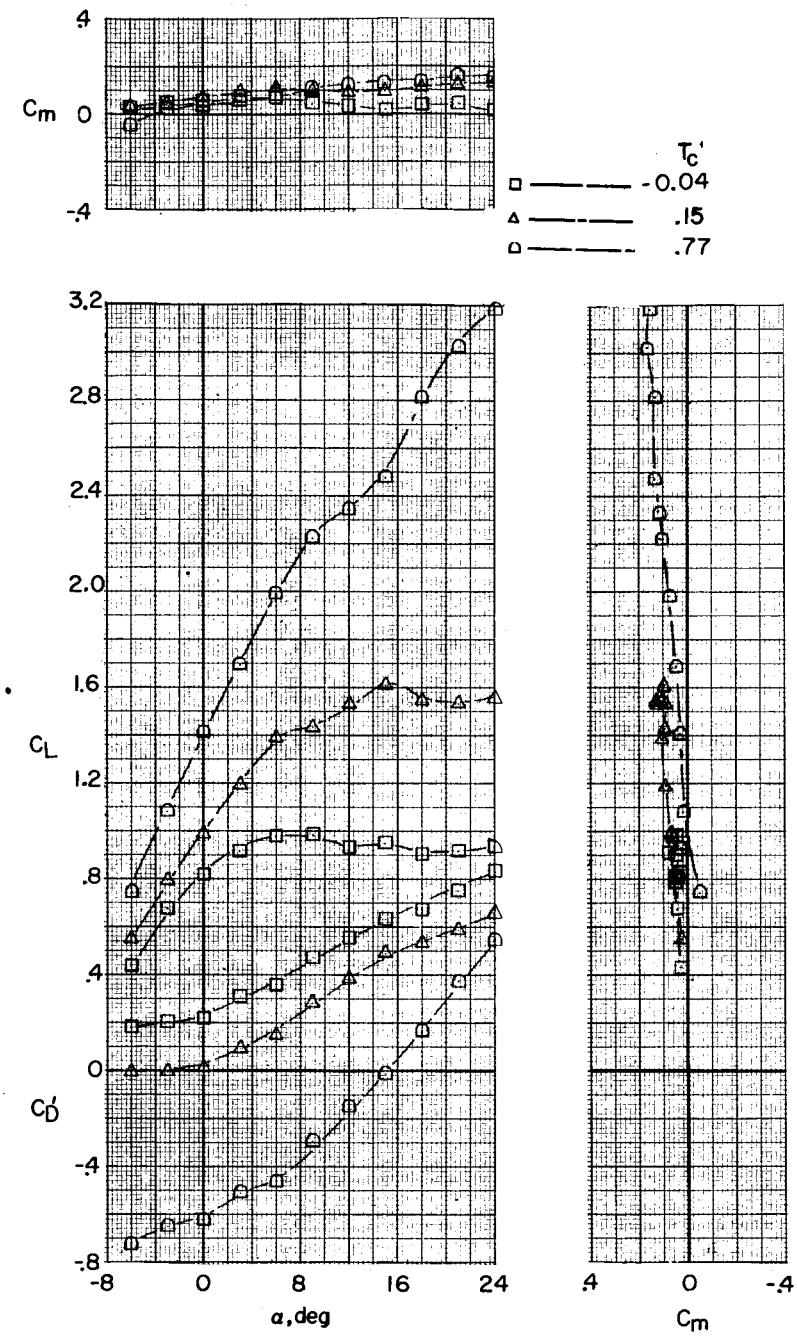

(a) Tails off.

Figure 16.- Longitudinal stability and control characteristics of long-wing configuration in normal forward flight at various thrust coefficients. $i_w = 10^\circ$; $\beta_F = 30^\circ$.

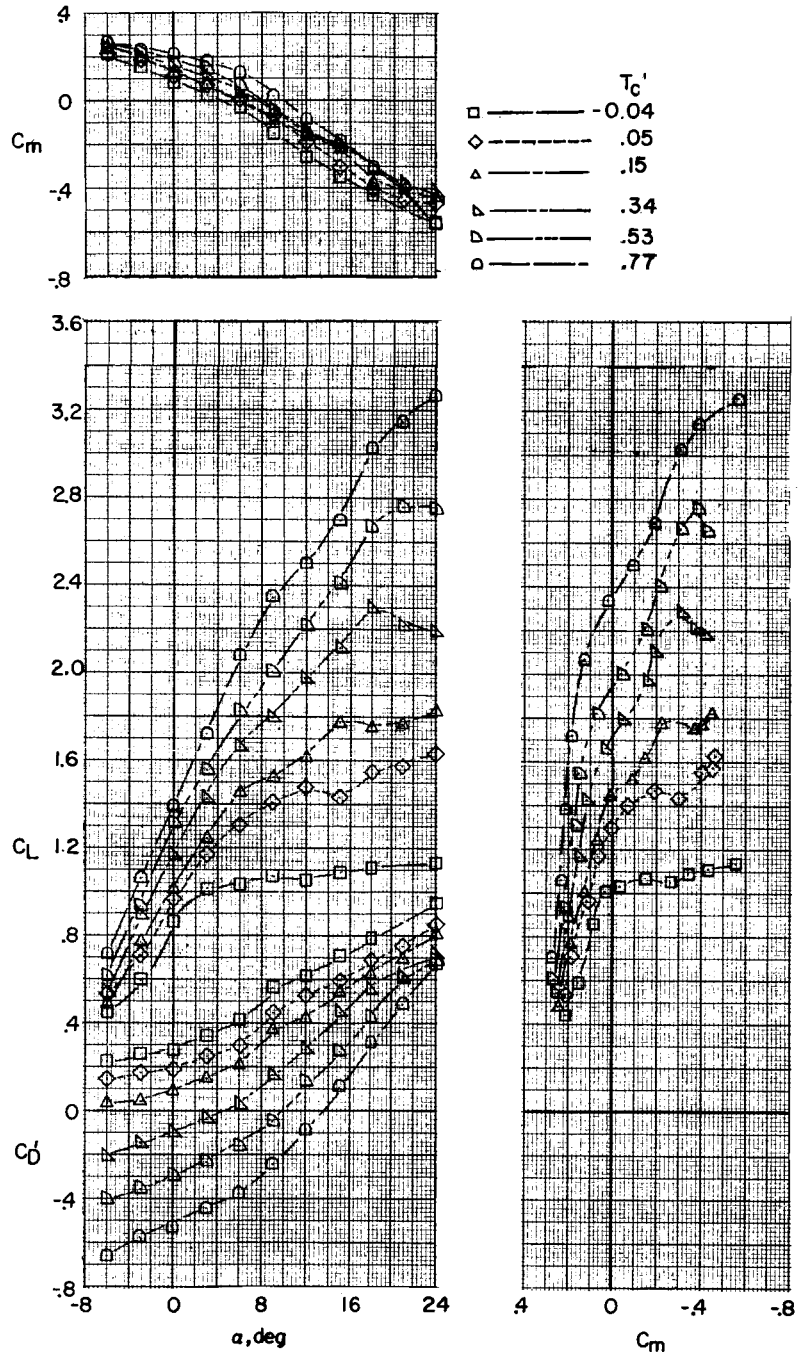

(b) $\delta_e = 0^\circ$; $i_t = 0.6^\circ$.

Figure 16.- Continued.

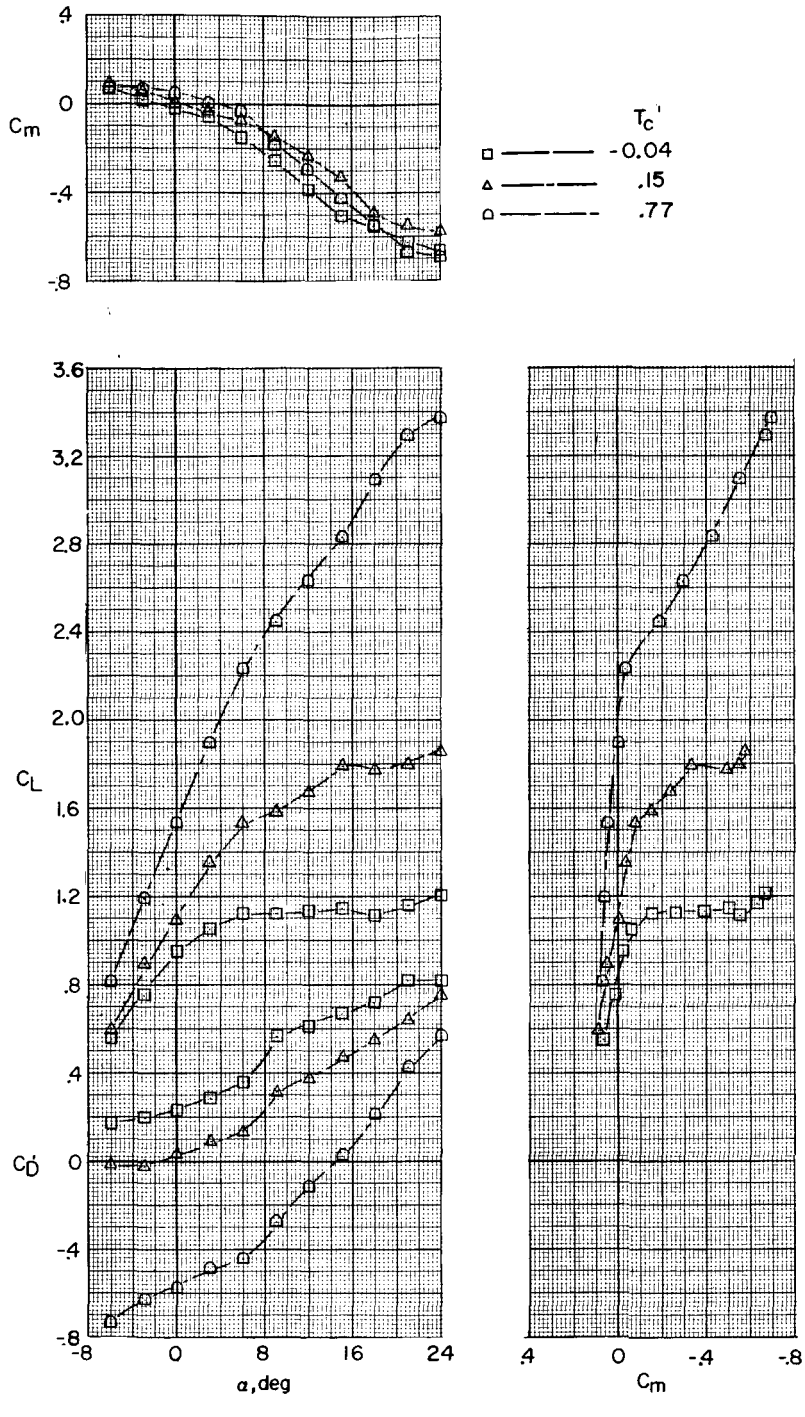

(c) $\delta_e = 10^\circ$; $i_t = 0.6^\circ$.

Figure 16.- Continued.

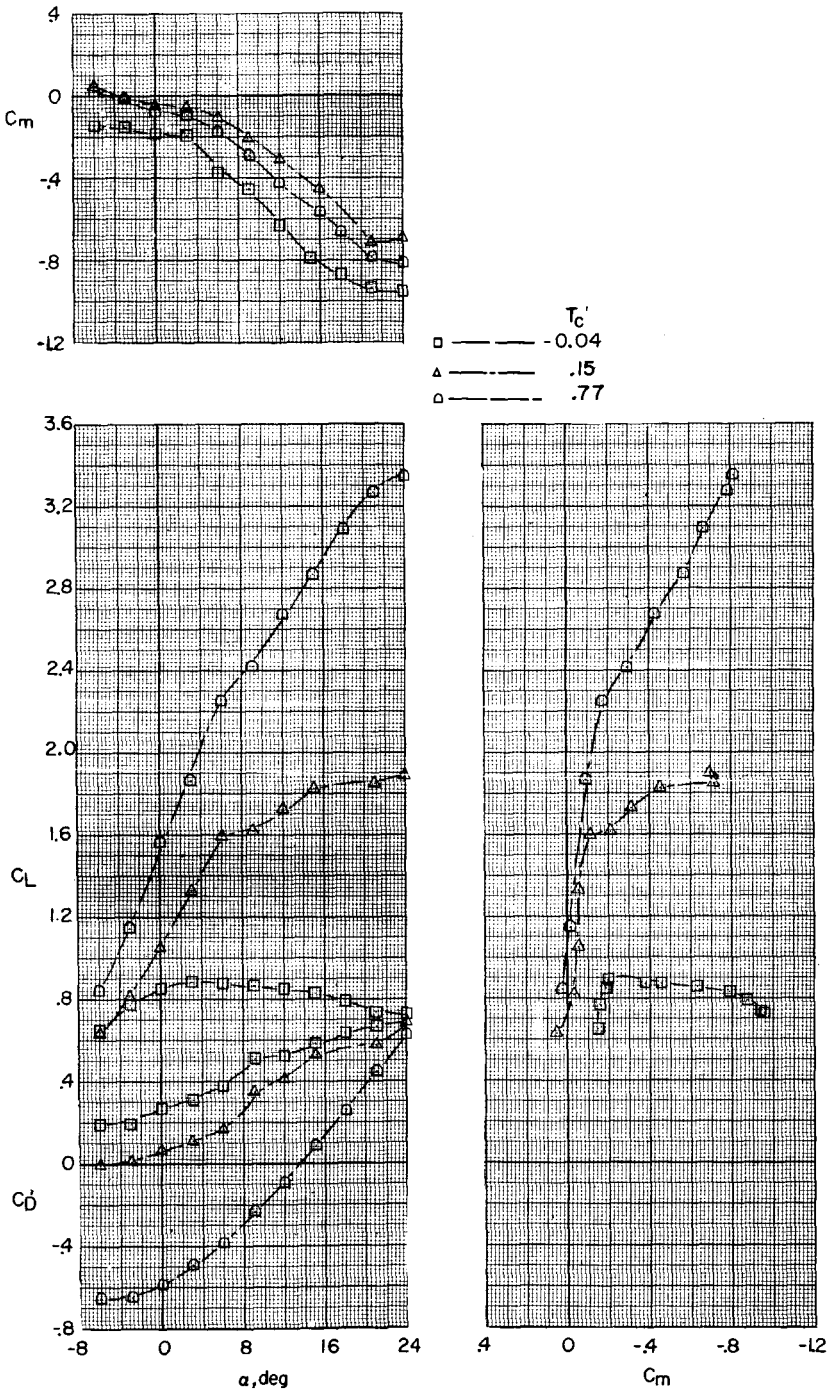

(d) $\delta_e = 20^\circ$; $i_t = 0.6^\circ$.

Figure 16.- Continued.

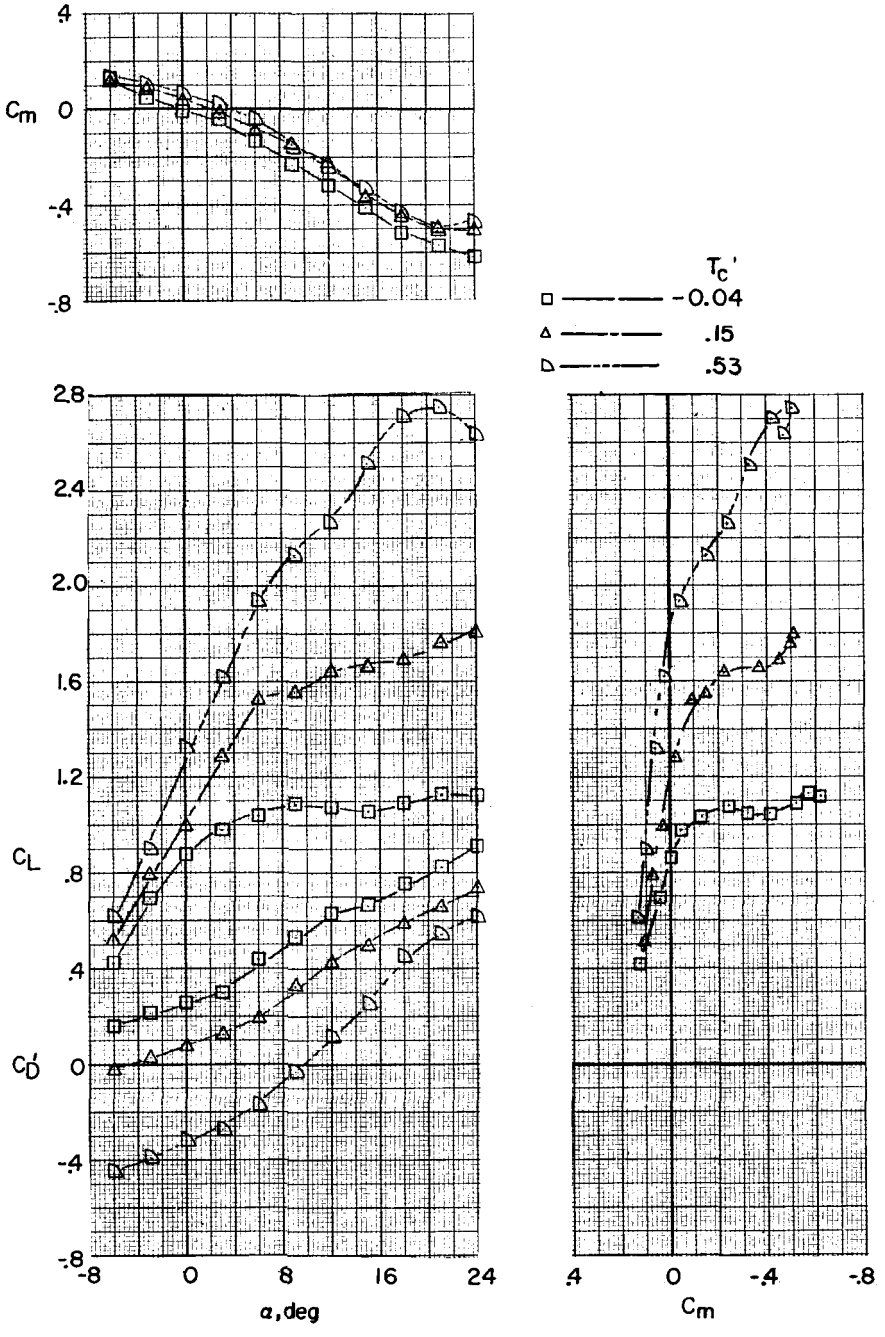

(e) $\delta_e = 0^\circ$; $i_t = 5^\circ$.

Figure 16.- Continued.

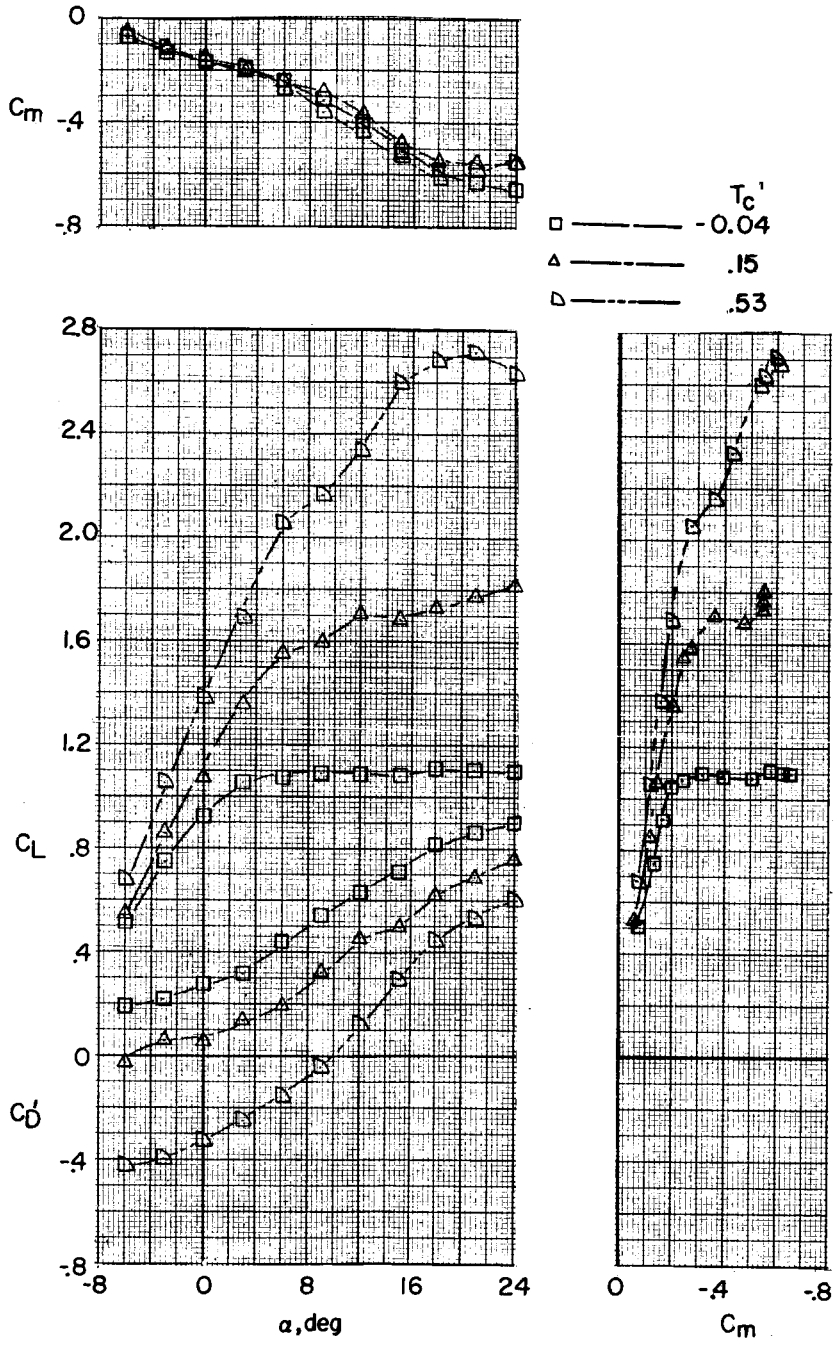

(f) $\delta_e = 0^\circ$; $i_t = 10^\circ$.

Figure 16.- Continued.

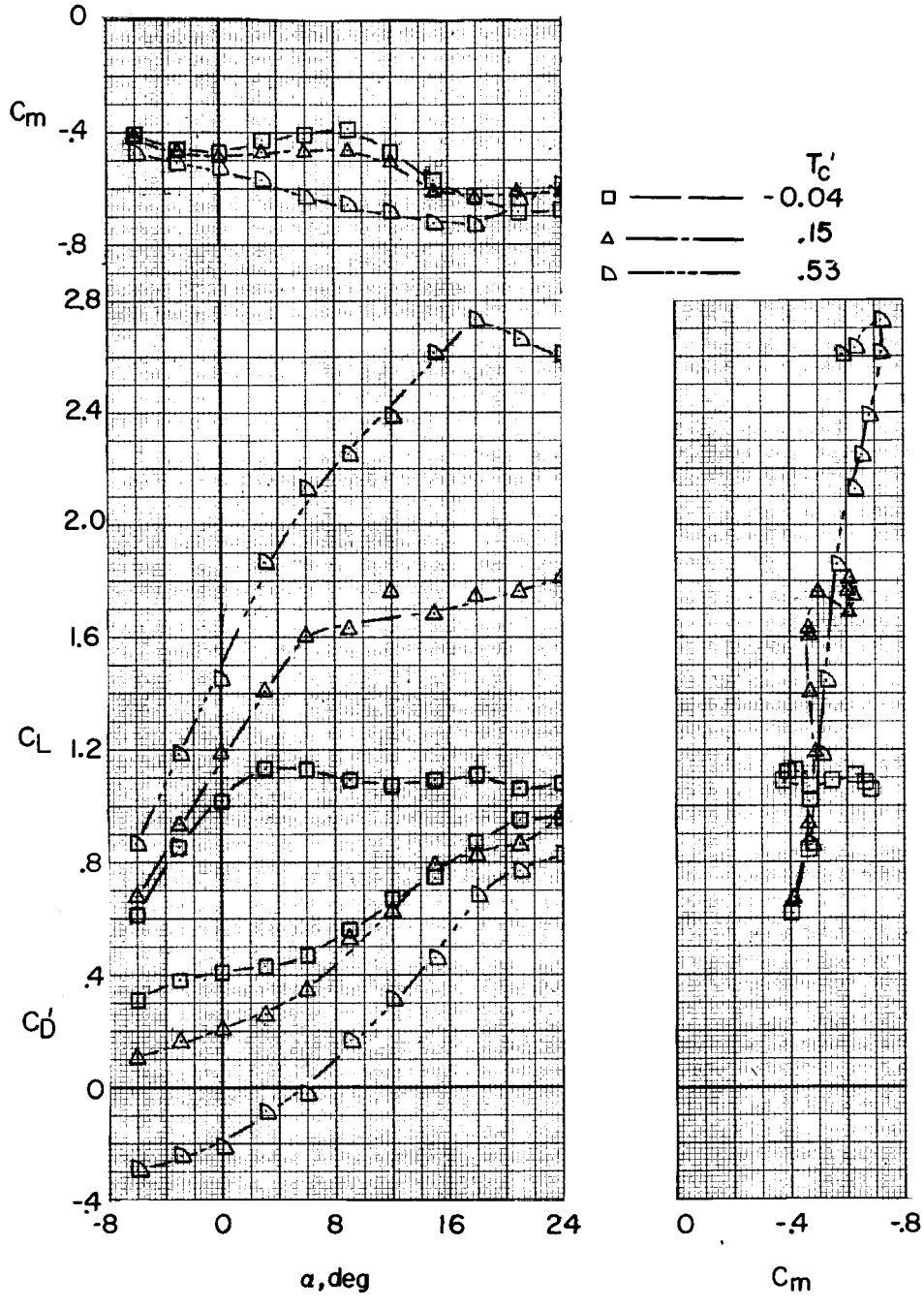

(g) $\delta_e = 0^\circ$; $i_t = 20^\circ$.

Figure 16.- Concluded.

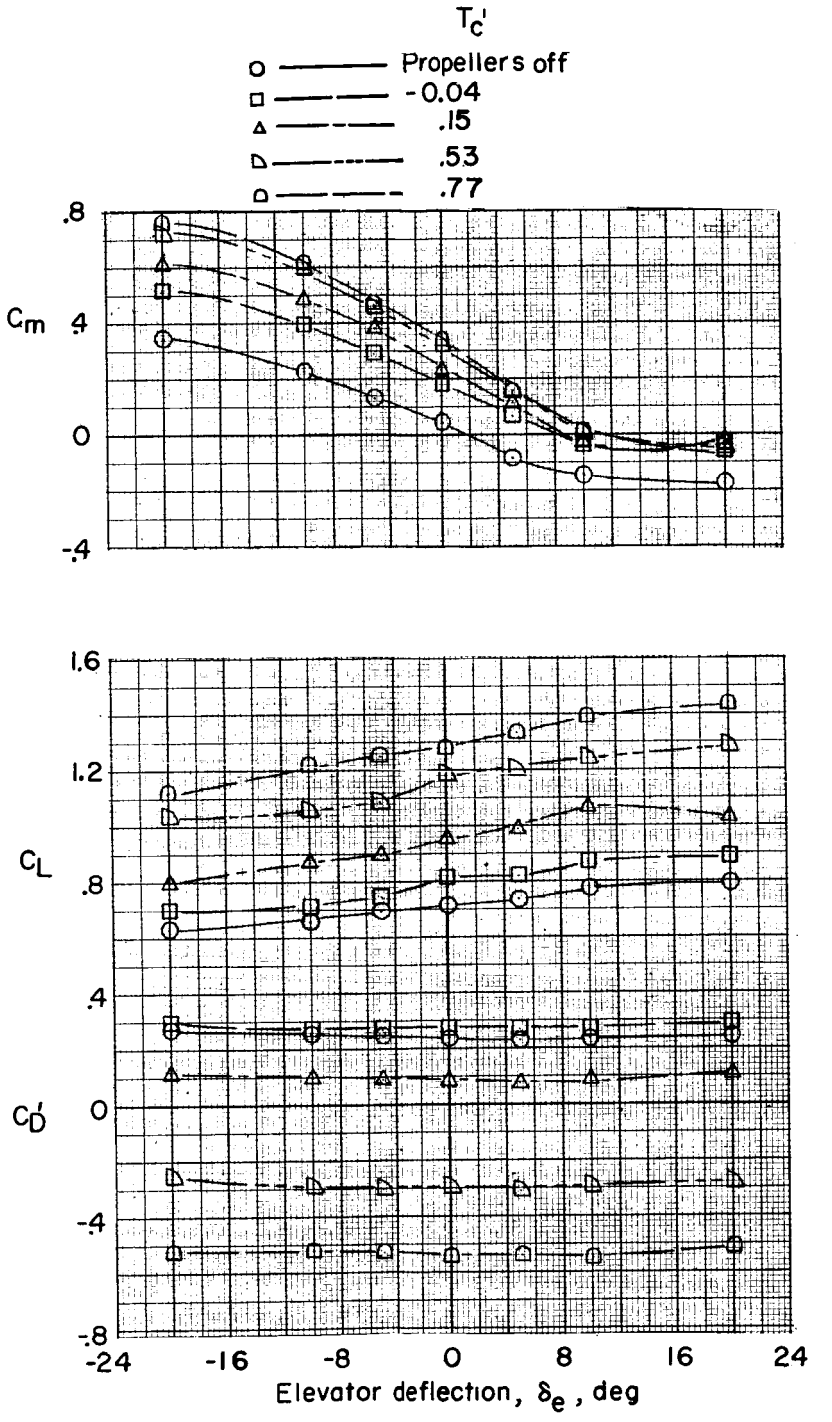

Figure 17.- Elevator effectiveness of long-wing configuration at various thrust coefficients. $i_w = 10^\circ$; $\alpha = 0^\circ$; $i_t = 0.6^\circ$; $\beta_F = 30^\circ$.

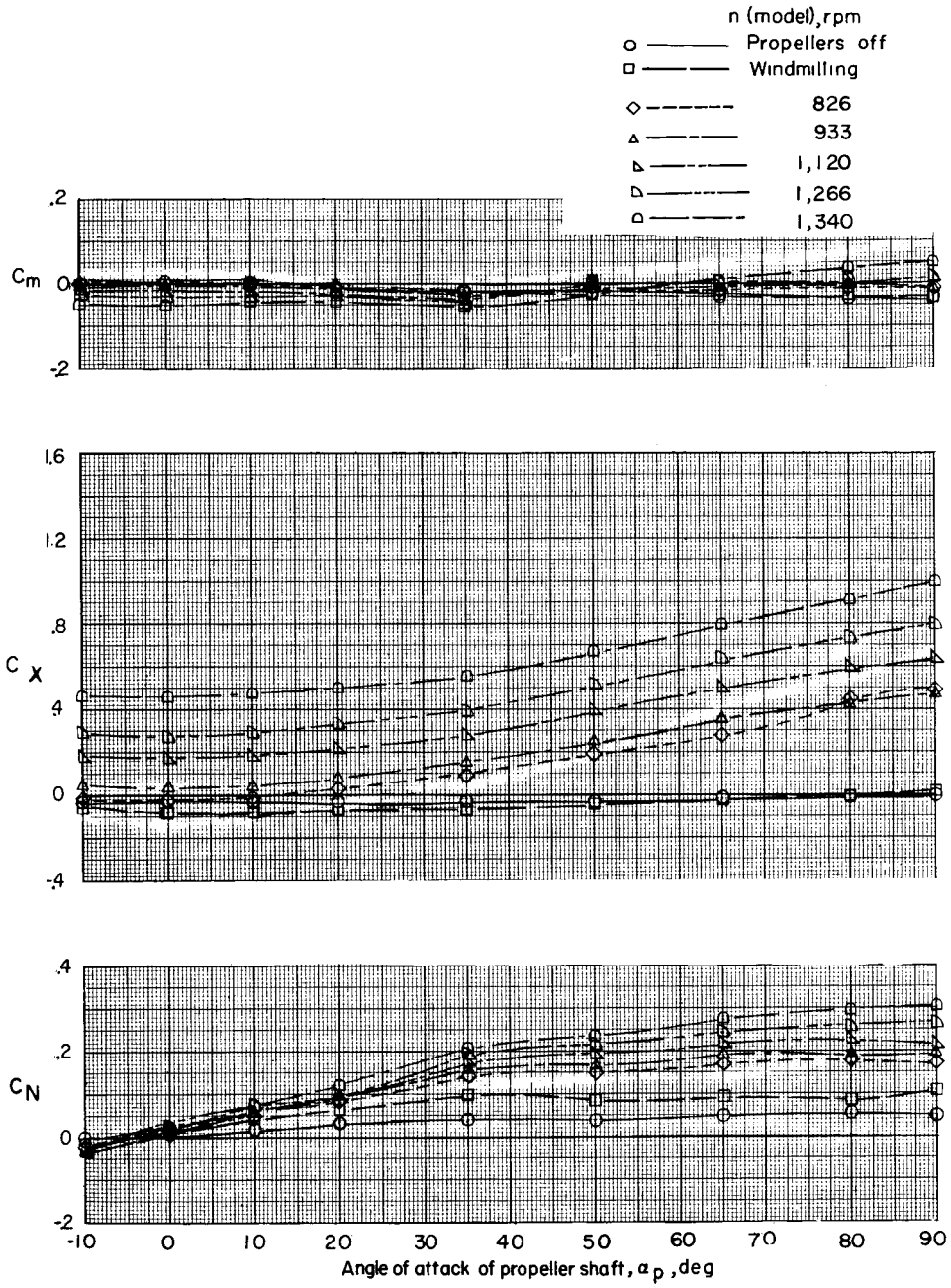

(a) $\beta_F = 30^\circ$.

Figure 18.- Longitudinal aerodynamic characteristics of one set of propellers alone at two blade angles and various propeller speeds and angles of attack. V_a = 22 knots.

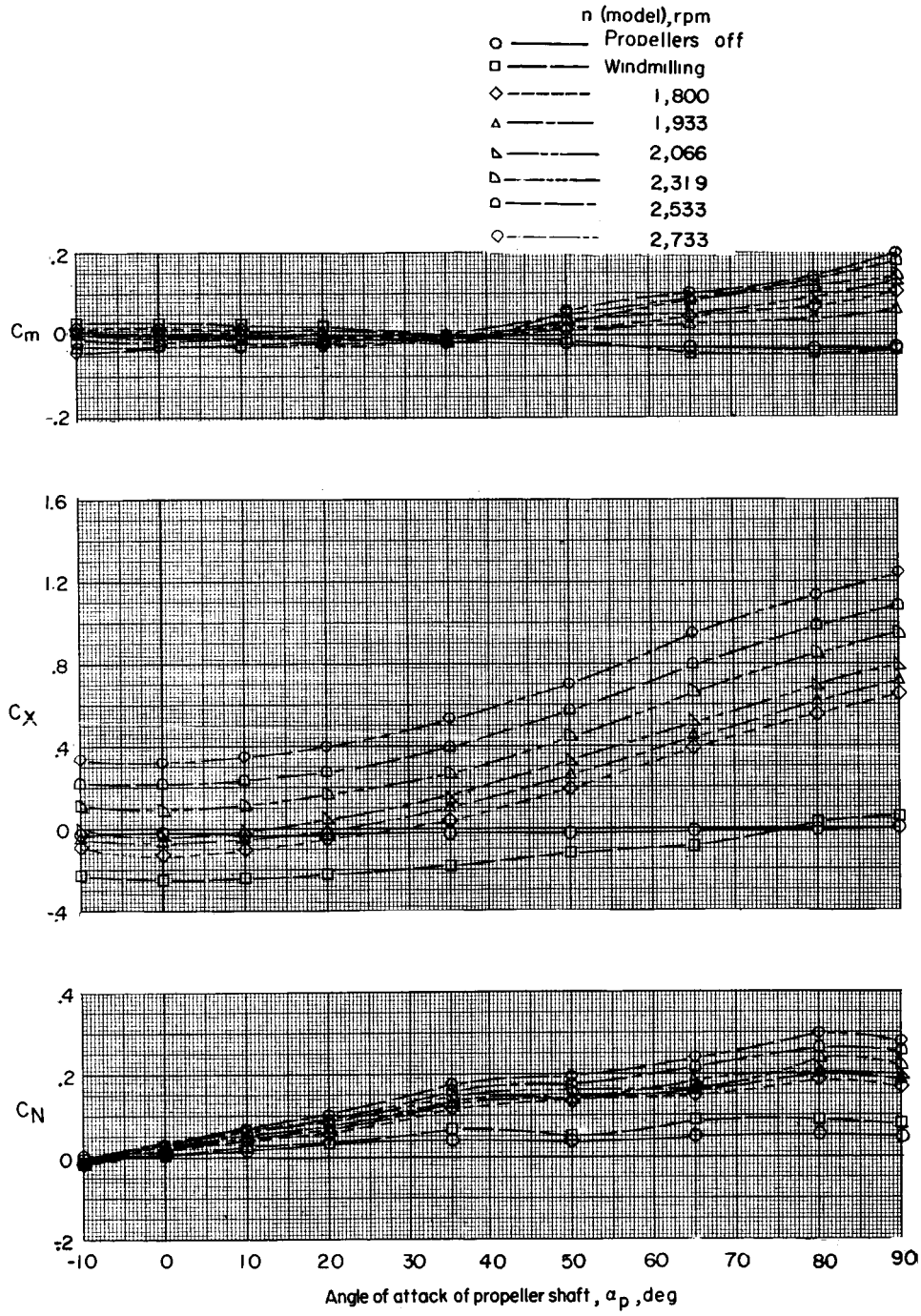

(b) $\beta_F = 10^\circ$.

Figure 18.- Concluded.

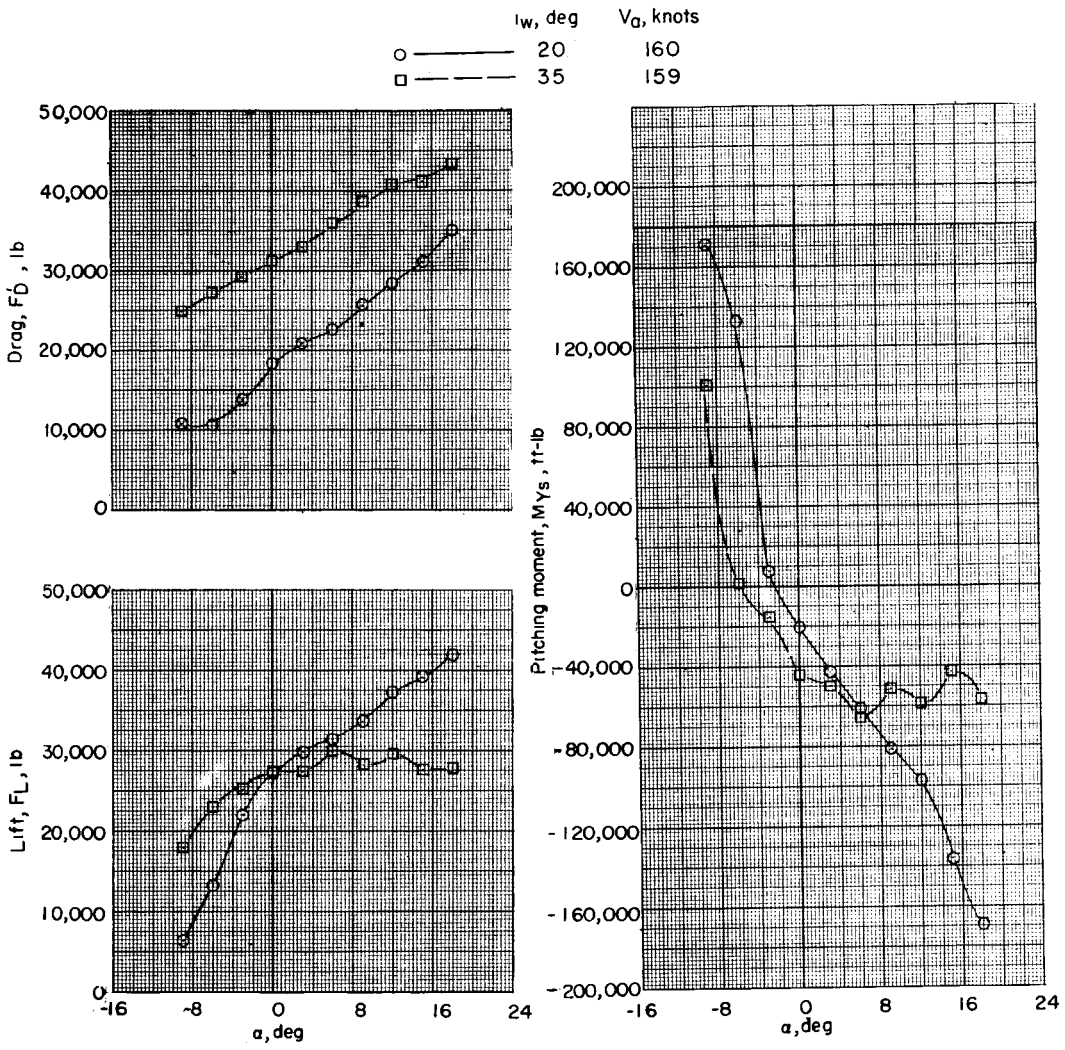

Figure 19.- Longitudinal stability characteristics in transition flight at wing incidences of 20° and 35°. Short wing; $i_t = 0.6°$; $\delta_e = 0°$; propellers off.

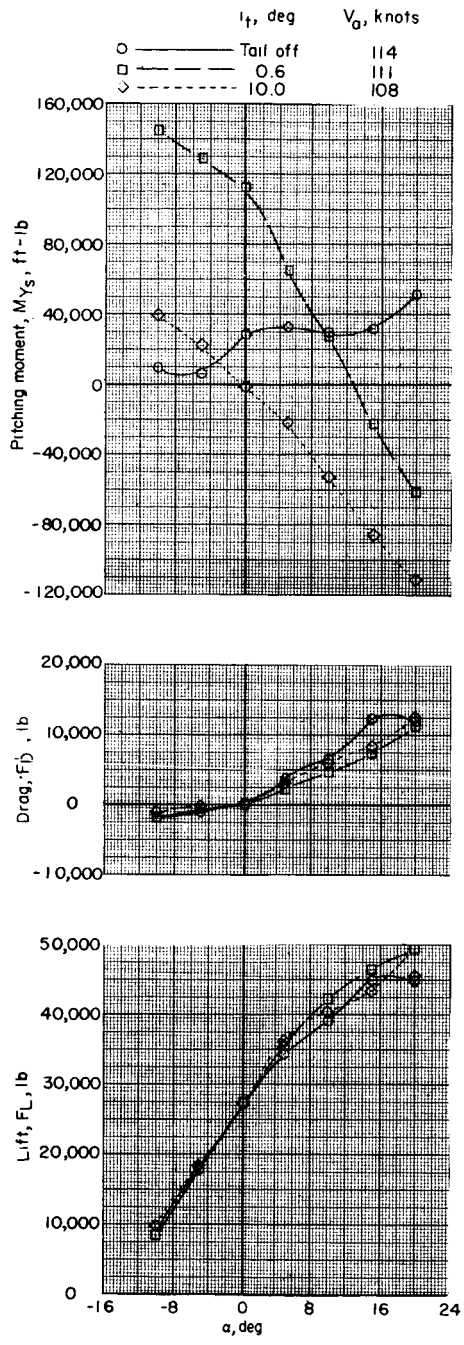

(a) $i_w = 20^\circ$.

Figure 20.- Tail effectiveness in transition flight with zero forward acceleration at $\alpha = 0^\circ$. Short wing; $\delta_e = 0^\circ$; $\beta_F = 10^\circ$.

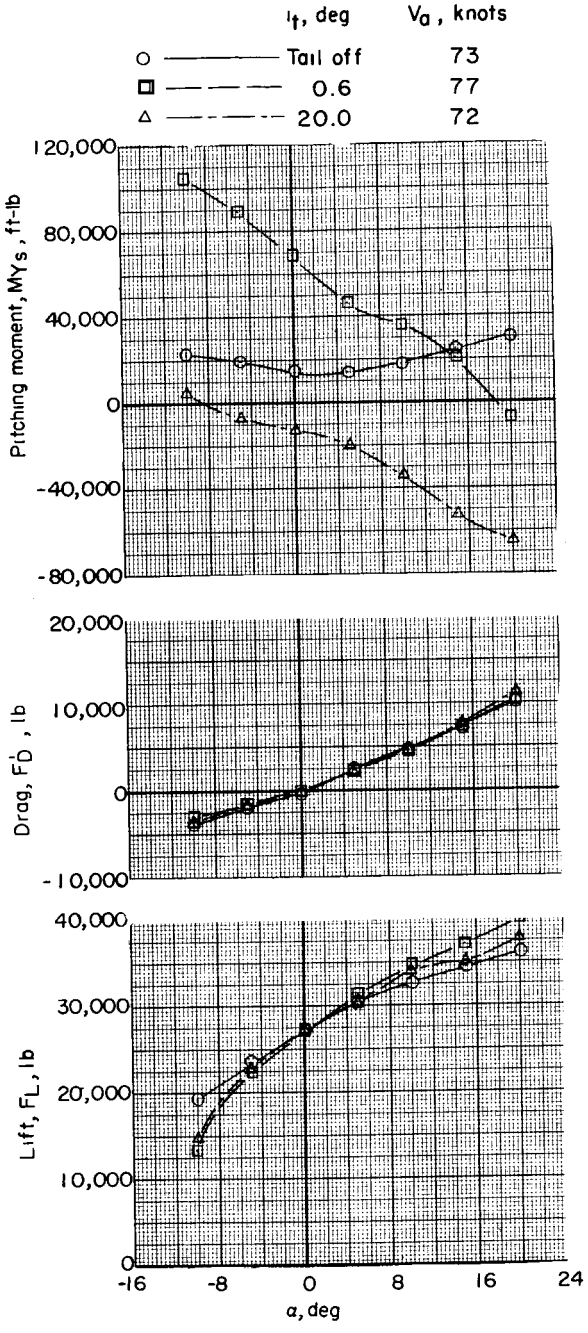

(b) $i_w = 35^\circ$.

Figure 20.- Continued.

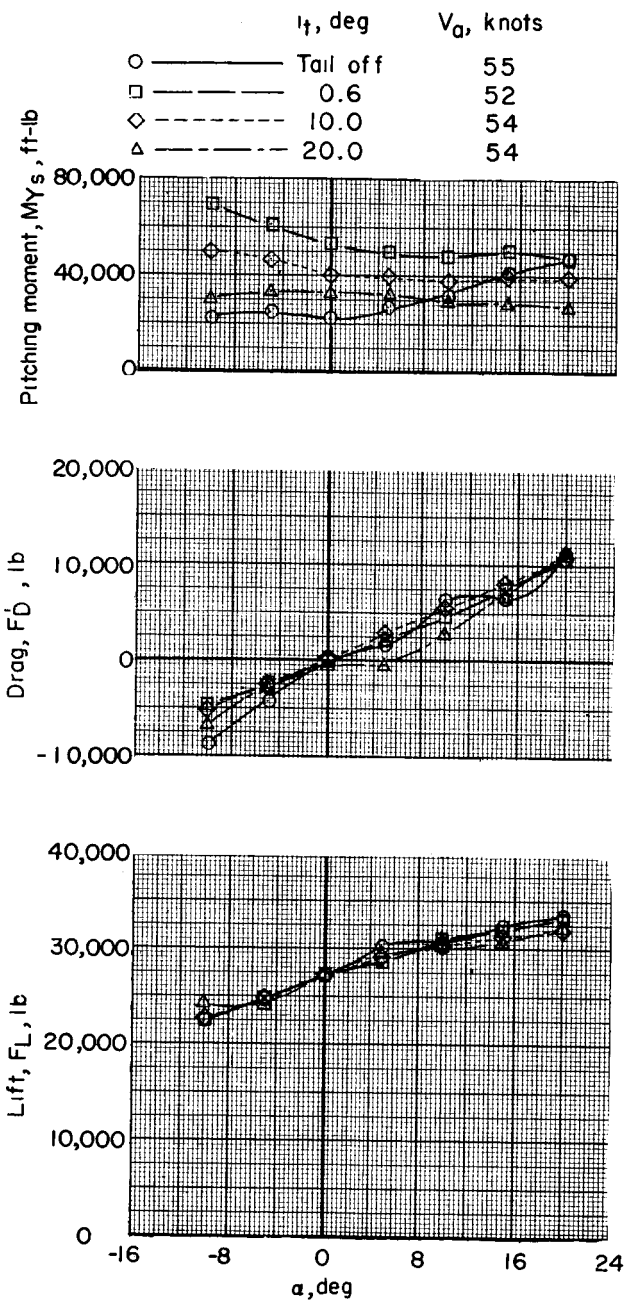

(c) $i_w = 50^\circ$.

Figure 20.- Continued.

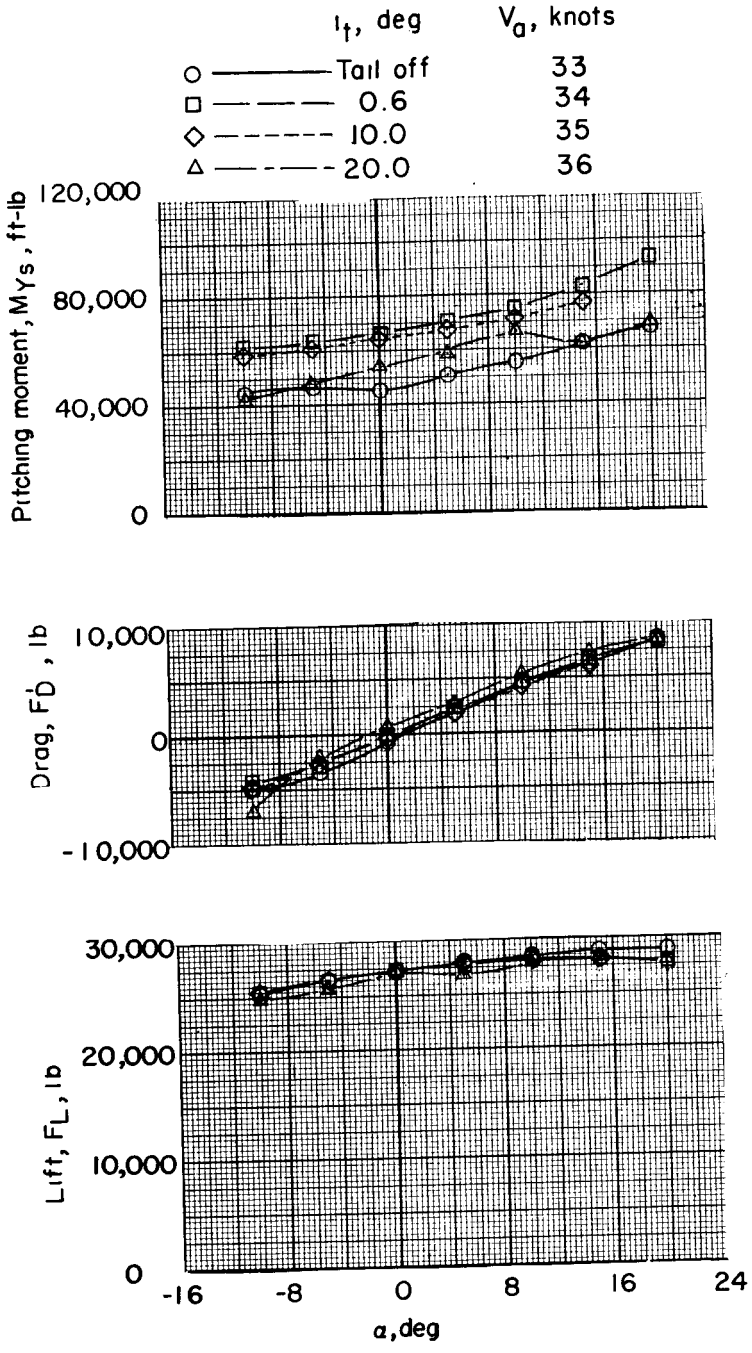

(d) $i_w = 65°$.

Figure 20.- Continued.

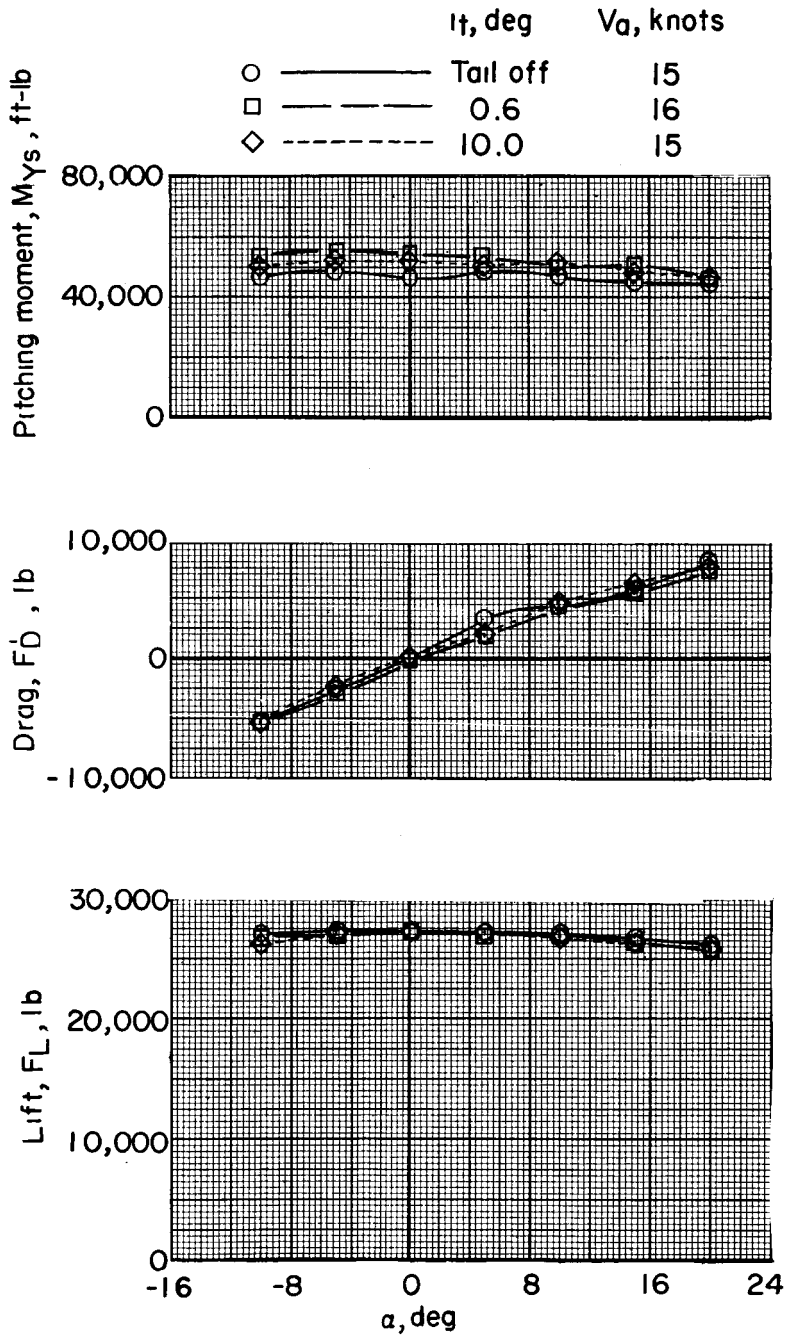

(e) $i_w = 80°$.

Figure 20.- Concluded.

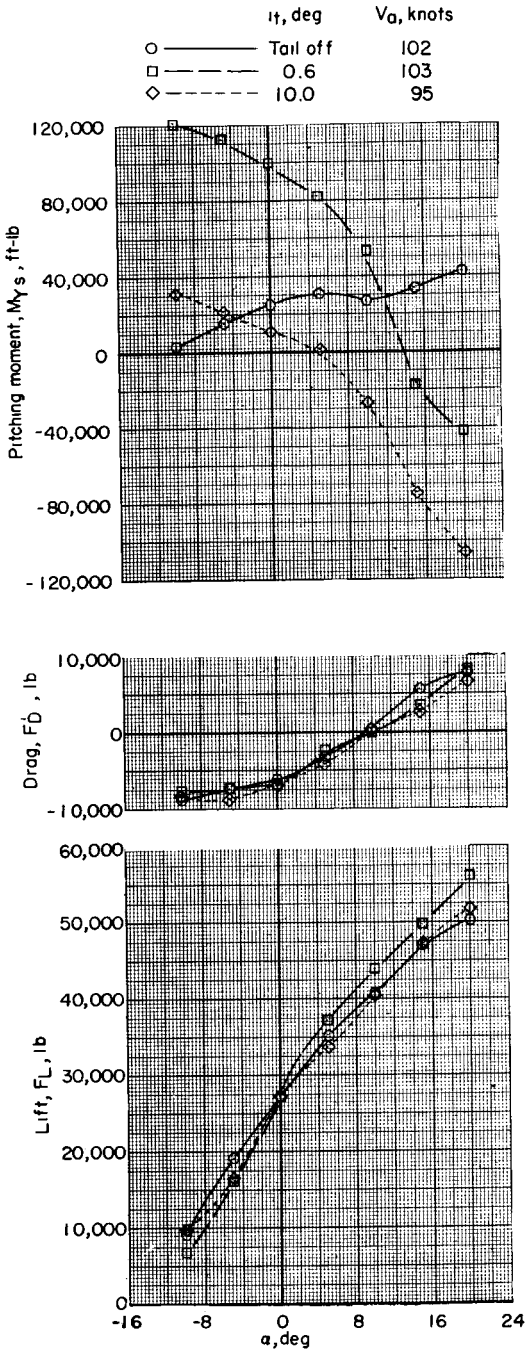

(a) $i_W = 20^\circ$.

Figure 21.- Tail effectiveness in transition flight with 0.25g forward acceleration at $\alpha = 0^\circ$. Short wing; $\delta_e = 0^\circ$; $\beta_F = 10^\circ$.

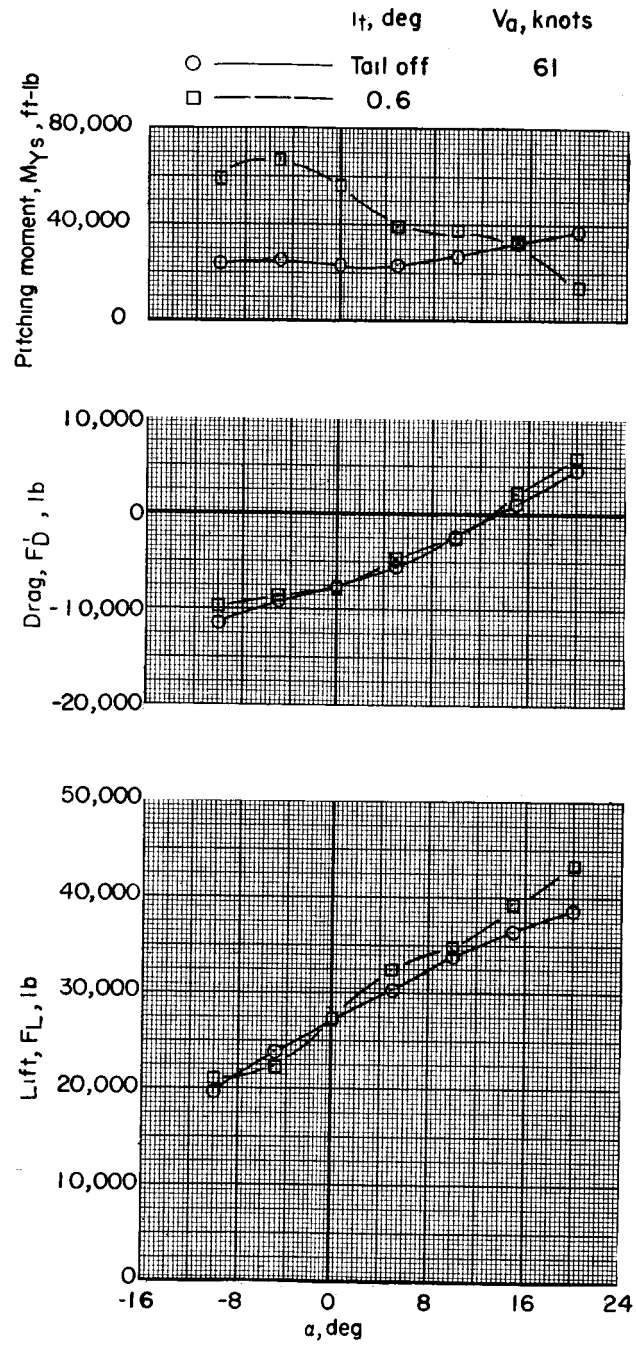

(b) $i_w = 35°$.

Figure 21.- Continued.

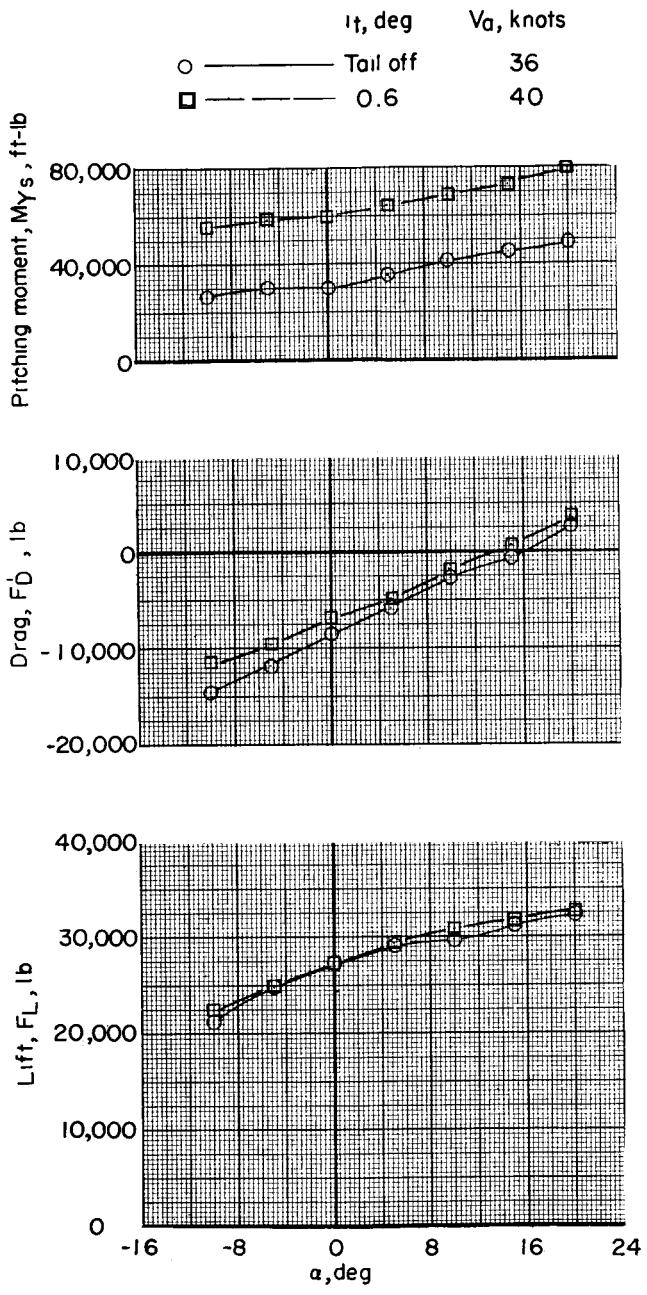

(c) $i_w = 50^\circ$.

Figure 21.- Continued.

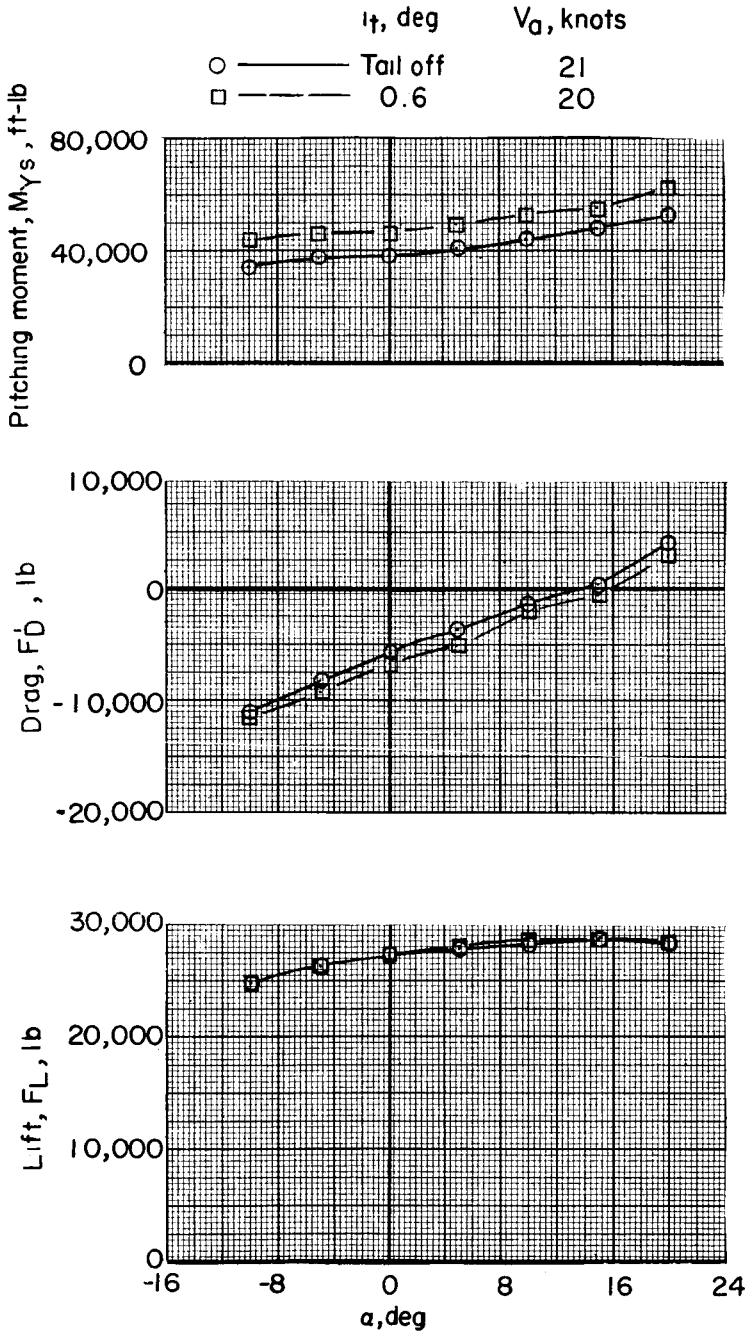

(d) $i_w = 65°$.

Figure 21.- Concluded.

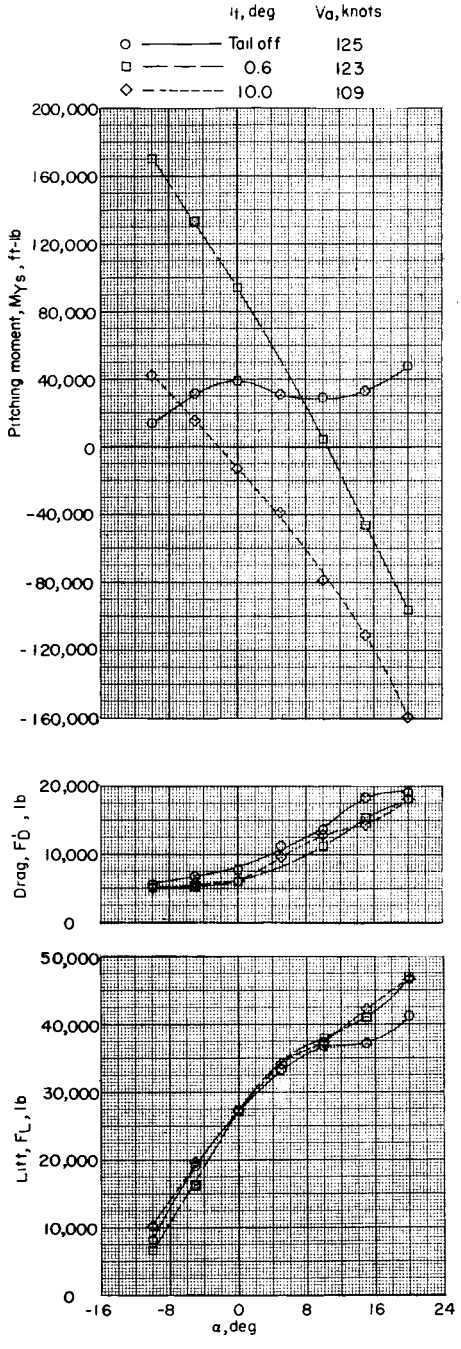

(a) $i_w = 20^\circ$.

Figure 22.- Tail effectiveness in transition flight with 0.25g deceleration at $\alpha = 0^\circ$. Short wing; $\delta_e = 0^\circ$; $\beta_F = 10^\circ$.

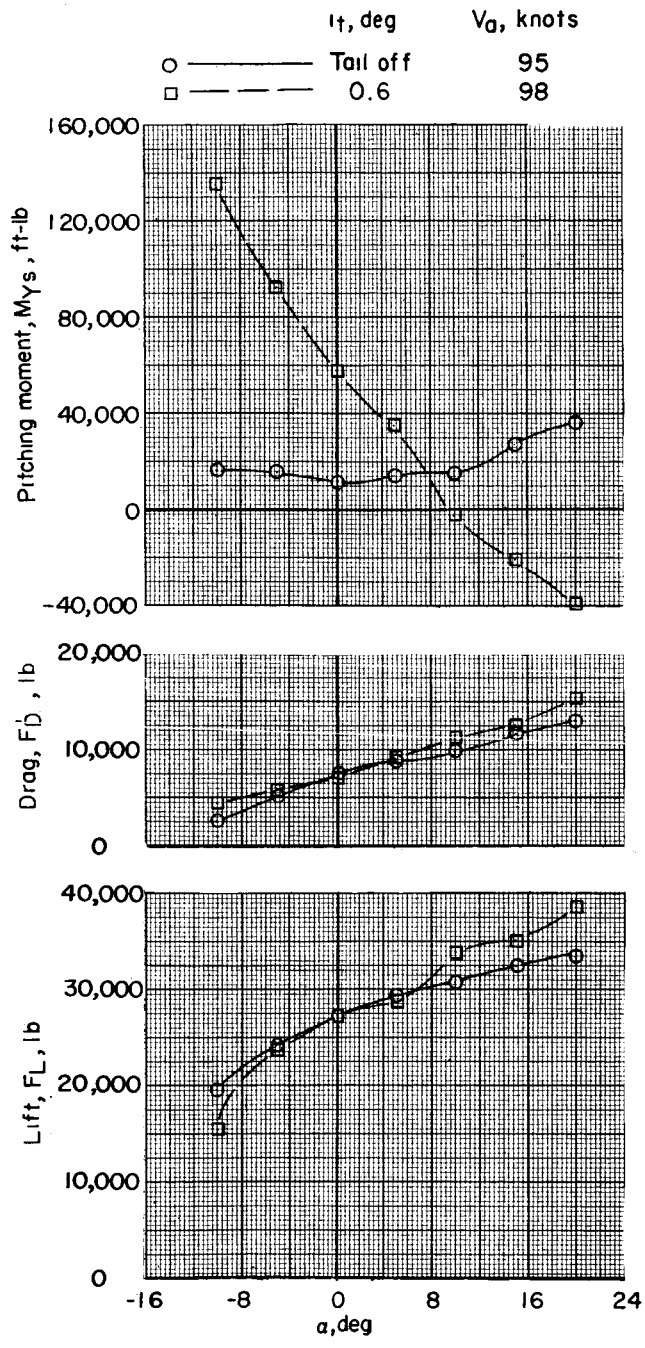

(b) $i_w = 35^\circ$.

Figure 22.- Continued.

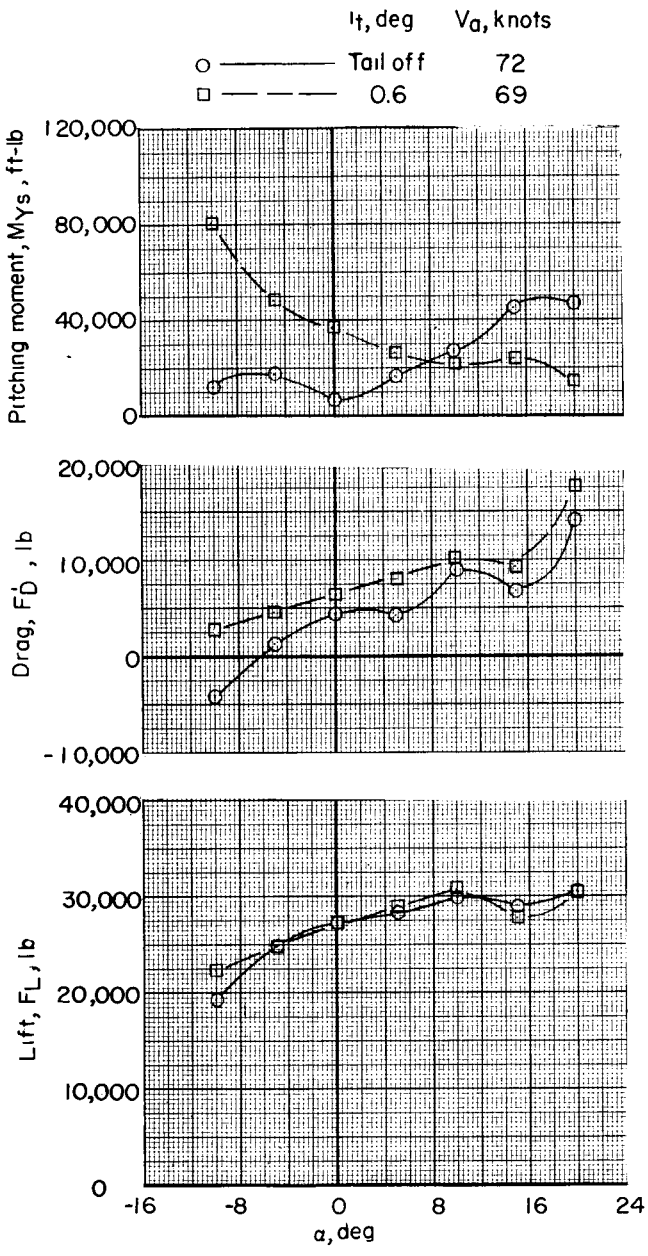

(c) $i_w = 50^\circ$.

Figure 22.- Continued.

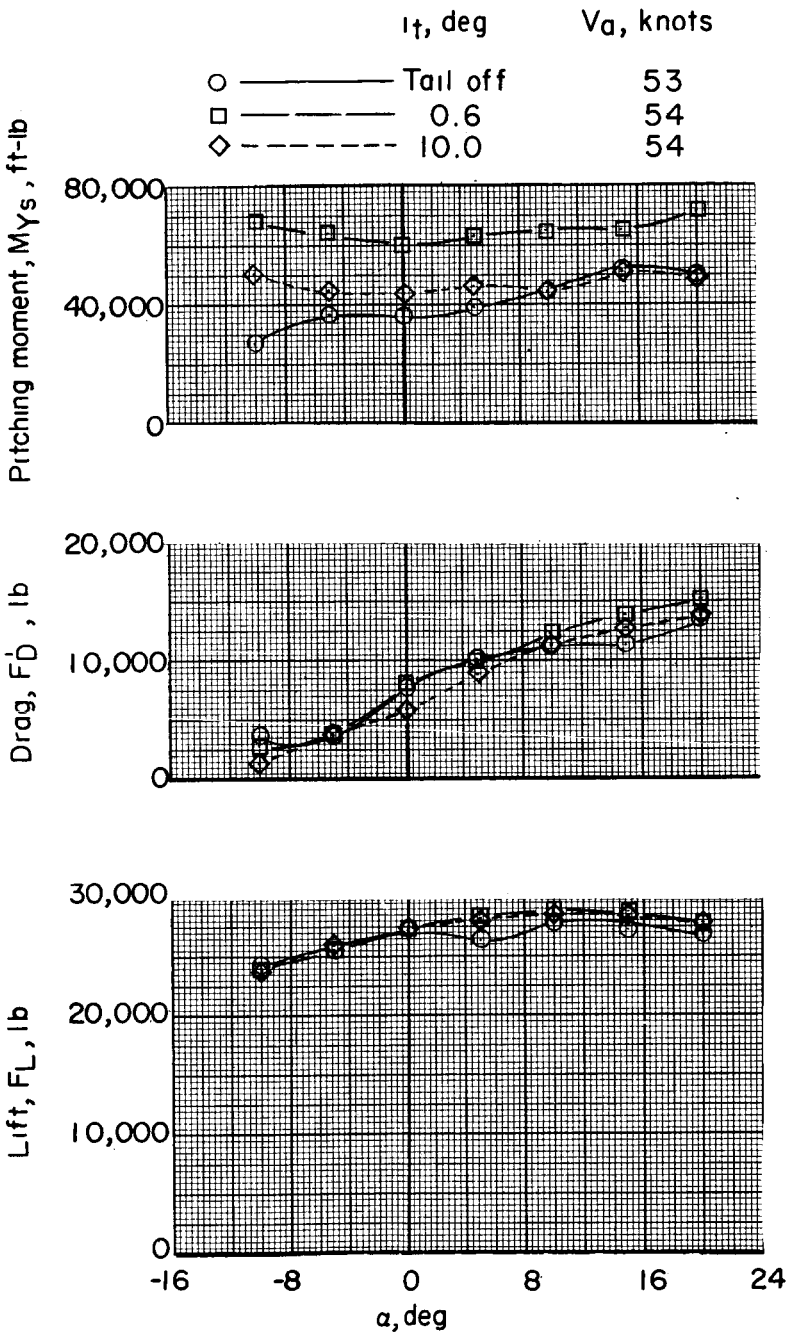

(d) $i_w = 65°$.

Figure 22.- Continued.

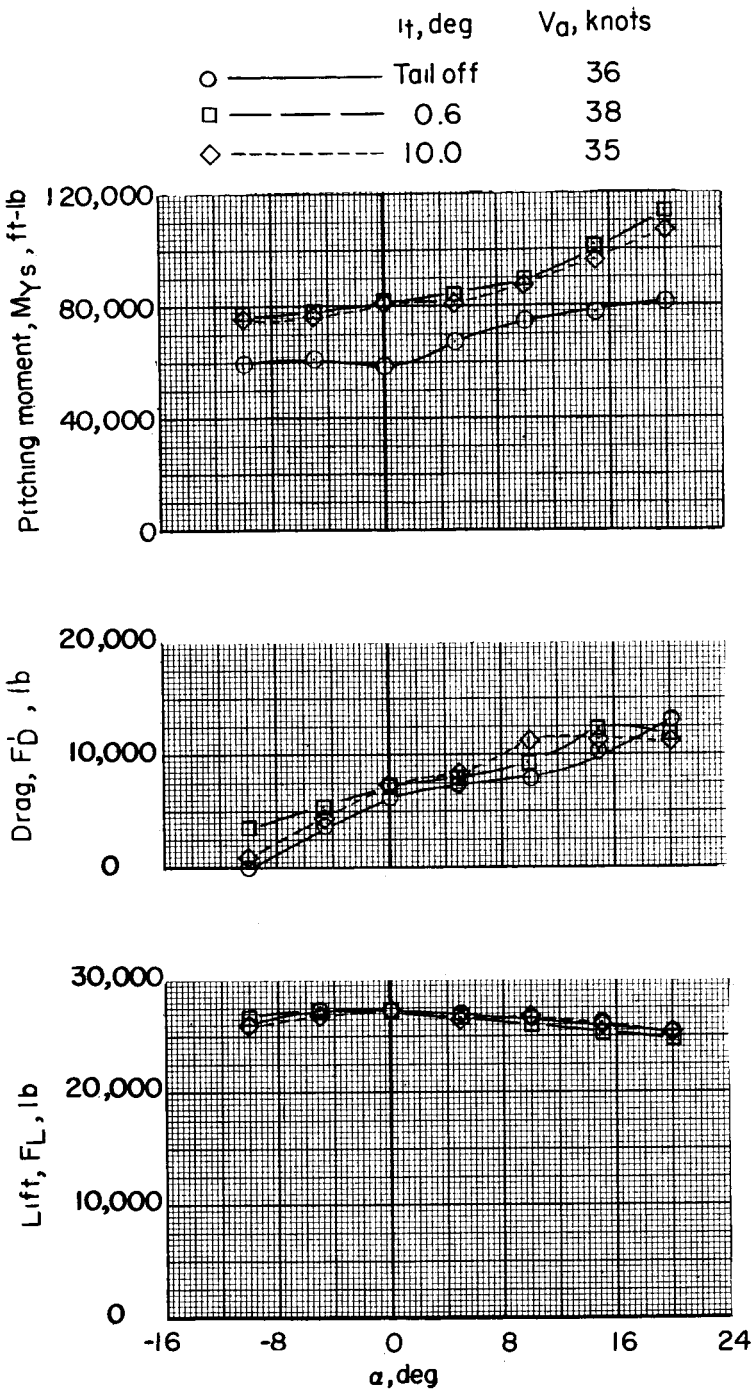

(e) $i_w = 80^\circ$.

Figure 22.- Continued.

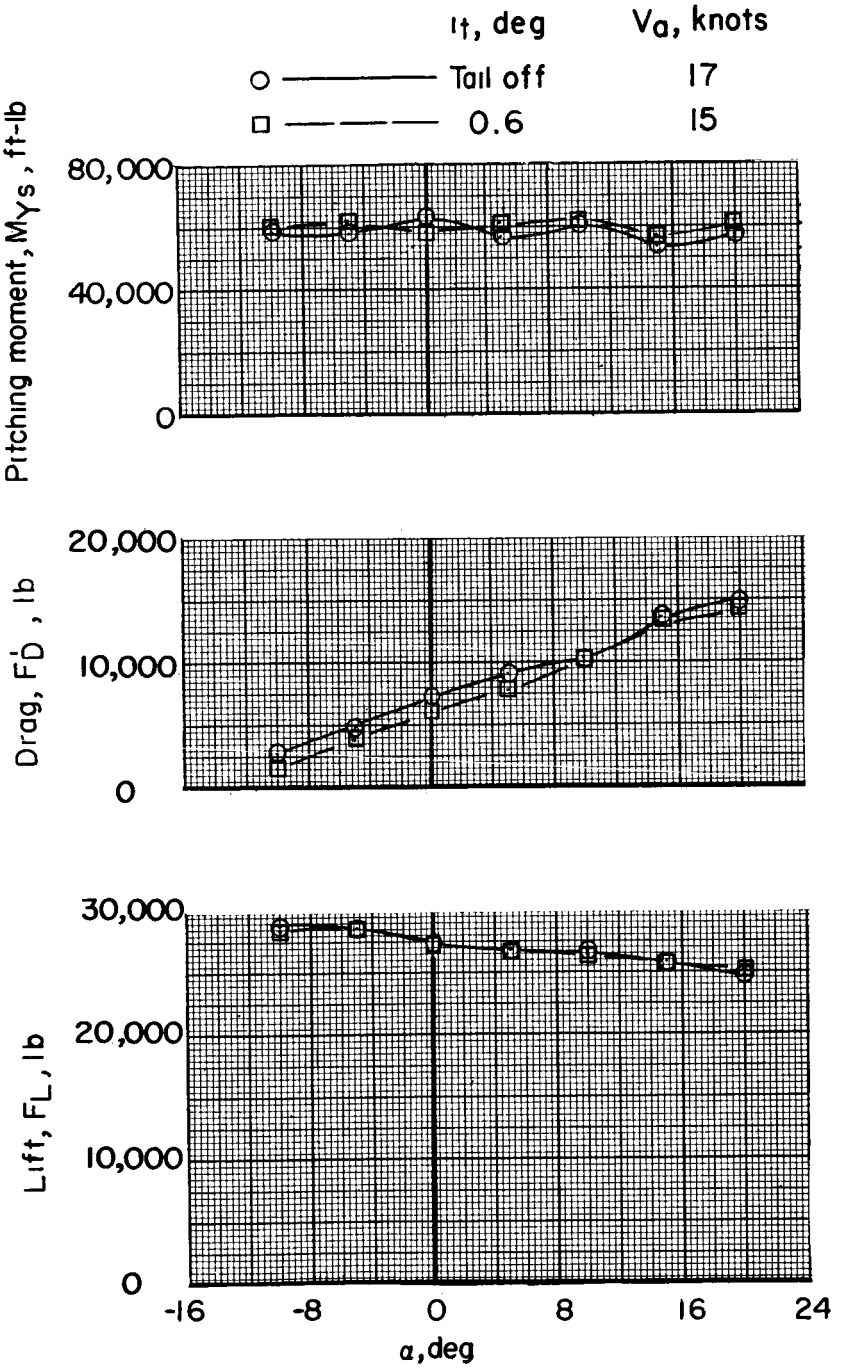

(f) $i_w = 90^\circ$.

Figure 22.- Concluded.

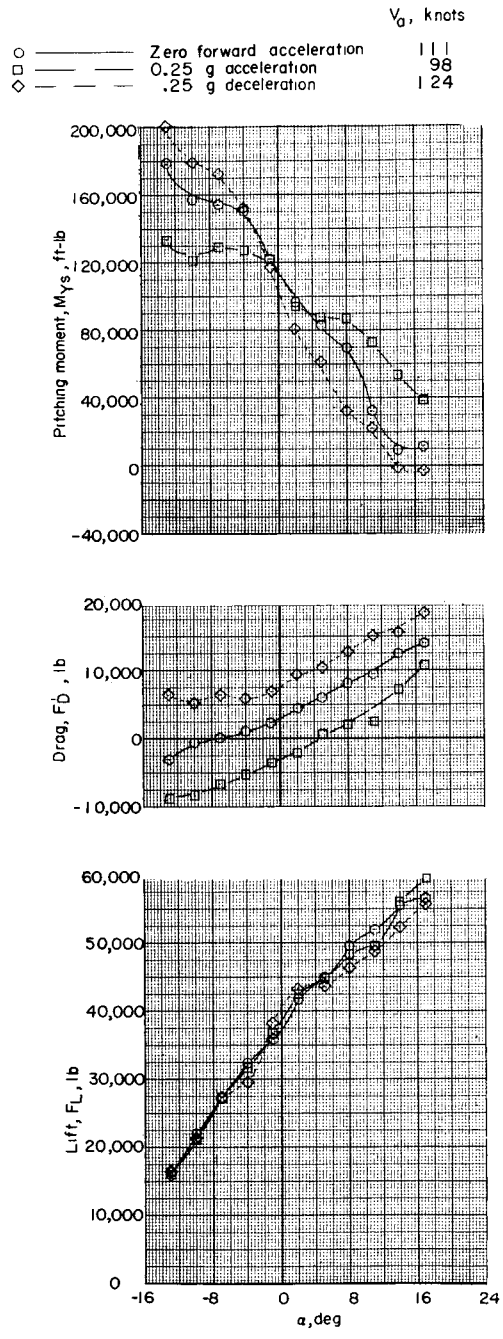

(a) $i_w = 24.5^\circ$.

Figure 23.- Longitudinal stability characteristics in transition flight for 0 and 0.25g forward acceleration and 0.25g deceleration at $\alpha = -7^\circ$. Short wing; $i_t = 0.6^\circ$; $\delta_e = 0^\circ$; $\beta_F = 10^\circ$.

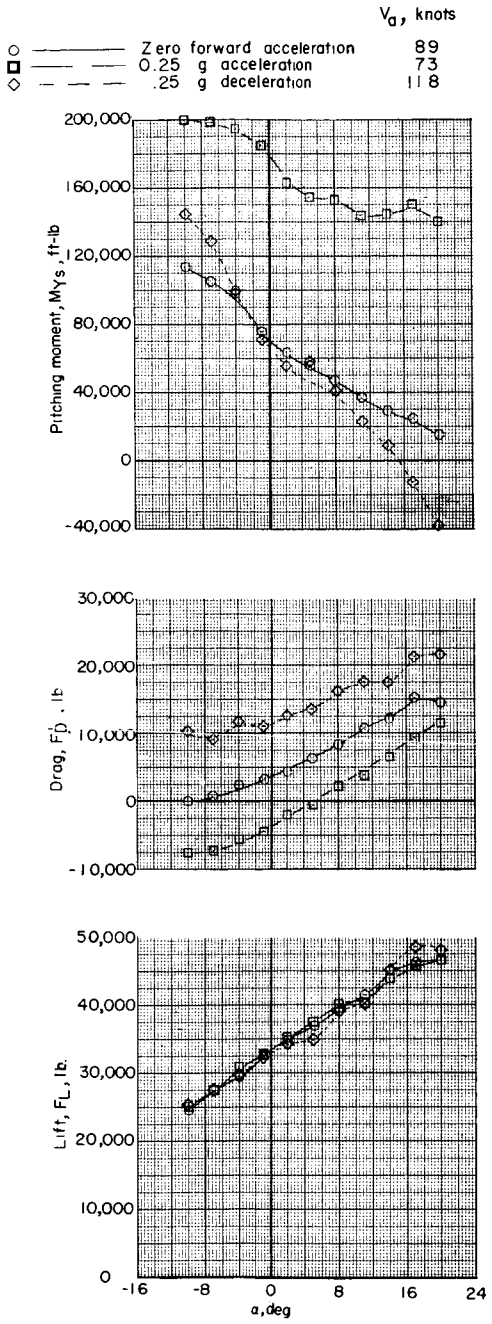

(b) $i_W = 39.5^\circ$.

Figure 23.- Continued.

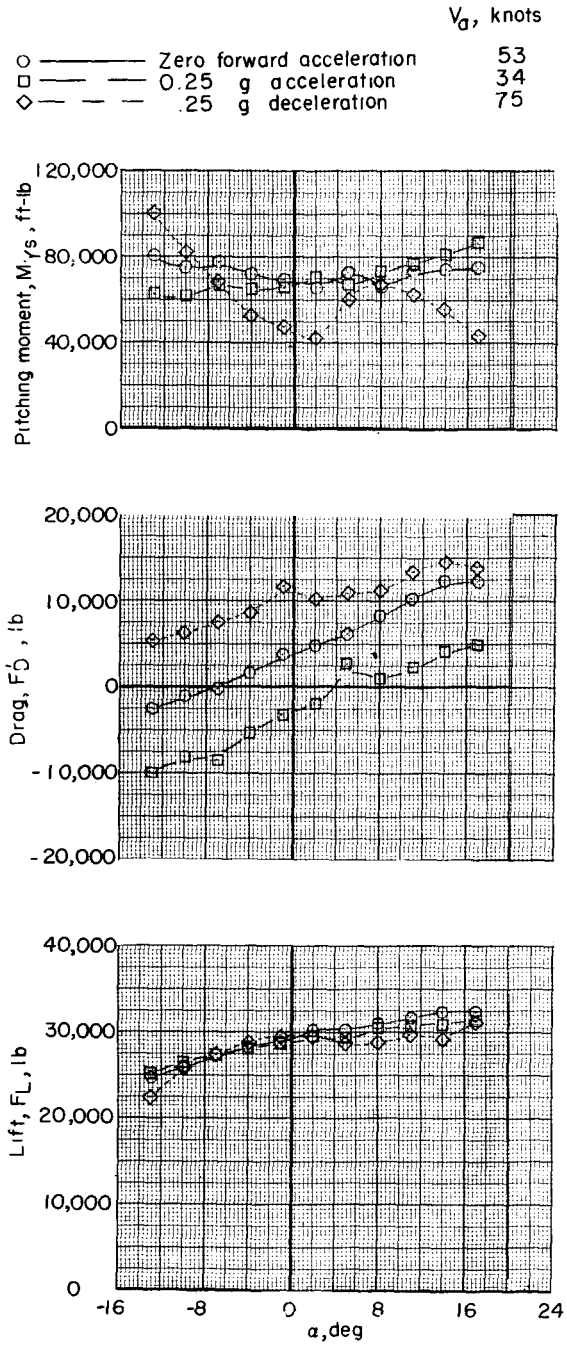

(c) $i_w = 54.5°$.

Figure 23.- Continued.

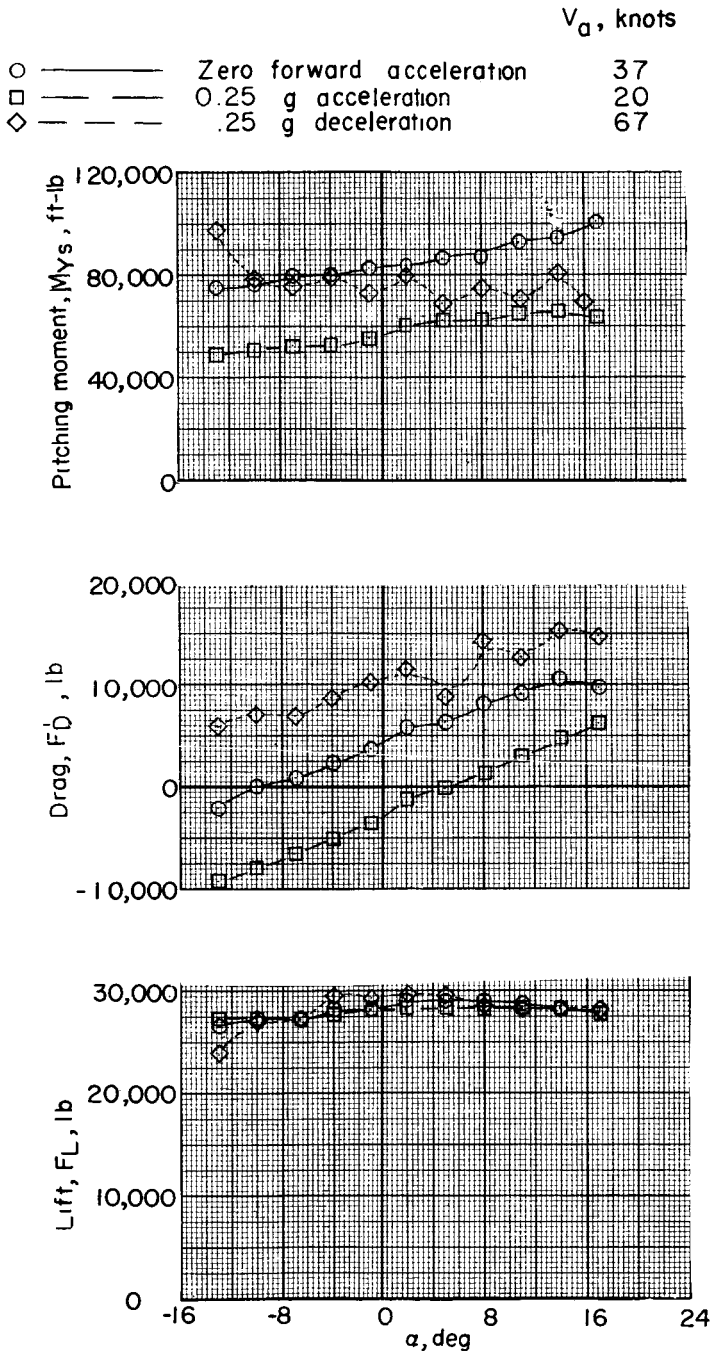

(d) $i_w = 69.5^\circ$.

Figure 23.- Concluded.

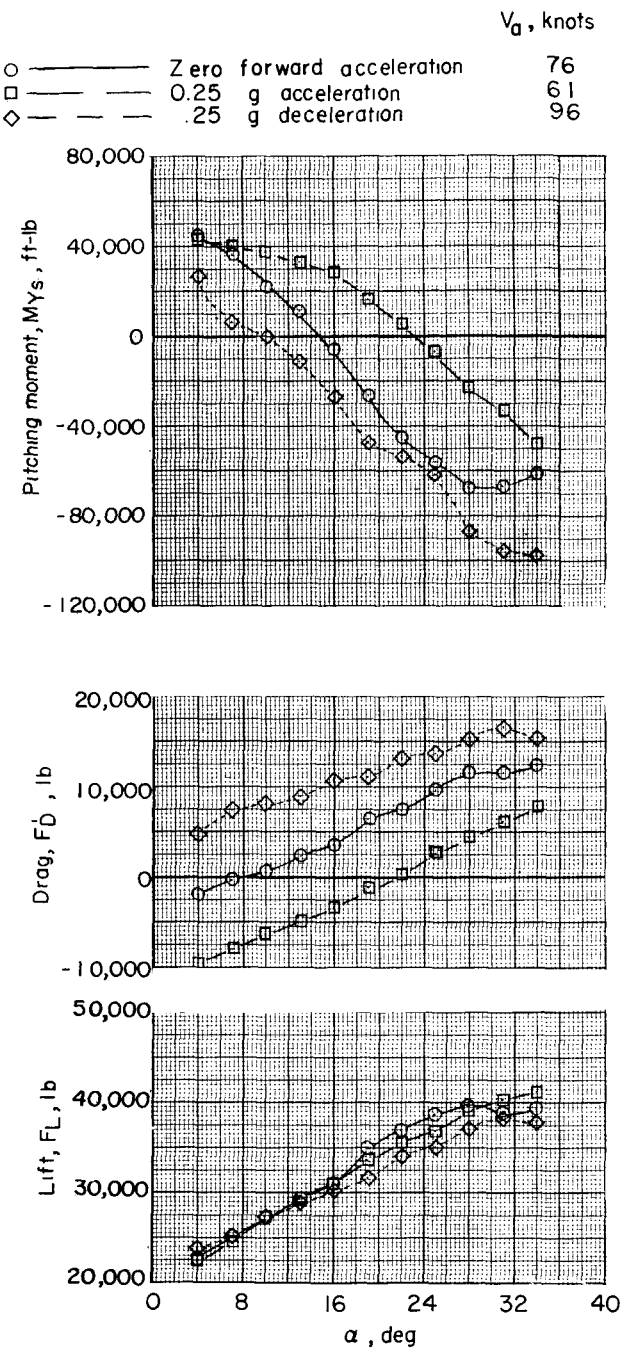

(a) $i_w = 20^\circ$.

Figure 24.- Longitudinal stability characteristics in transition flight for 0 and 0.25g forward acceleration and 0.25g deceleration at $\alpha = 10^\circ$. Short wing; $i_t = 0.6^\circ$; $\delta_e = 0^\circ$; $\beta = 10^\circ$.

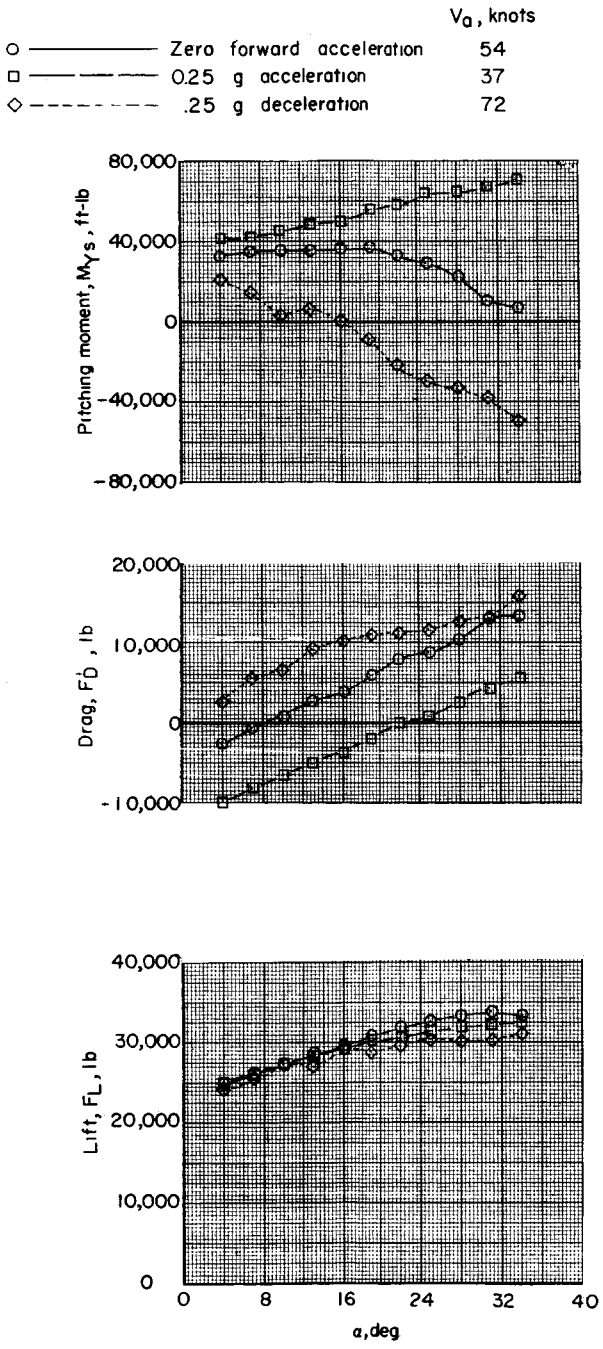

(b) $i_w = 35^\circ$.

Figure 24.- Continued.

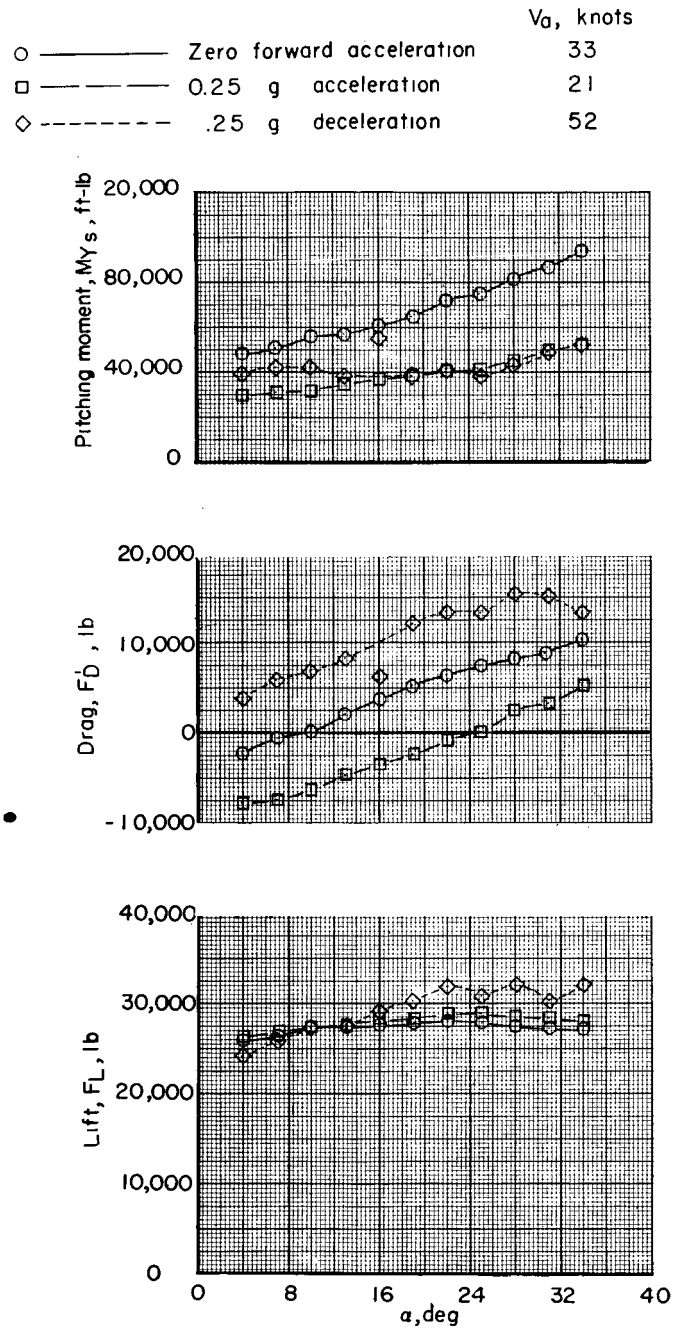

(c) $i_w = 50°$.

Figure 24.- Continued.

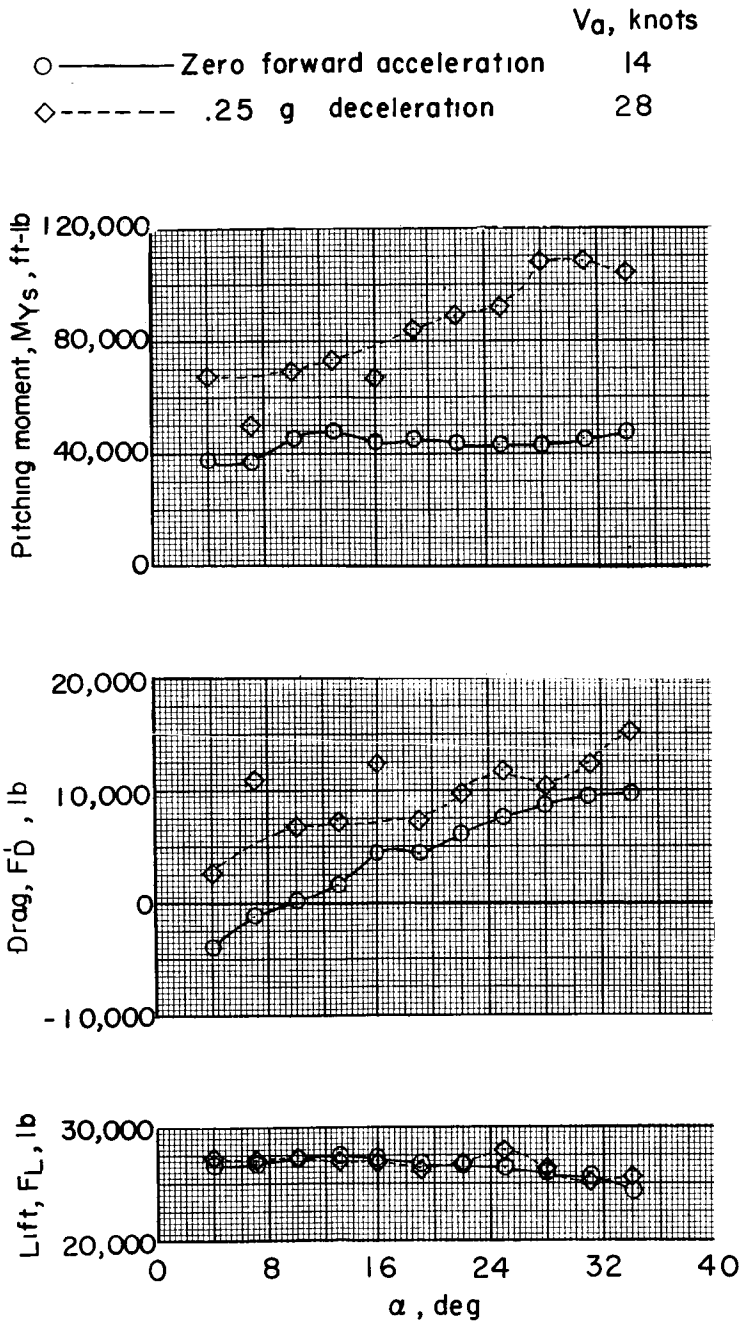

(d) $i_w = 65^\circ$.

Figure 24.- Concluded.

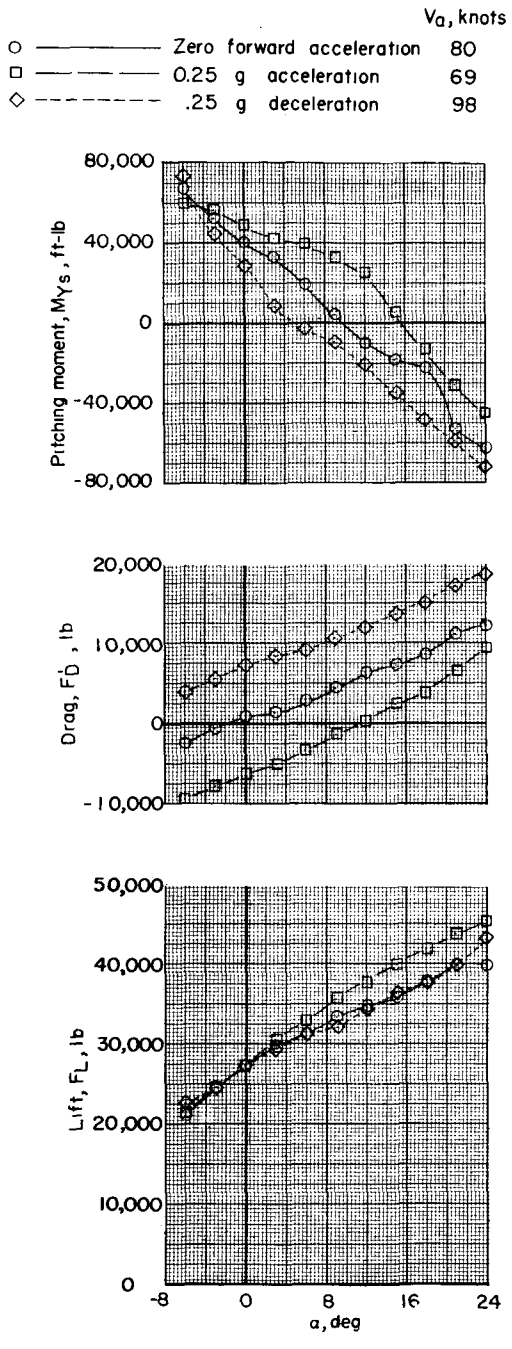

(a) $i_w = 20^\circ$.

Figure 25.- Longitudinal stability characteristics of long-wing configuration in transition flight for 0 and 0.25g forward acceleration and 0.25g deceleration at $\alpha = 0^\circ$. $i_t = 0.6^\circ$; $\delta_e = 0^\circ$; $\beta_F = 10^\circ$.

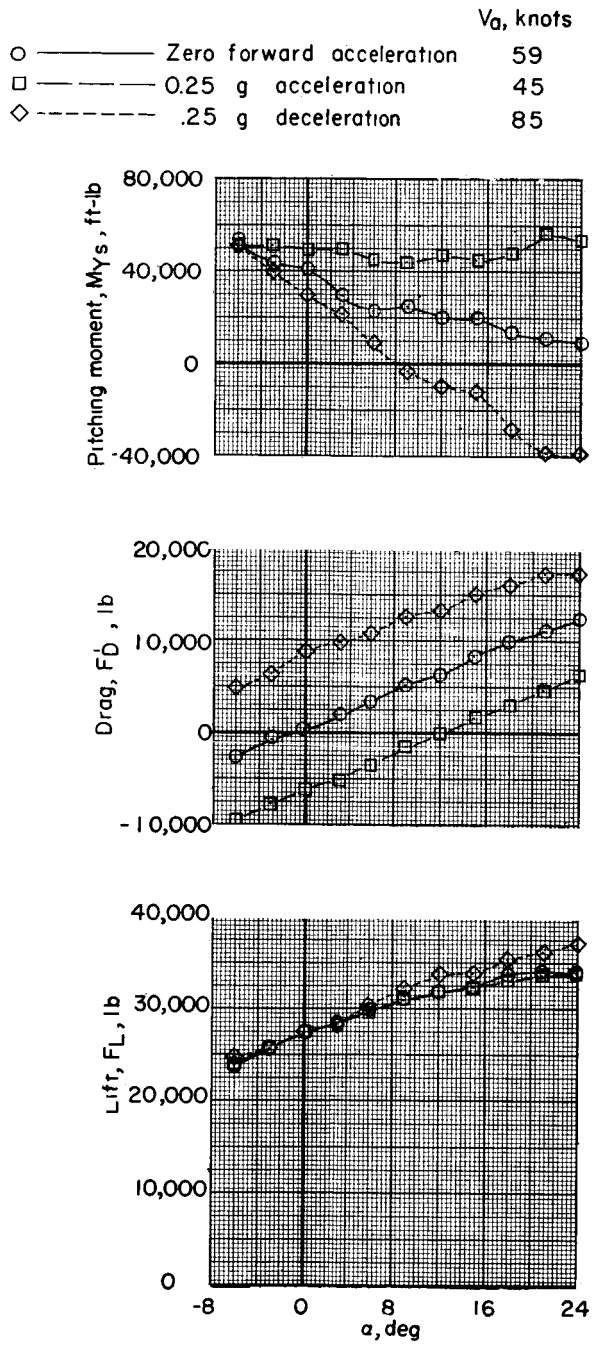

(b) $i_w = 35°$.

Figure 25.- Continued.

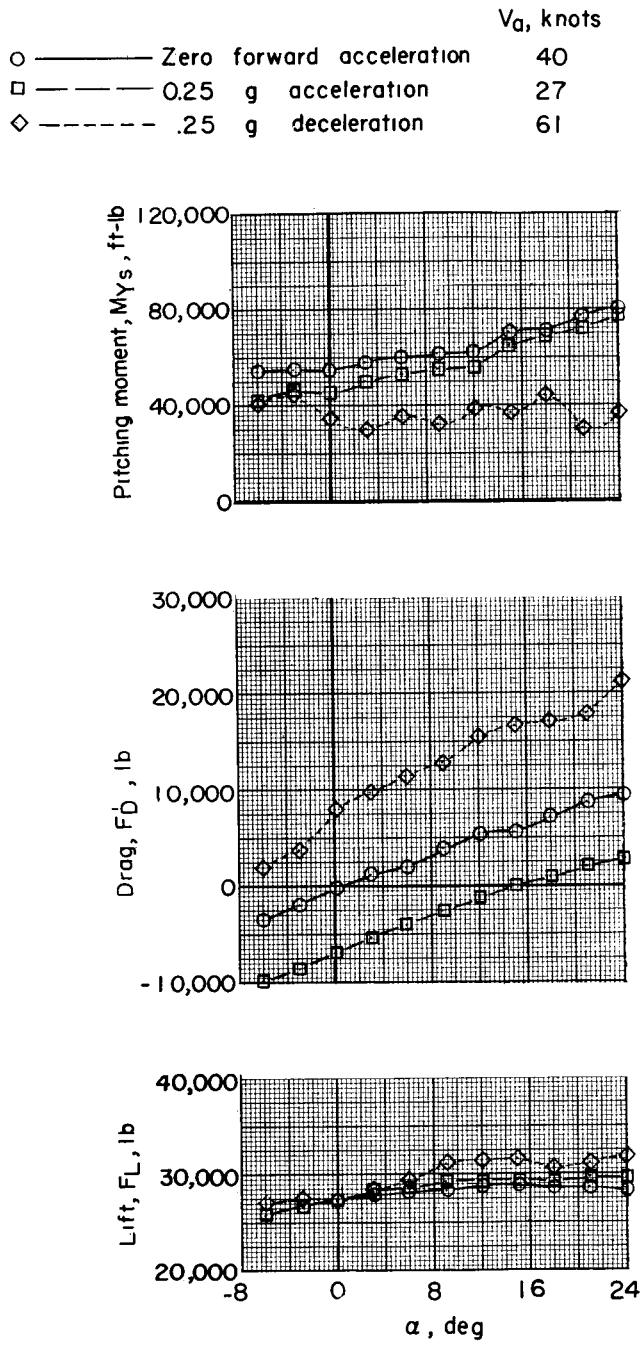

(c) $i_w = 50^\circ$.

Figure 25.- Continued.

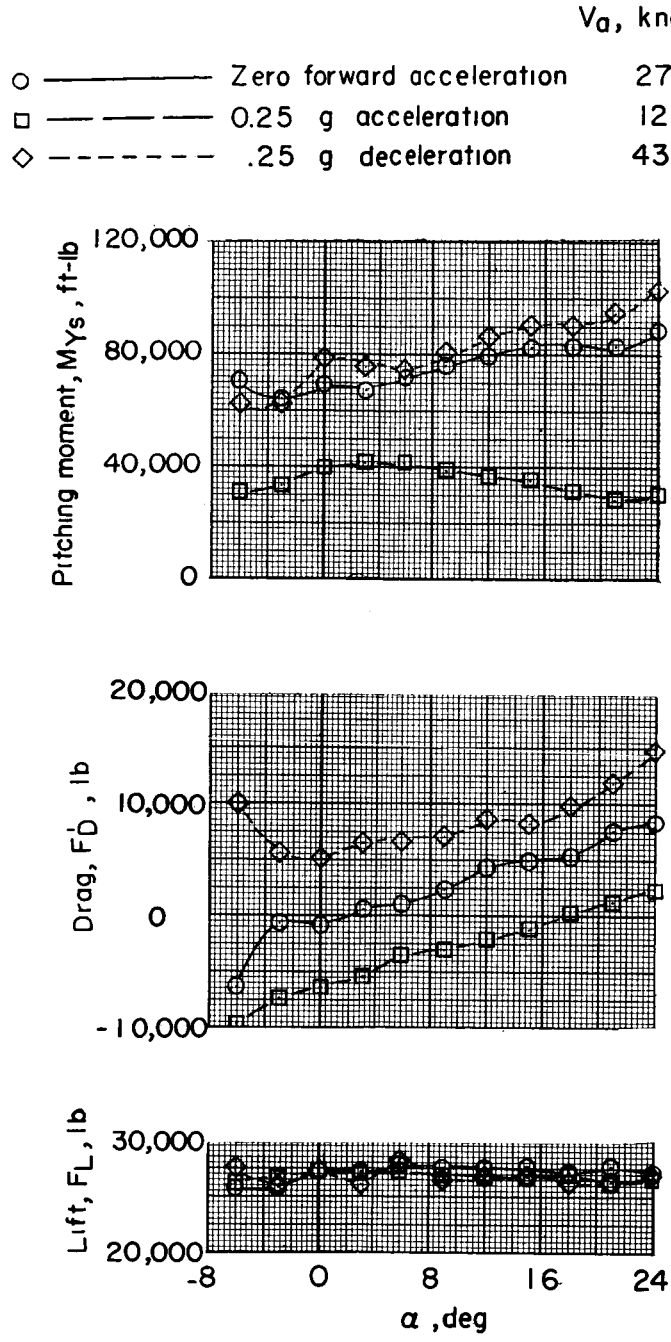

(d) $i_w = 65°$.

Figure 25.- Concluded.

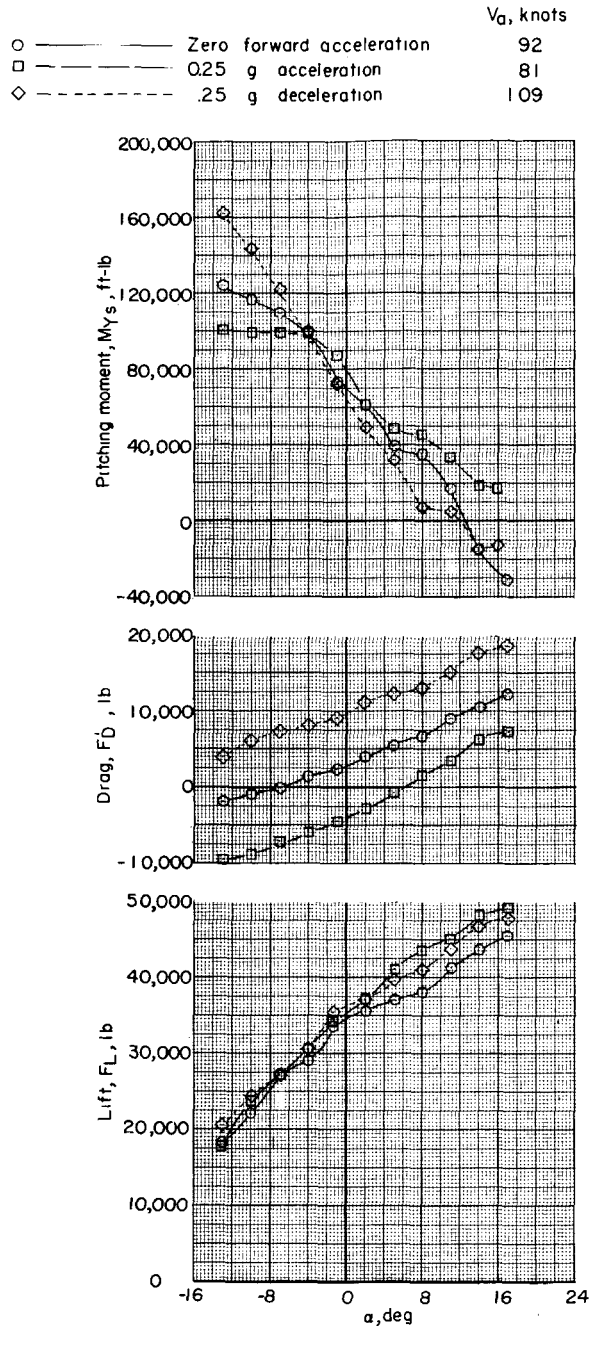

(a) $i_w = 24.5^\circ$.

Figure 26.- Longitudinal stability characteristics of long-wing configuration in transition flight for 0 and 0.25g forward acceleration and 0.25g deceleration at $\alpha = -7^\circ$. $i_t = 0.6^\circ$; $\delta_e = 0^\circ$; $\beta_F = 10^\circ$.

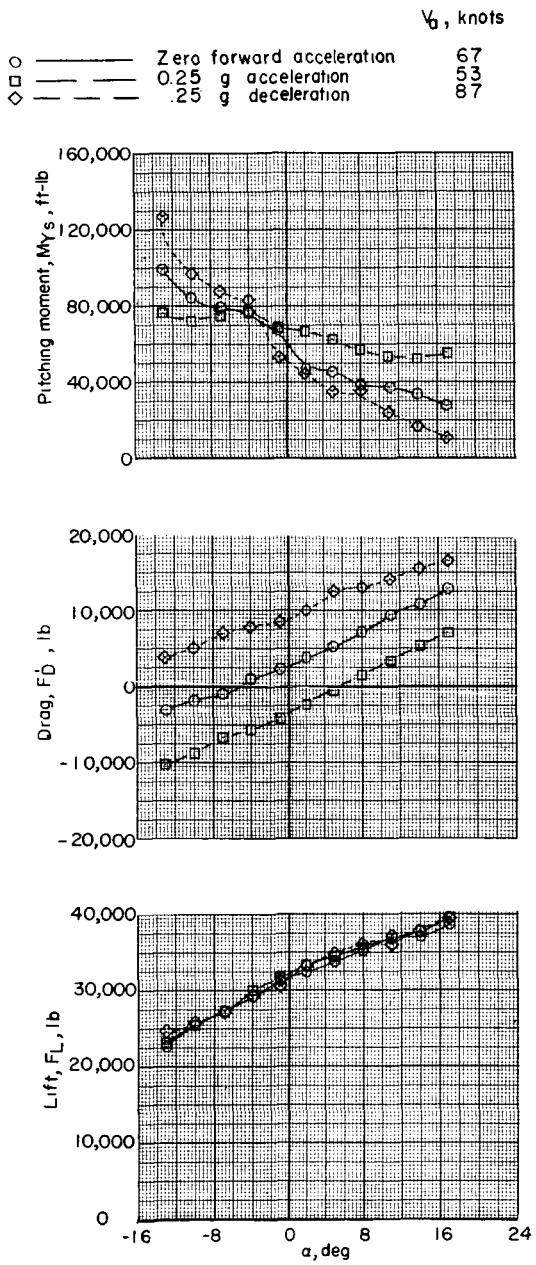

(b) $i_w = 39.5°$.

Figure 26.- Continued.

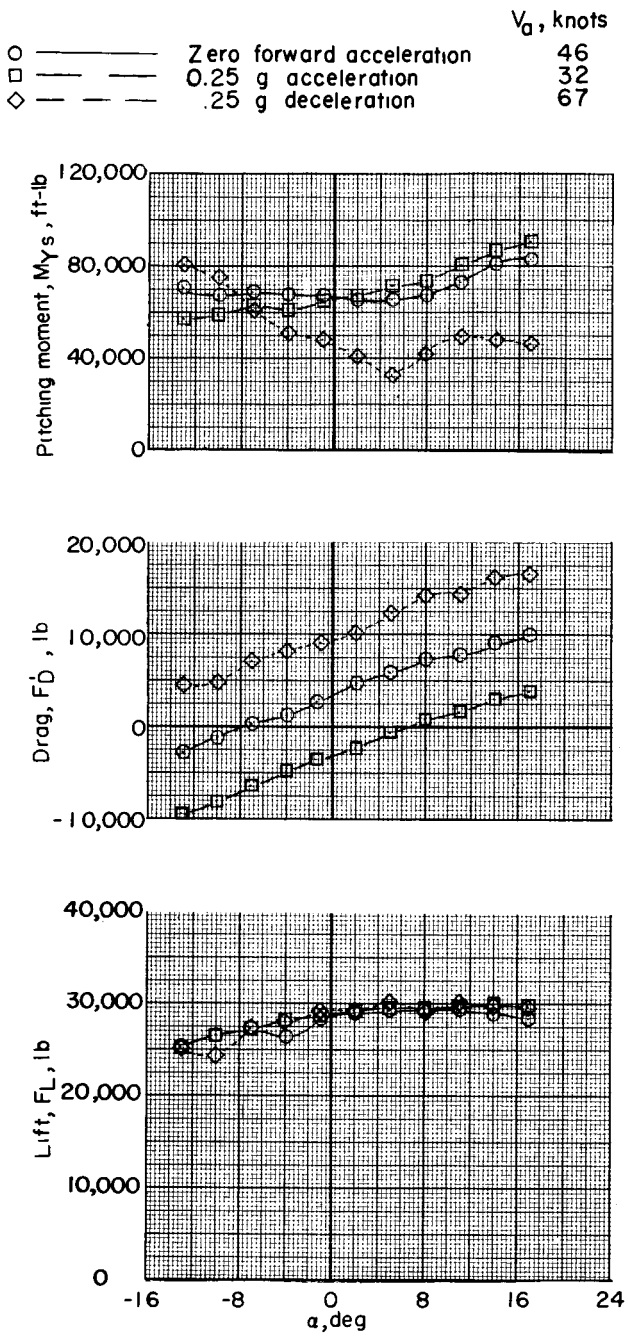

(c) $i_w = 54.5^\circ$.

Figure 26.- Continued.

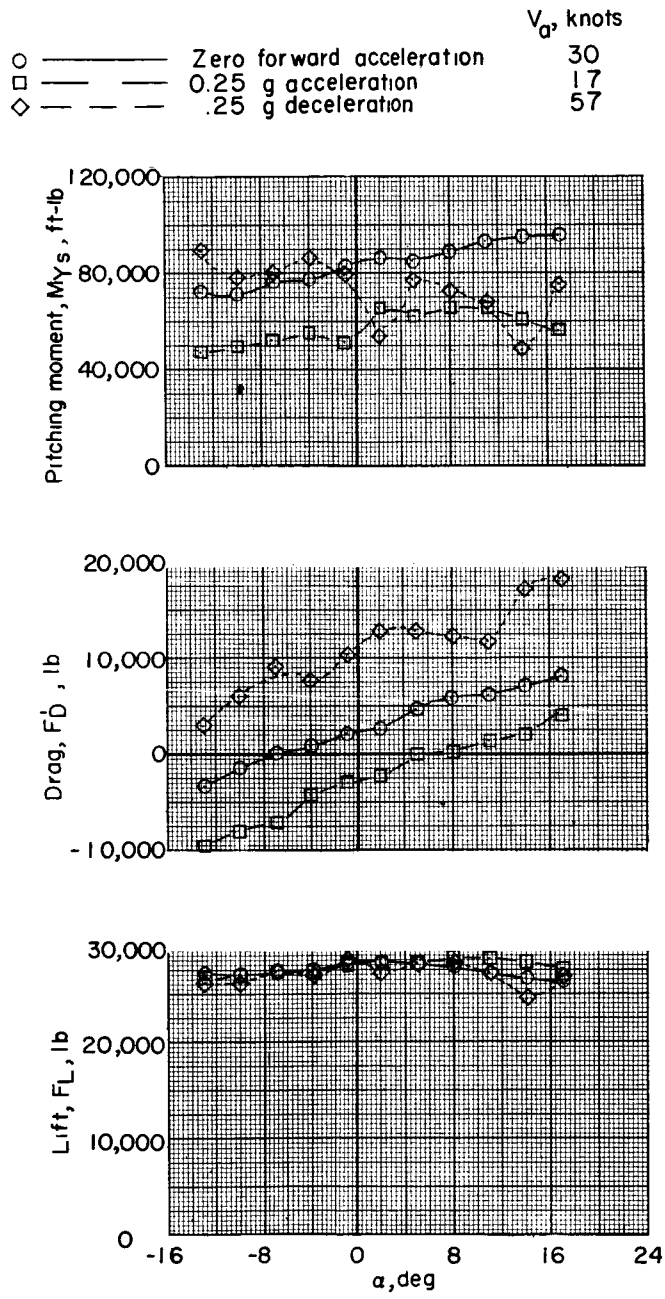

(d) $i_w = 69.5°$.

Figure 26.- Concluded.

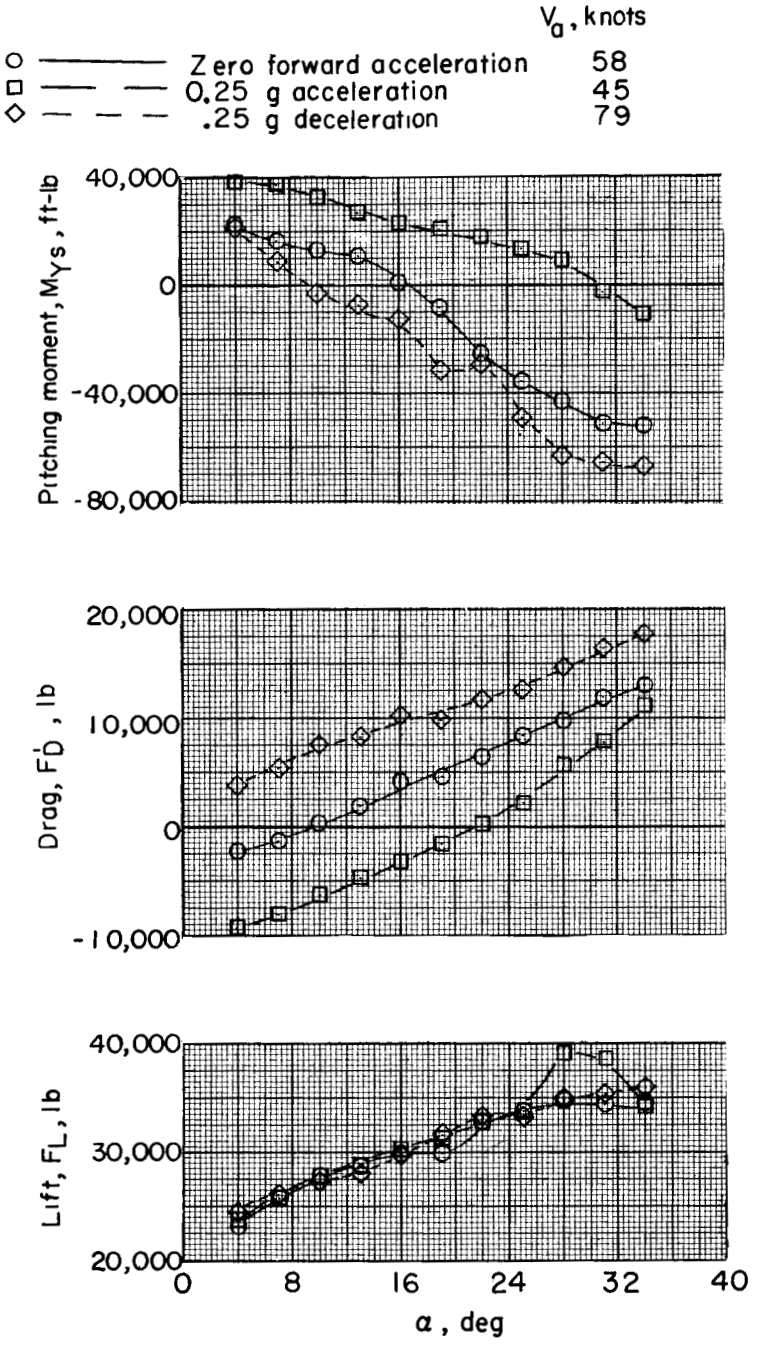

(a) $i_w = 20^\circ$.

Figure 27.- Longitudinal stability characteristics of long-wing configuration in transition flight for 0 and 0.25g forward acceleration and 0.25g deceleration at $\alpha = 10^\circ$. $i_t = 0.6^\circ$; $\delta_e = 0^\circ$; $\beta_F = 10^\circ$.

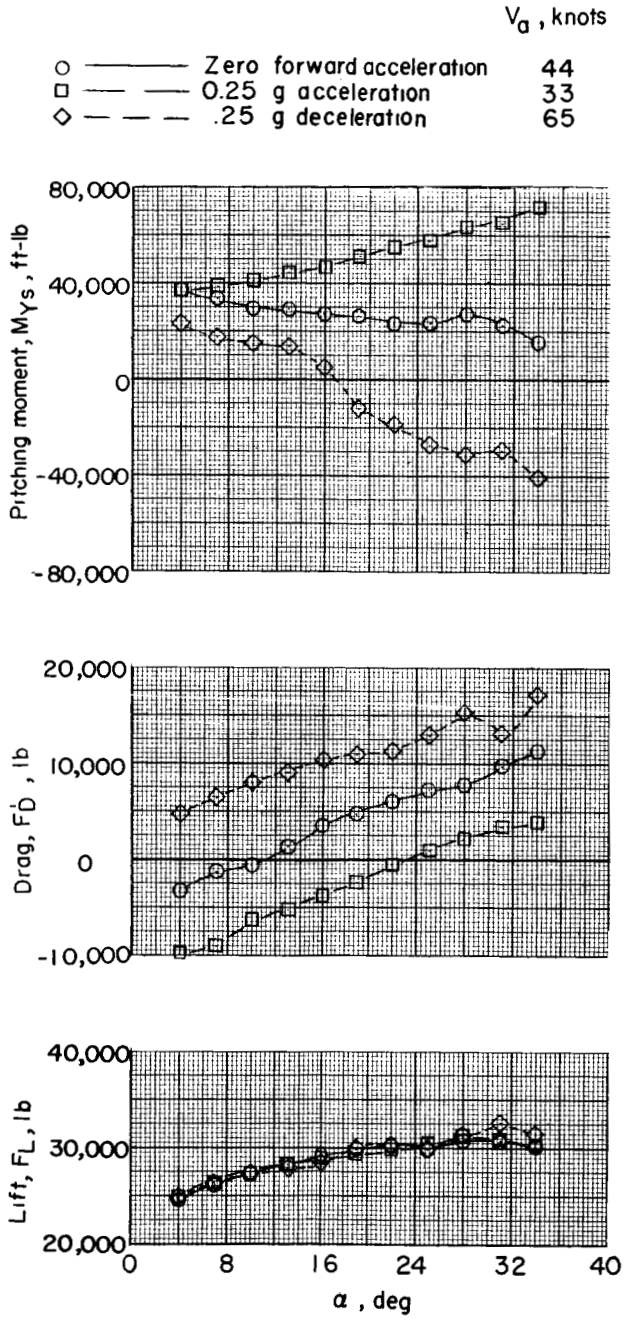

(b) $i_w = 35°$.

Figure 27.- Continued.

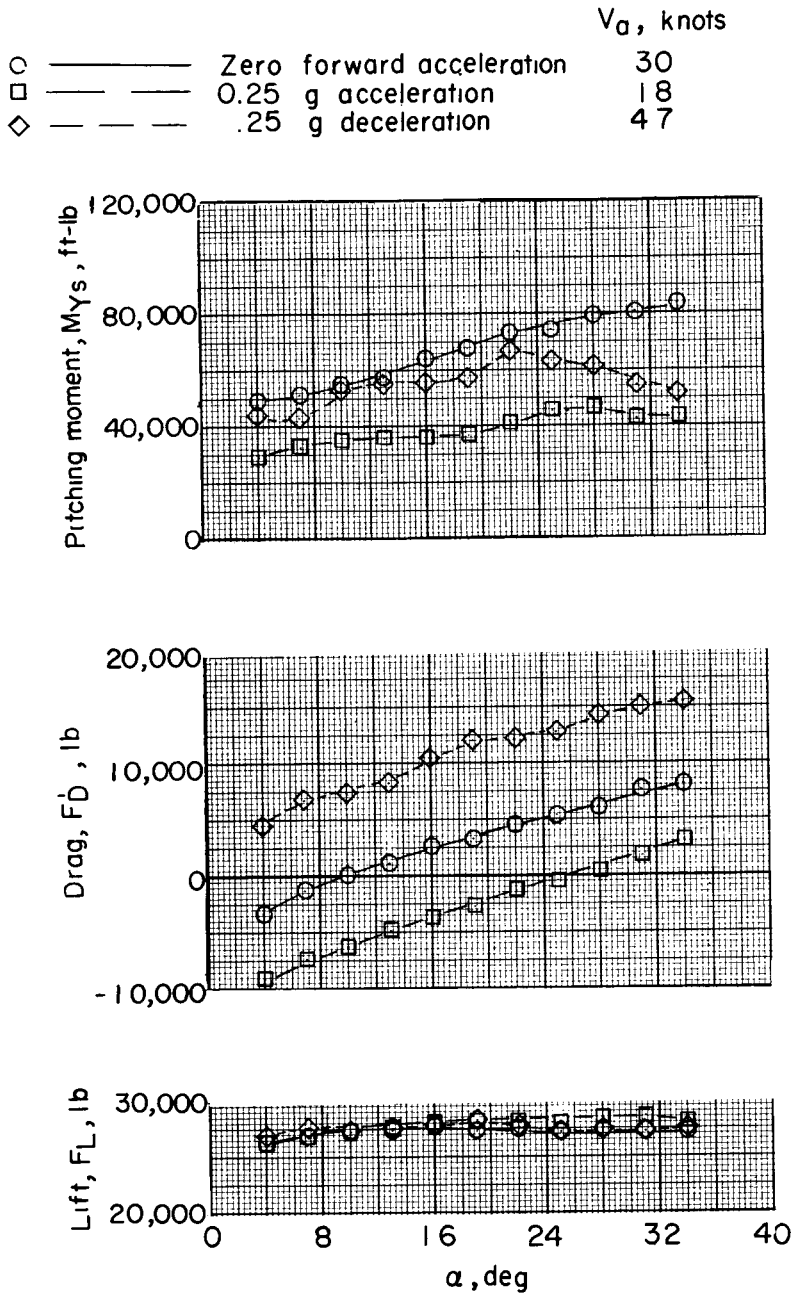

(c) $i_w = 50^\circ$.

Figure 27.- Continued.

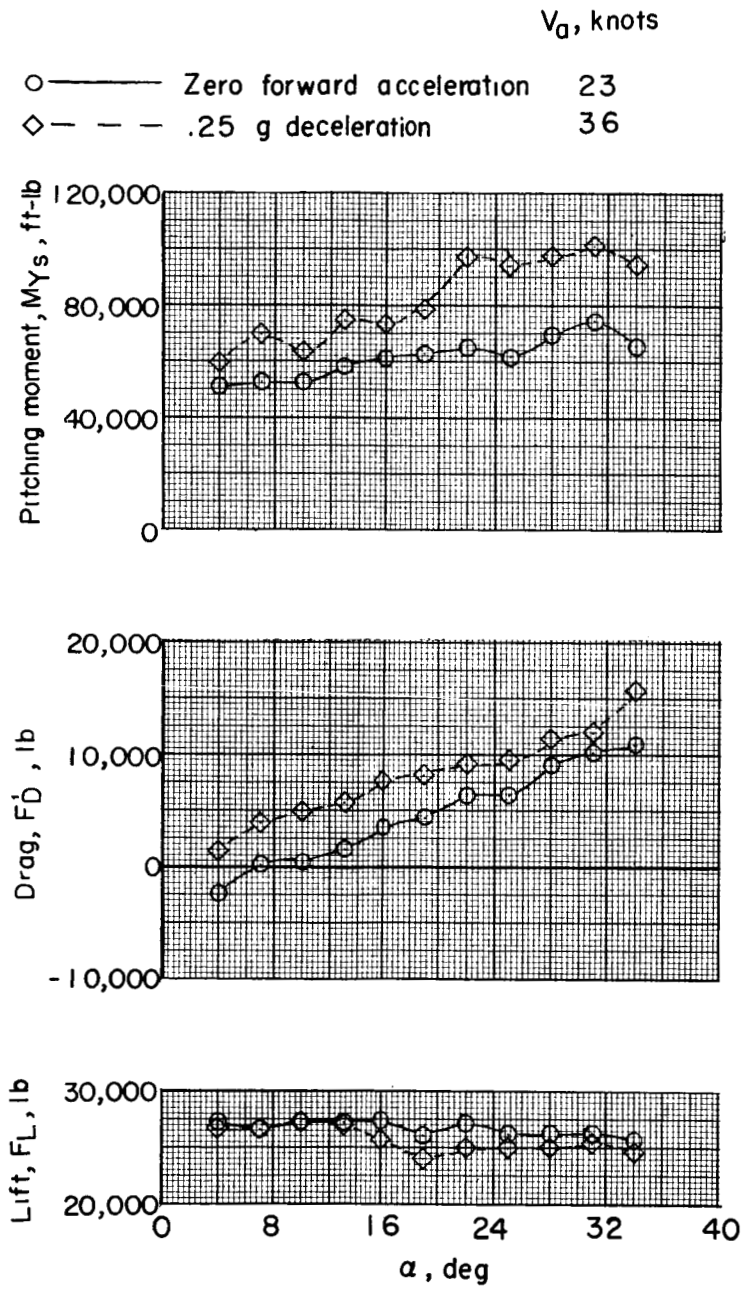

(d) $i_w = 65°$.

Figure 27.- Concluded.

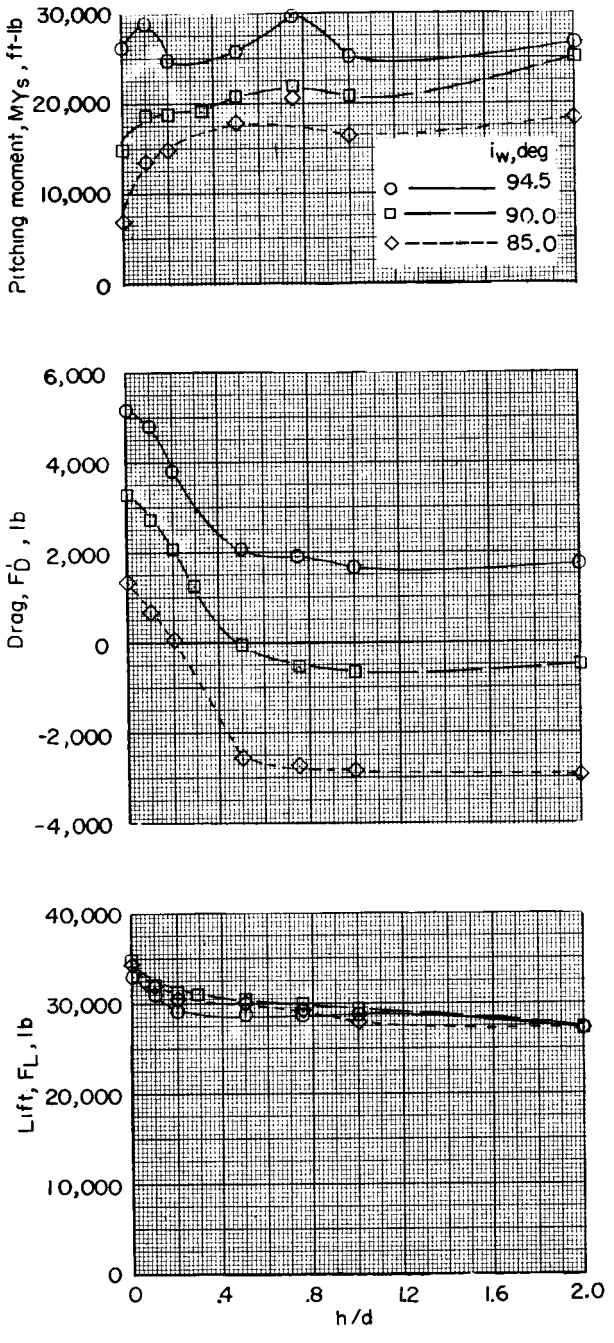

(a) $i_w = 85^\circ$, 90°, and 94.5°; $\alpha = 0^\circ$.

Figure 28.- Longitudinal characteristics in hovering flight when in ground proximity. Short wing; $i_t = 0.6^\circ$; $\delta_e = 0^\circ$; $\beta_F = 10^\circ$; $V_a = 0$.

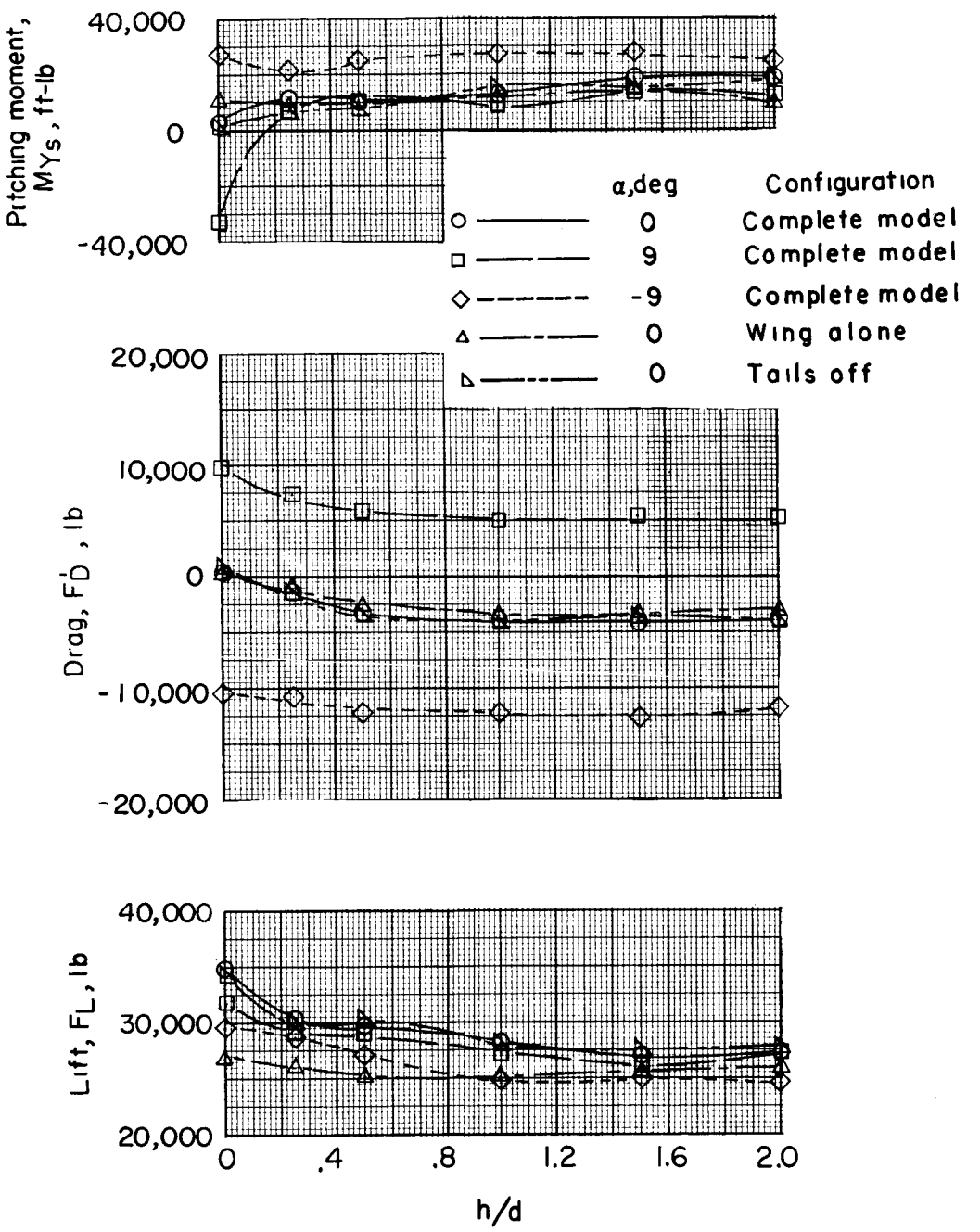

(b) $i_w = 85°$.

Figure 28.- Continued.

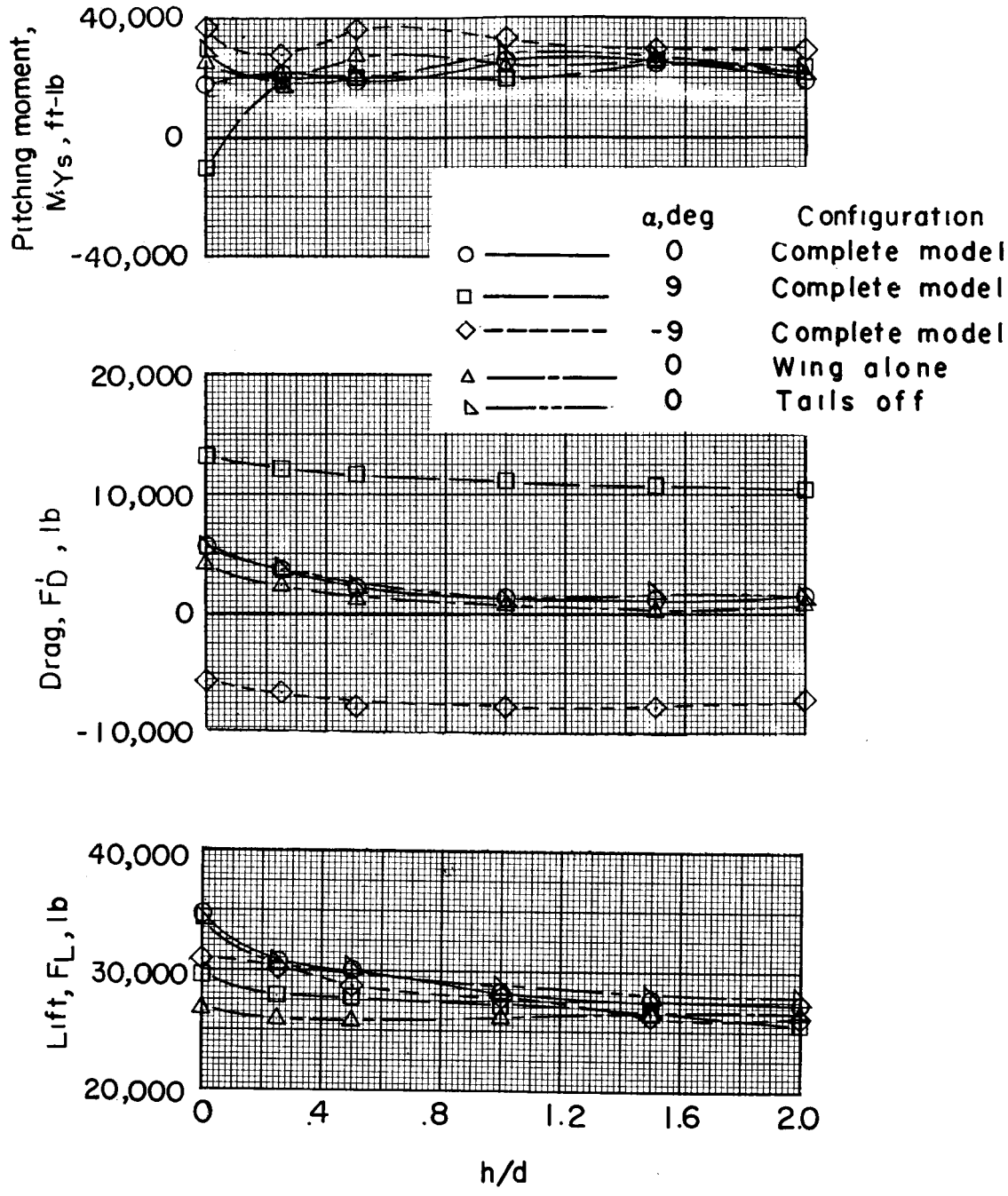

(c) $i_w = 94.5°$.

Figure 28.- Concluded.

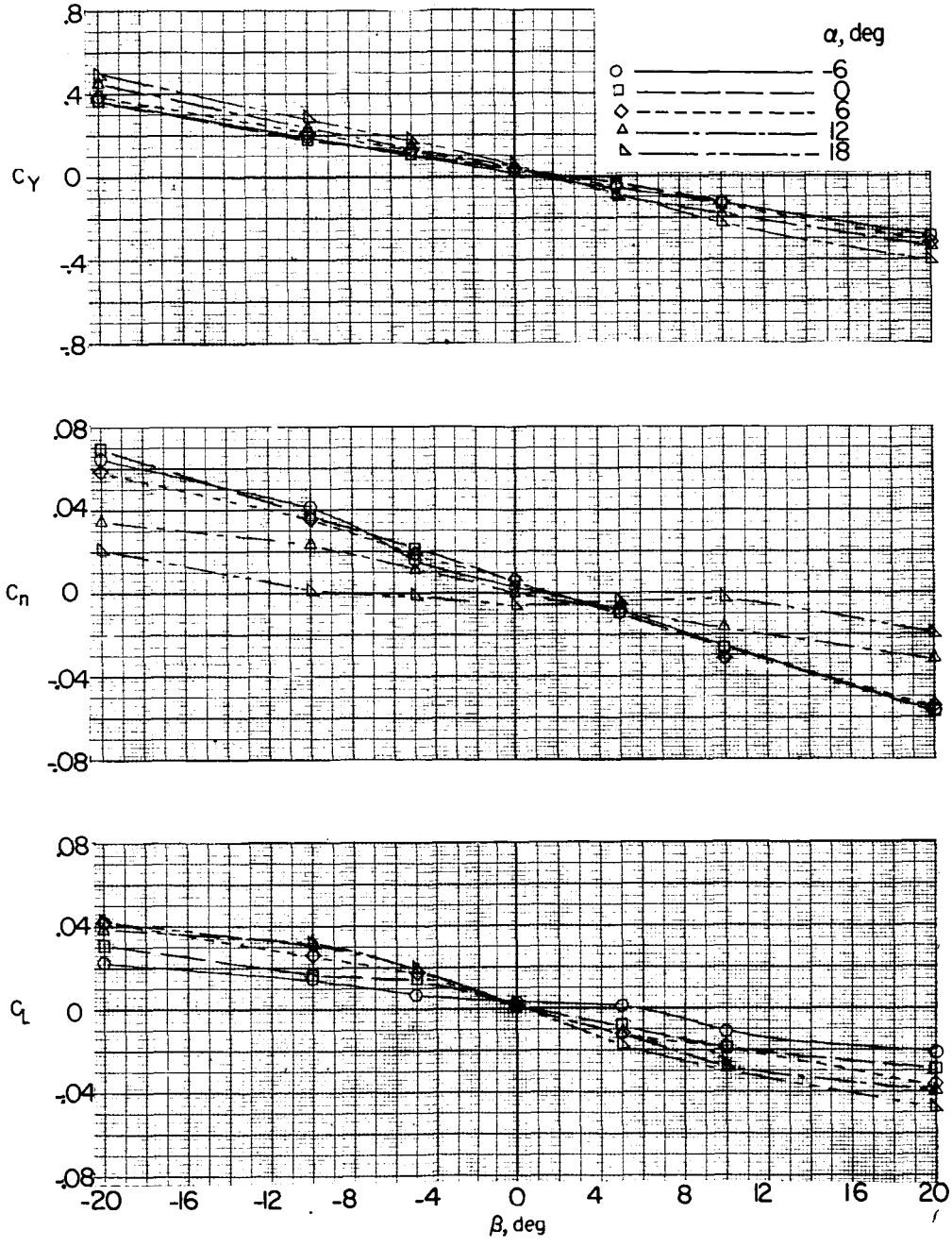

(a) Propellers off.

Figure 29.- Lateral stability characteristics at various thrust coefficients. $i_w = 4.5^\circ$; short wing; tails off; $\delta_a = \delta_r = 0^\circ$; $\beta_F = 30^\circ$.

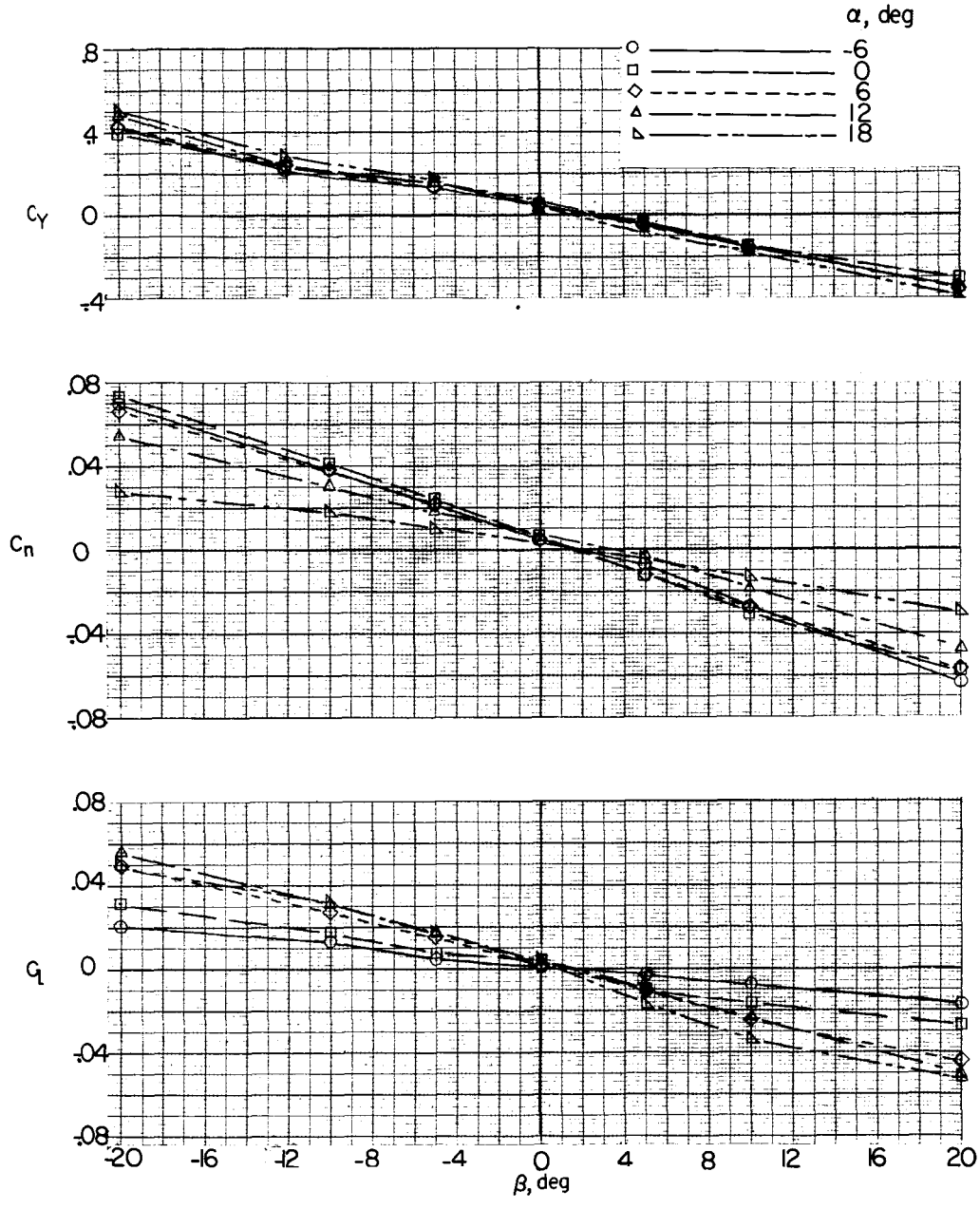

(b) $T_c' = -0.15$.

Figure 29.- Continued.

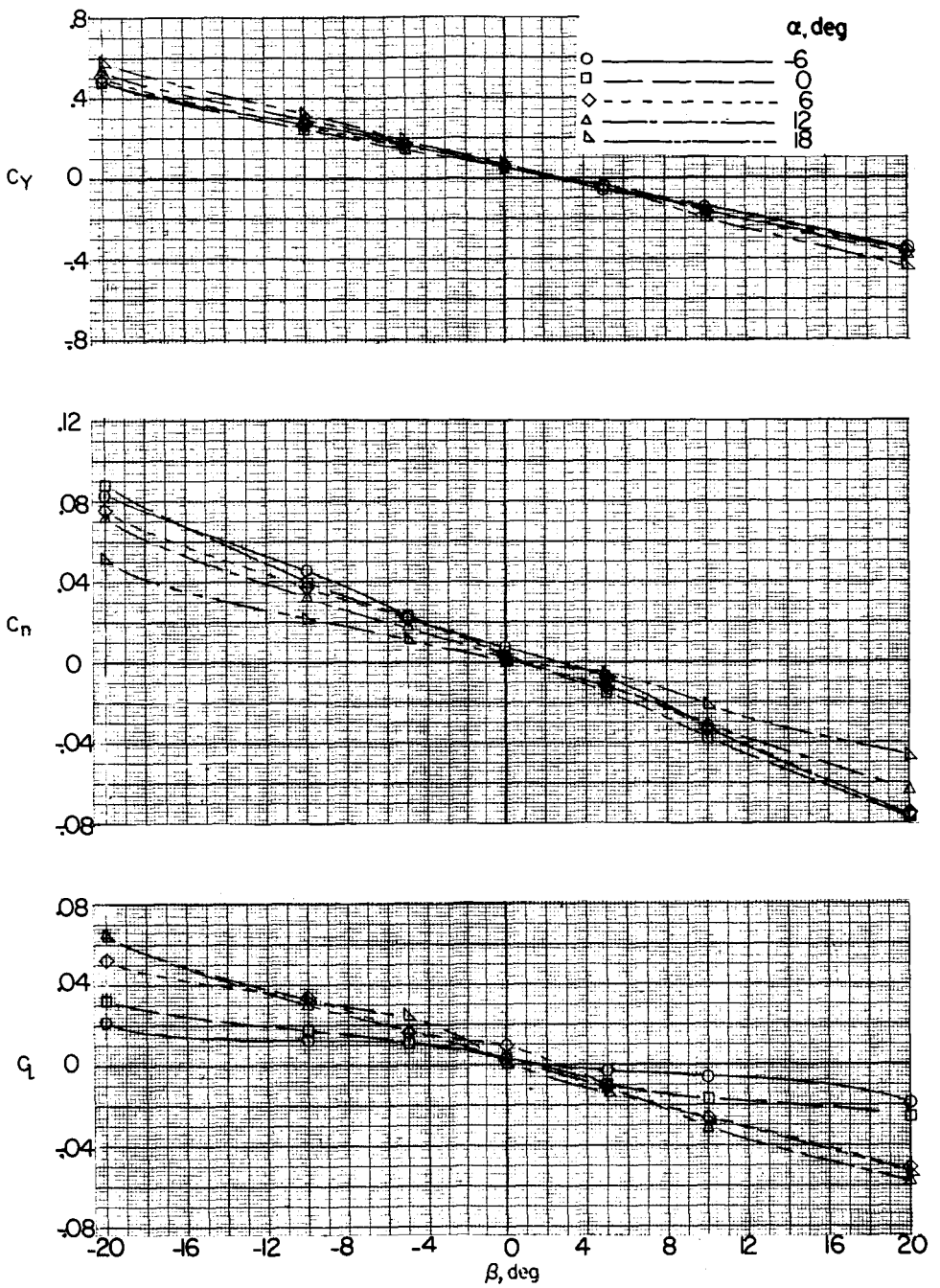

(c) $T_c' = 0.06$.

Figure 29.- Continued.

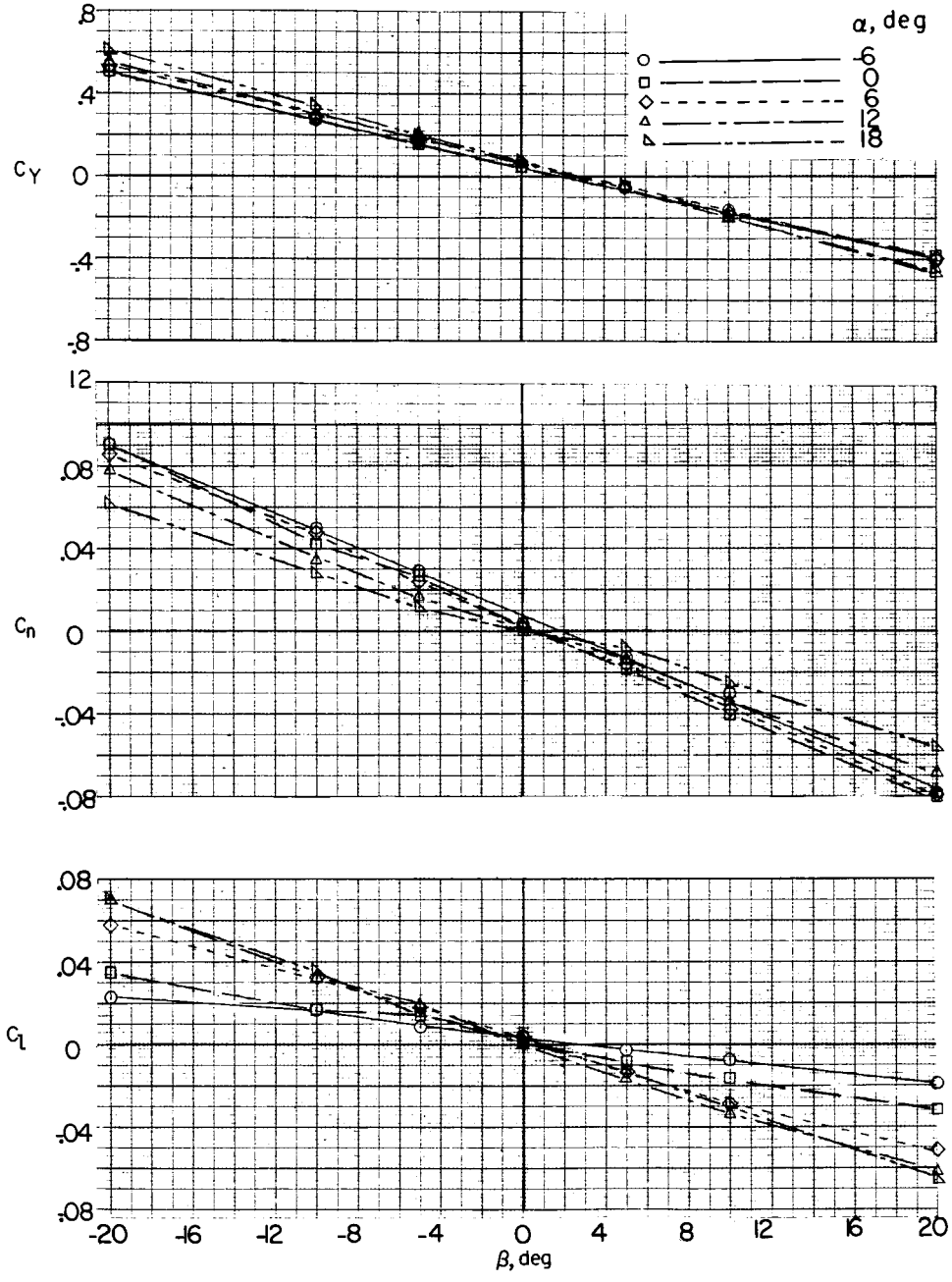

(d) $T_c' = 0.24$.

Figure 29.- Continued.

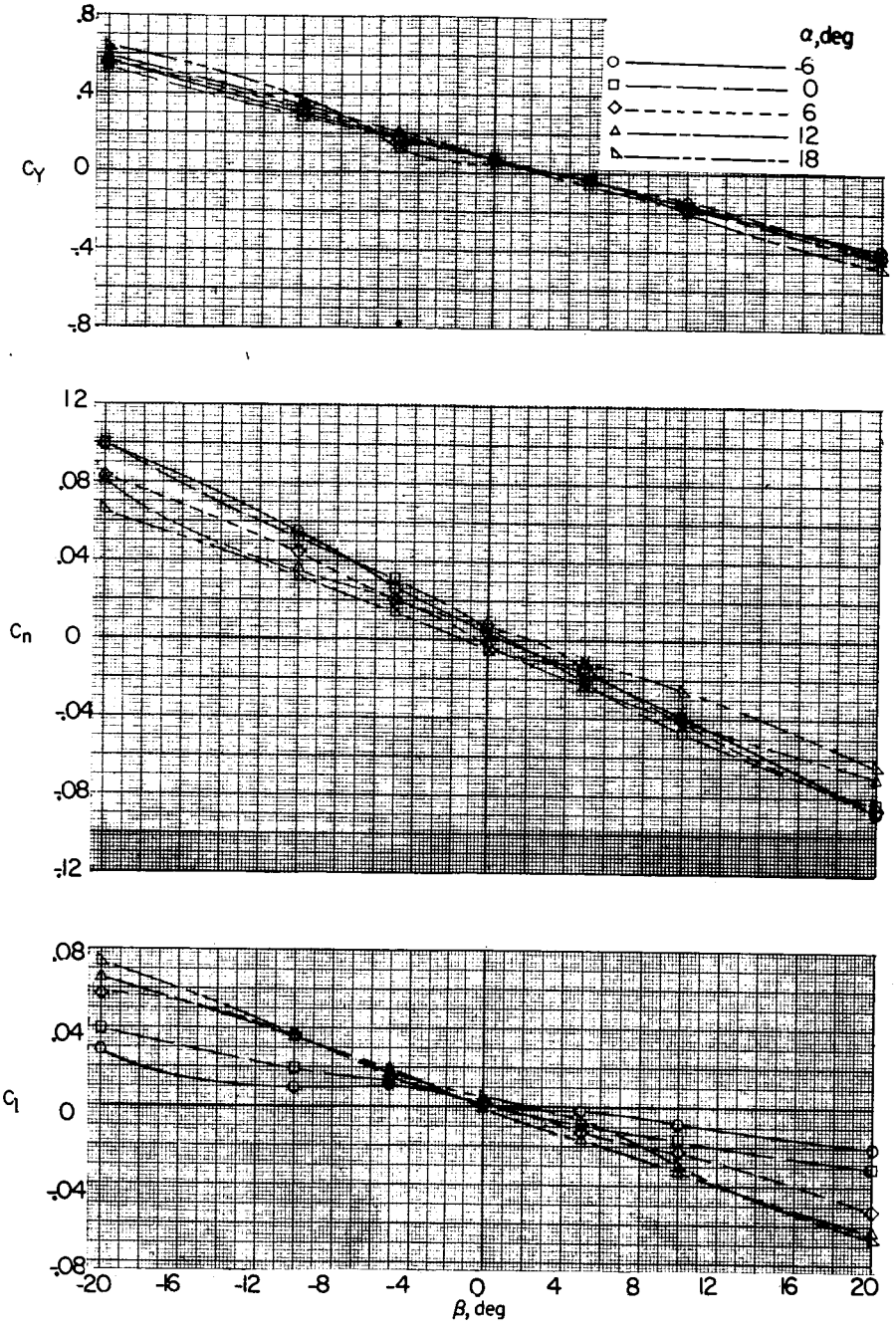

(e) $T_c' = 0.51$.

Figure 29.- Continued.

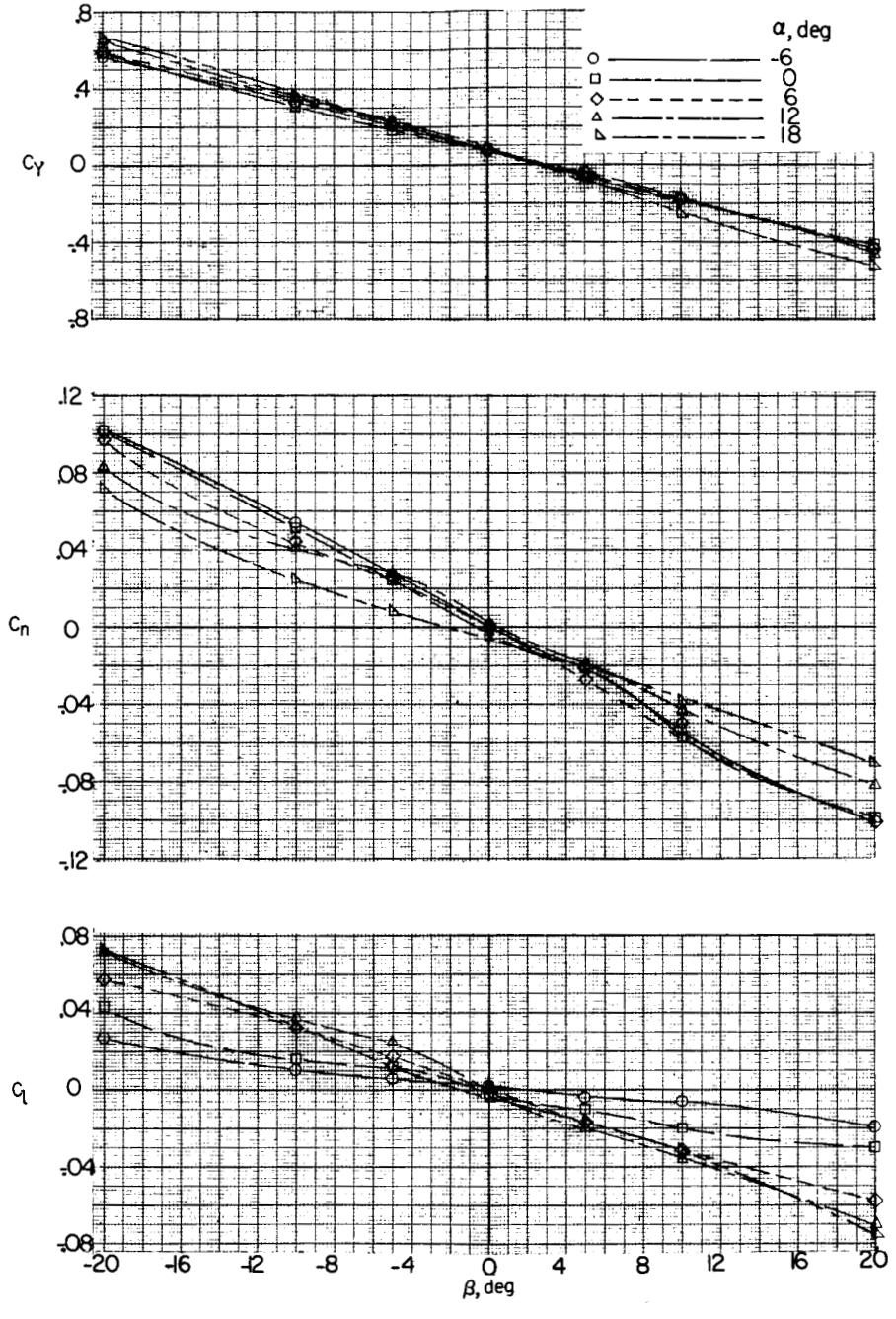

(f) $T_c' = 0.77$.

Figure 29.- Concluded.

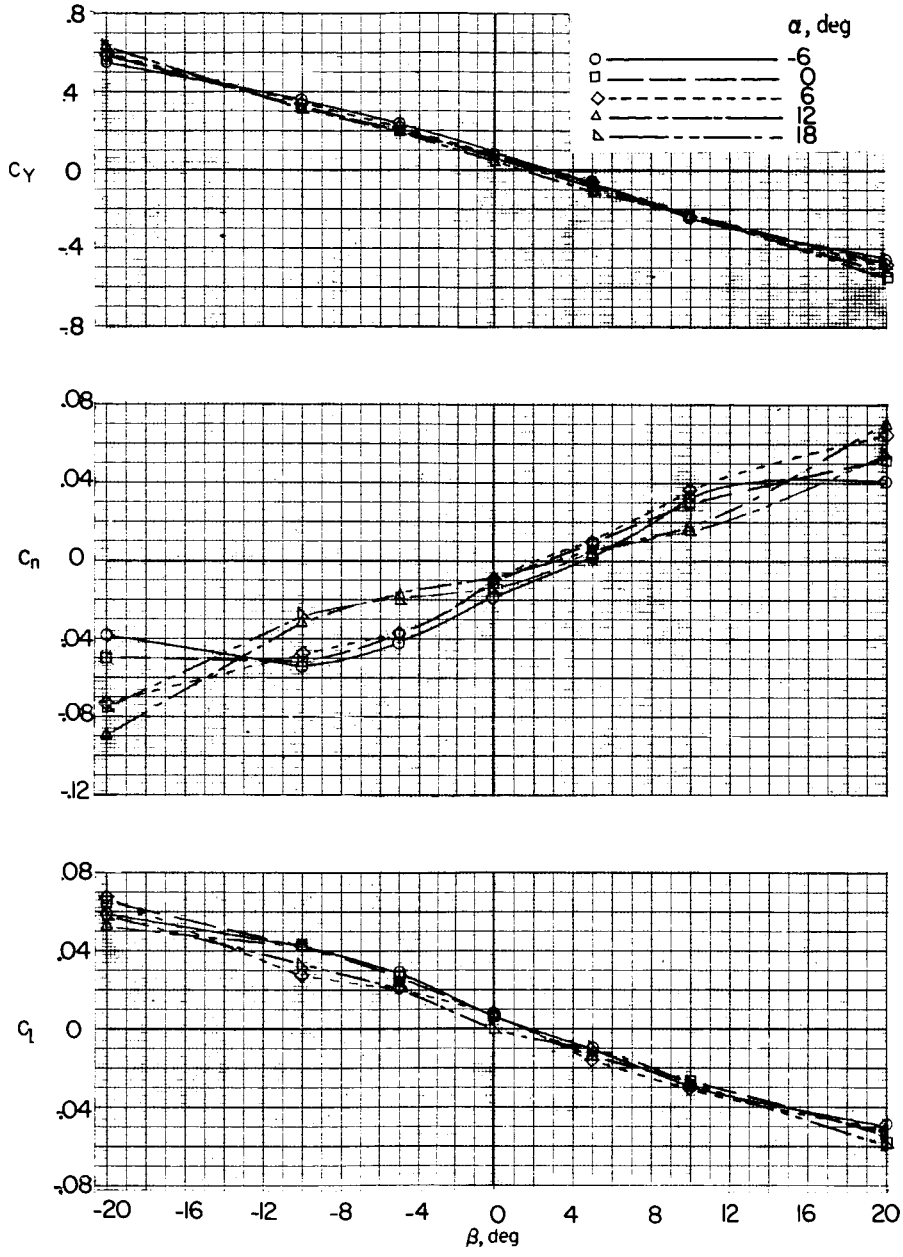

(a) Propellers off.

Figure 30.- Lateral stability characteristics at various thrust coefficients. $i_w = 4.5^\circ$; short wing; $i_t = 0.6^\circ$; $\delta_e = \delta_a = \delta_r = 0^\circ$; $\beta_F = 30^\circ$.

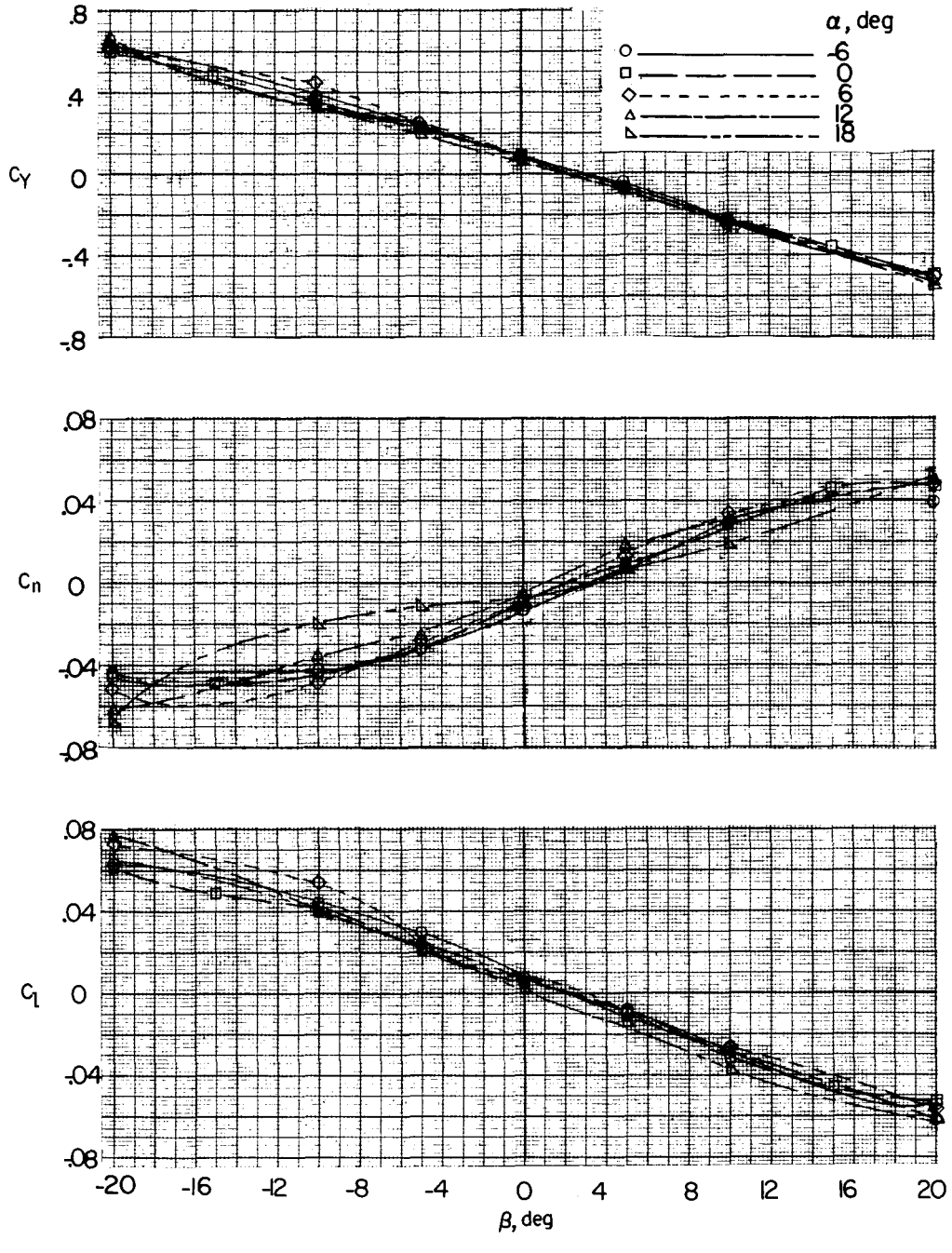

(b) $T_c' = -0.15$.

Figure 30.- Continued.

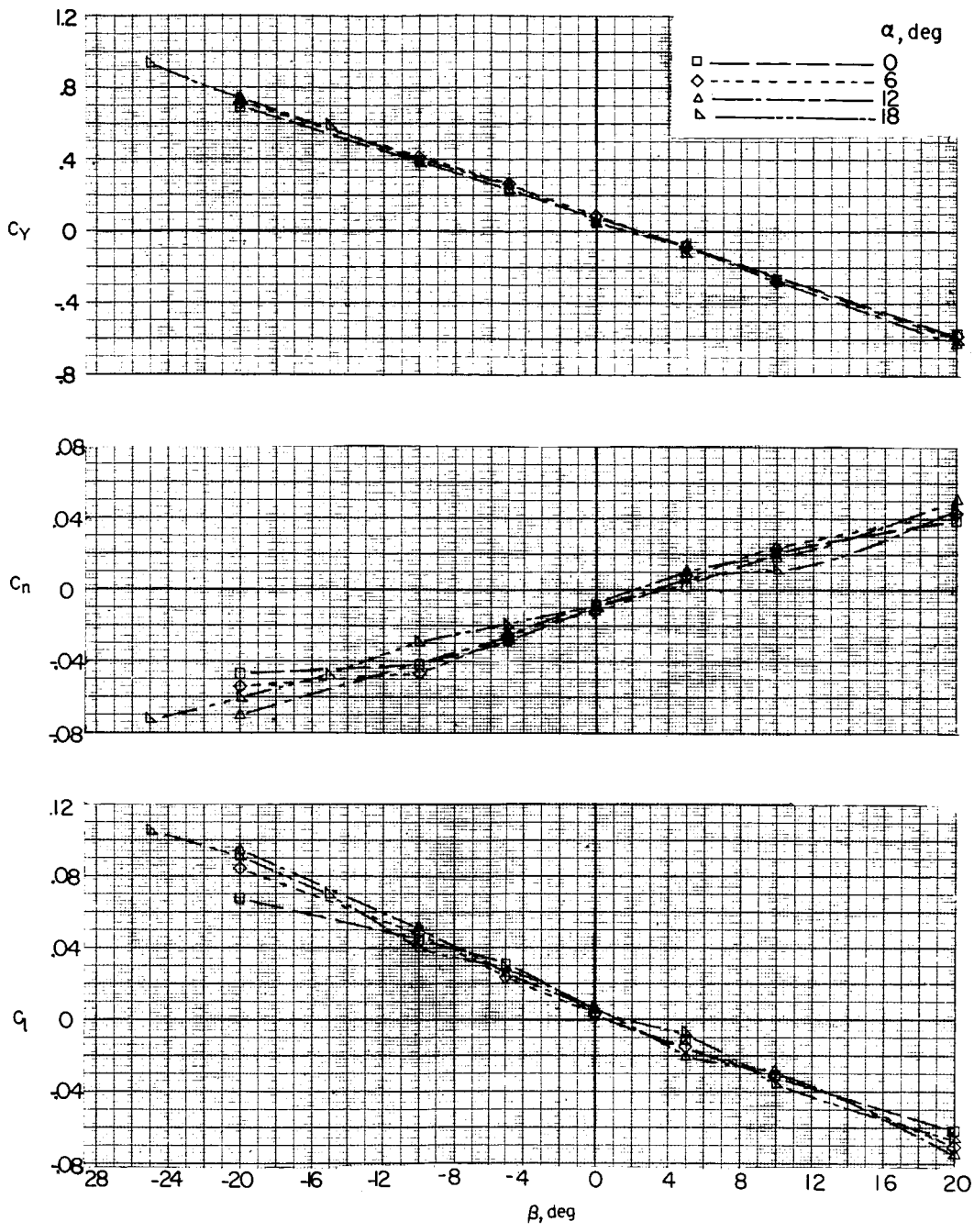

(c) $T_c' = 0.06$.

Figure 30.- Continued.

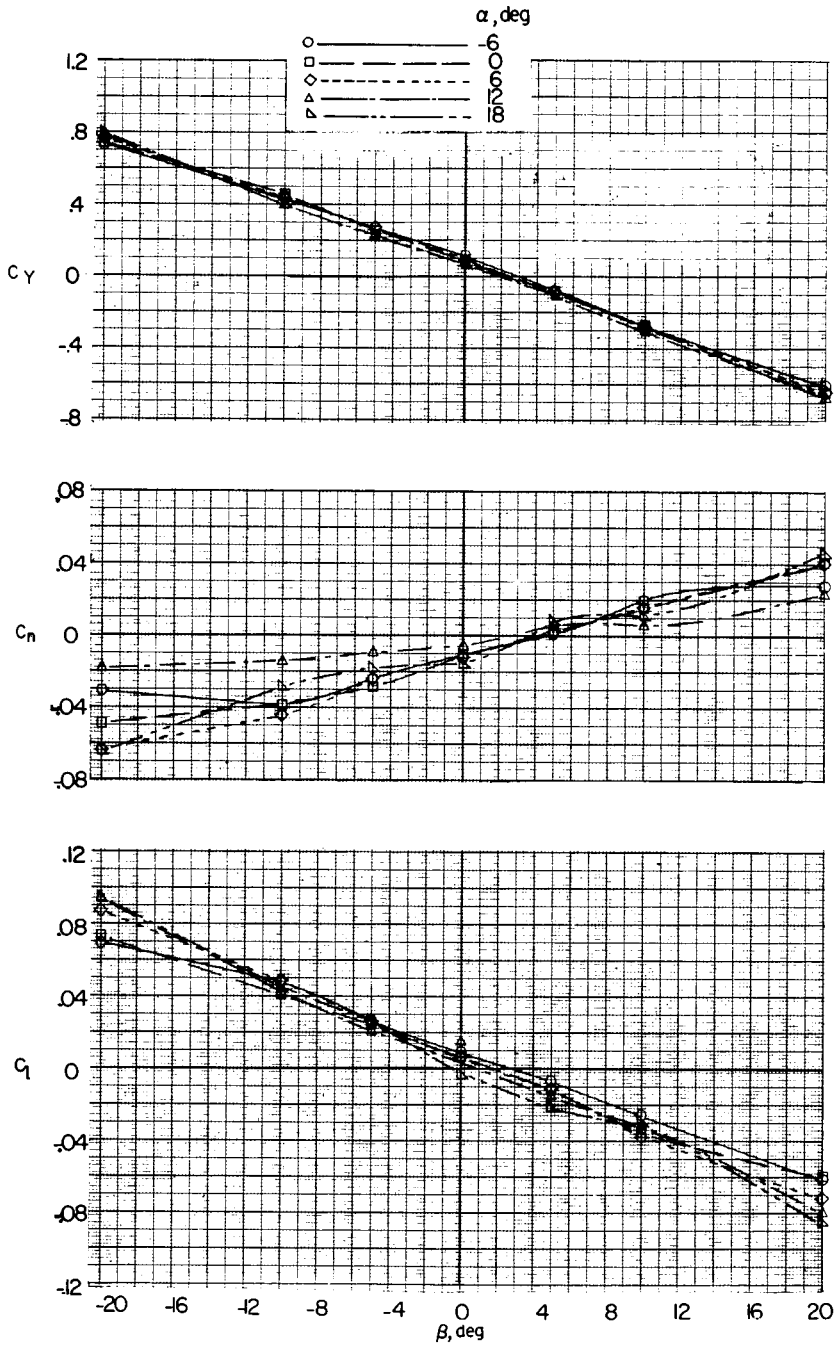

(d) $T_c' = 0.24$.

Figure 30.- Continued.

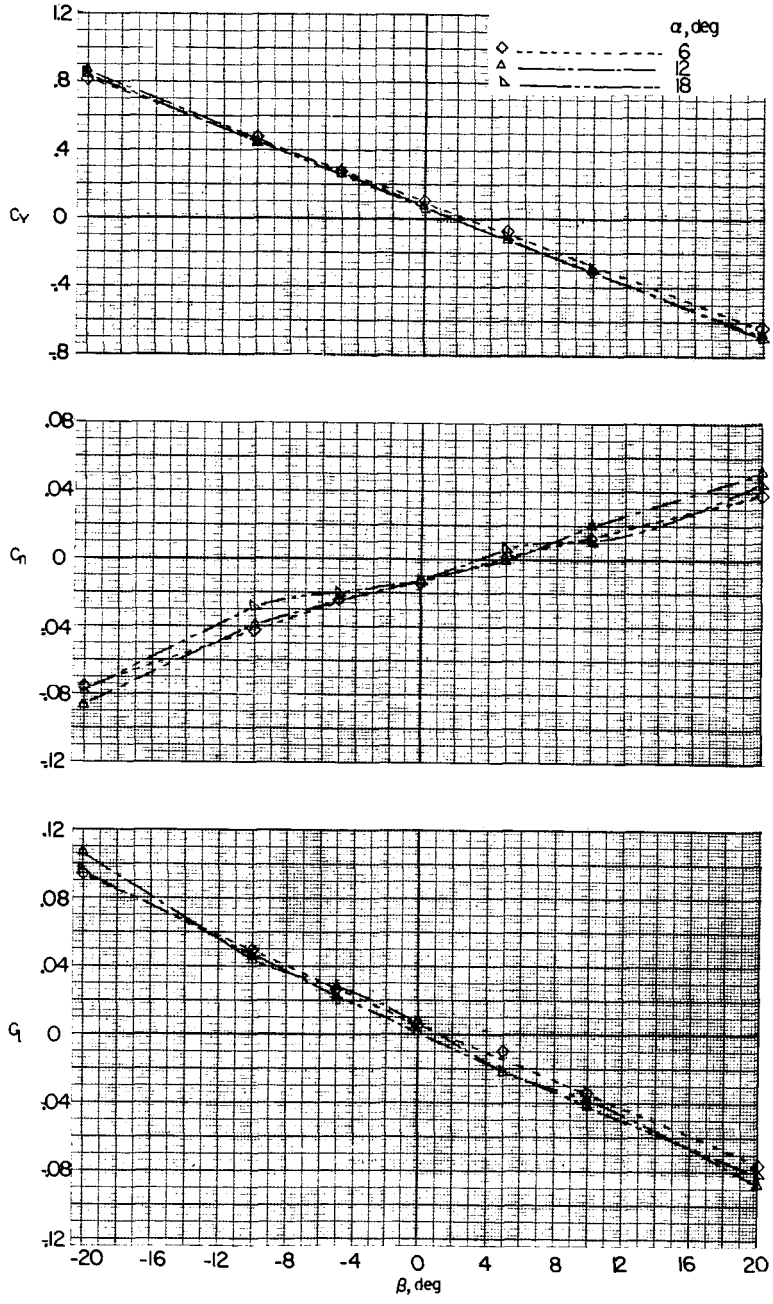

(e) $T_c' = 0.51$.

Figure 30.- Continued.

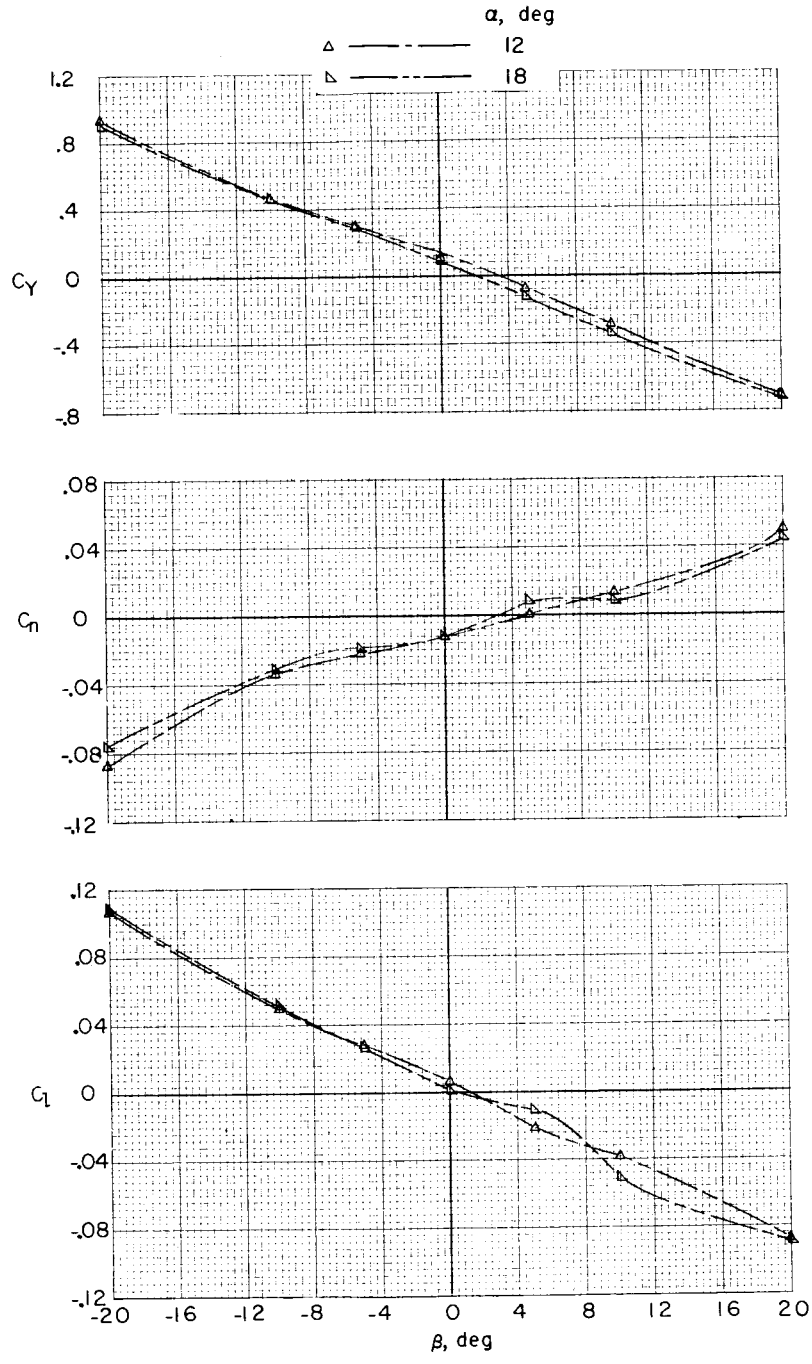

(f) $T_c' = 0.77$.

Figure 30.- Concluded.

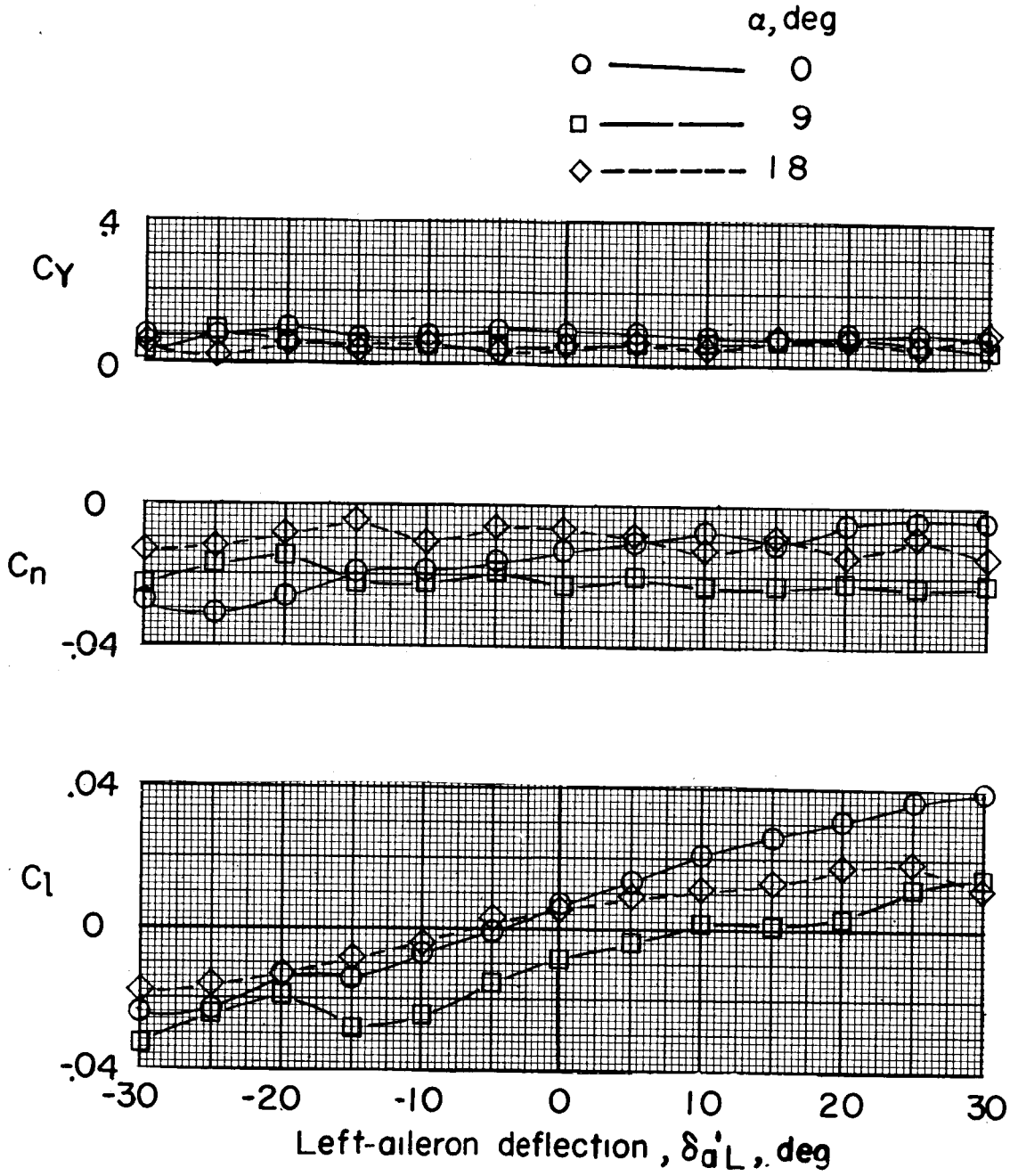

(a) Propellers off; $\delta_r = 0^\circ$.

Figure 31.- Lateral control characteristics in normal forward flight. $i_w = 4.5^\circ$; short wing; $\delta_{a'R} = 0^\circ$; $\beta = 0^\circ$; $\beta_F = 30^\circ$.

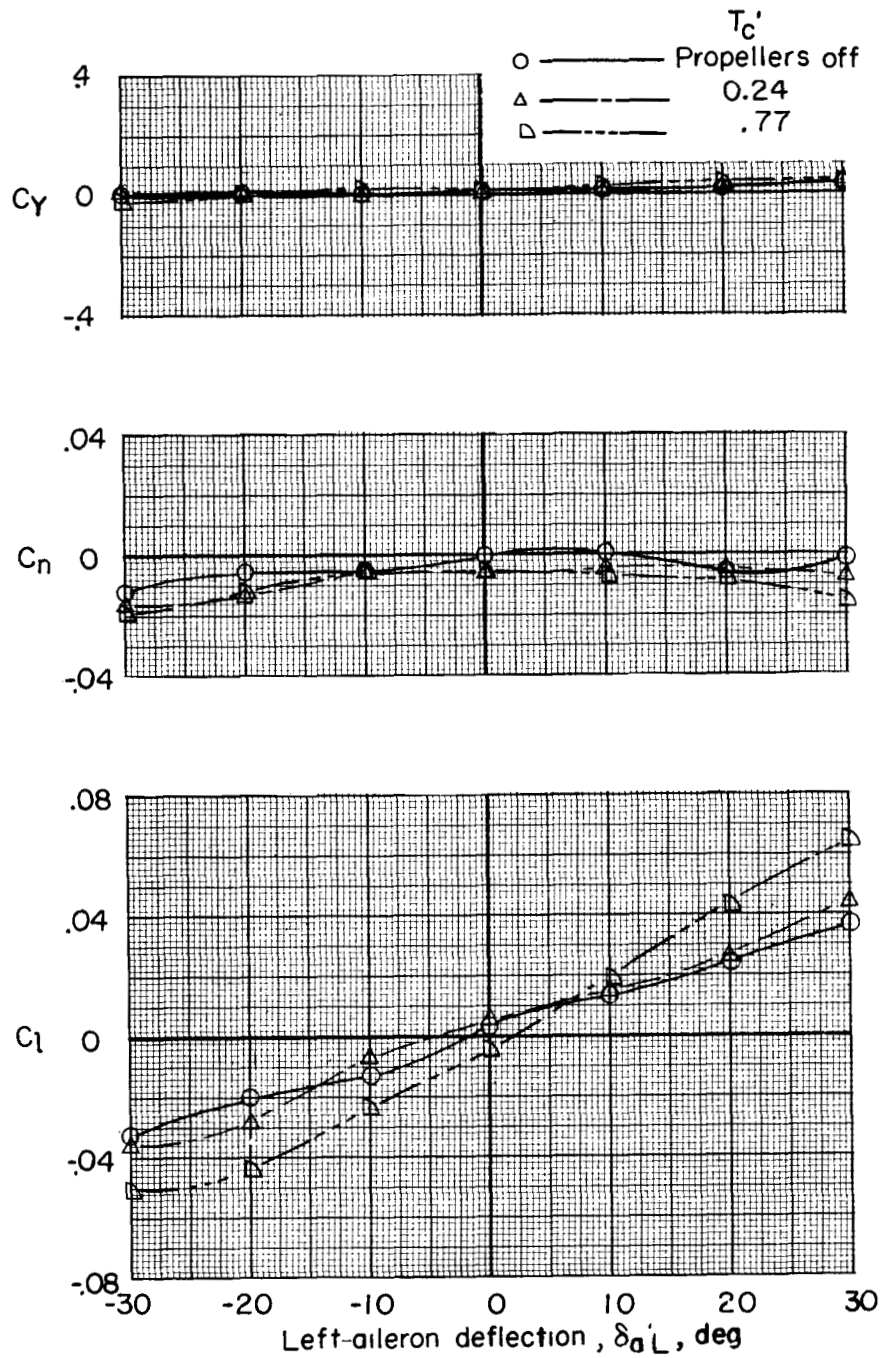

(b) $\delta_r = 0^\circ$; $\alpha = 0^\circ$.

Figure 31.- Continued.

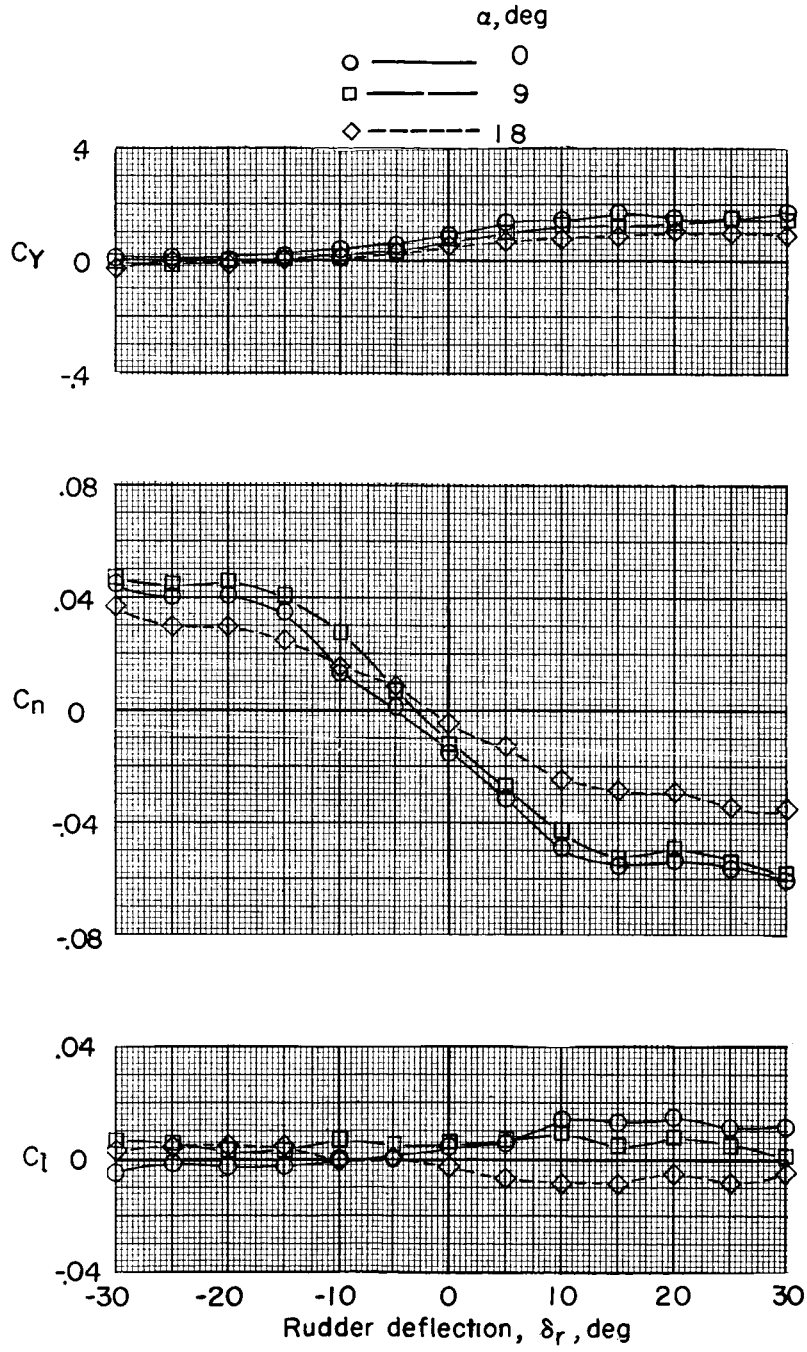

(c) $\delta_a{}'_L = 0^o$; $T_c{}' = -0.15$.

Figure 31.- Concluded.

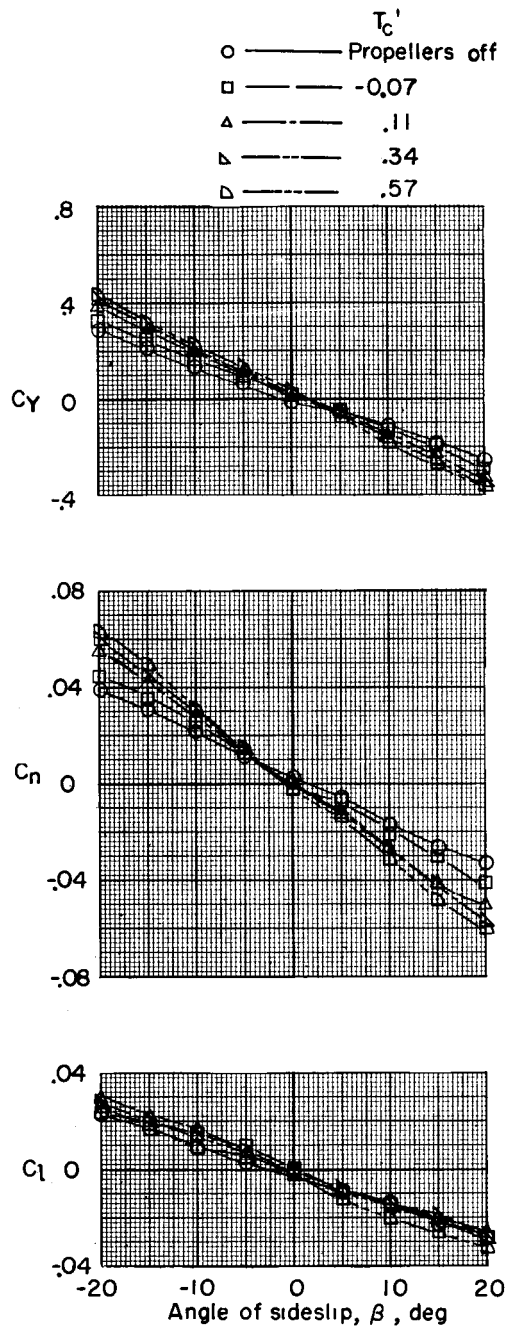

(a) Tails off.

Figure 32.- Lateral stability characteristics of long-wing configuration at various thrust coefficients. $i_w = 4.5^\circ$; $\delta_a = \delta_r = \alpha = 0^\circ$; $\beta_F = 30^\circ$.

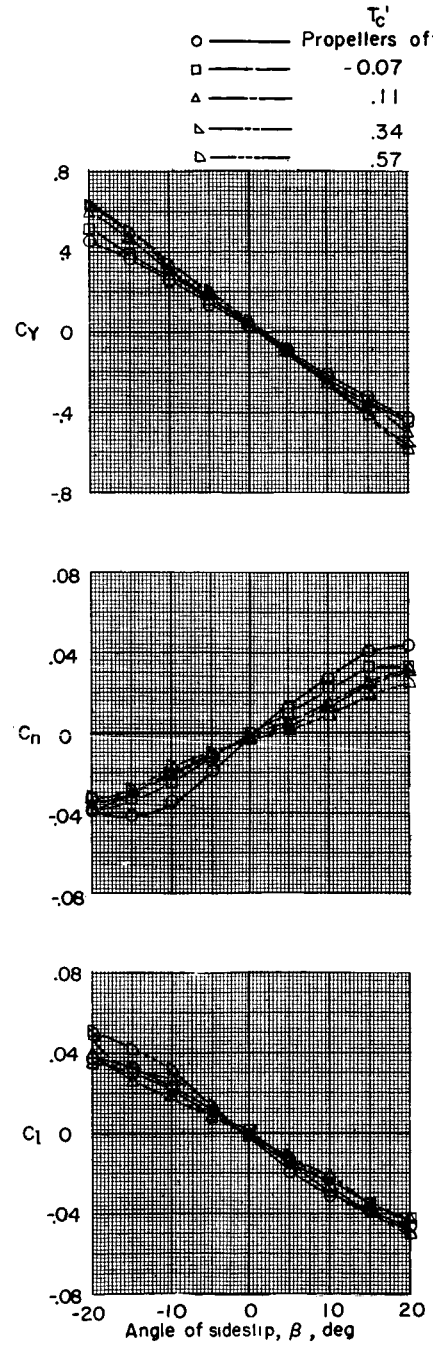

(b) Complete model.

Figure 32.- Concluded.

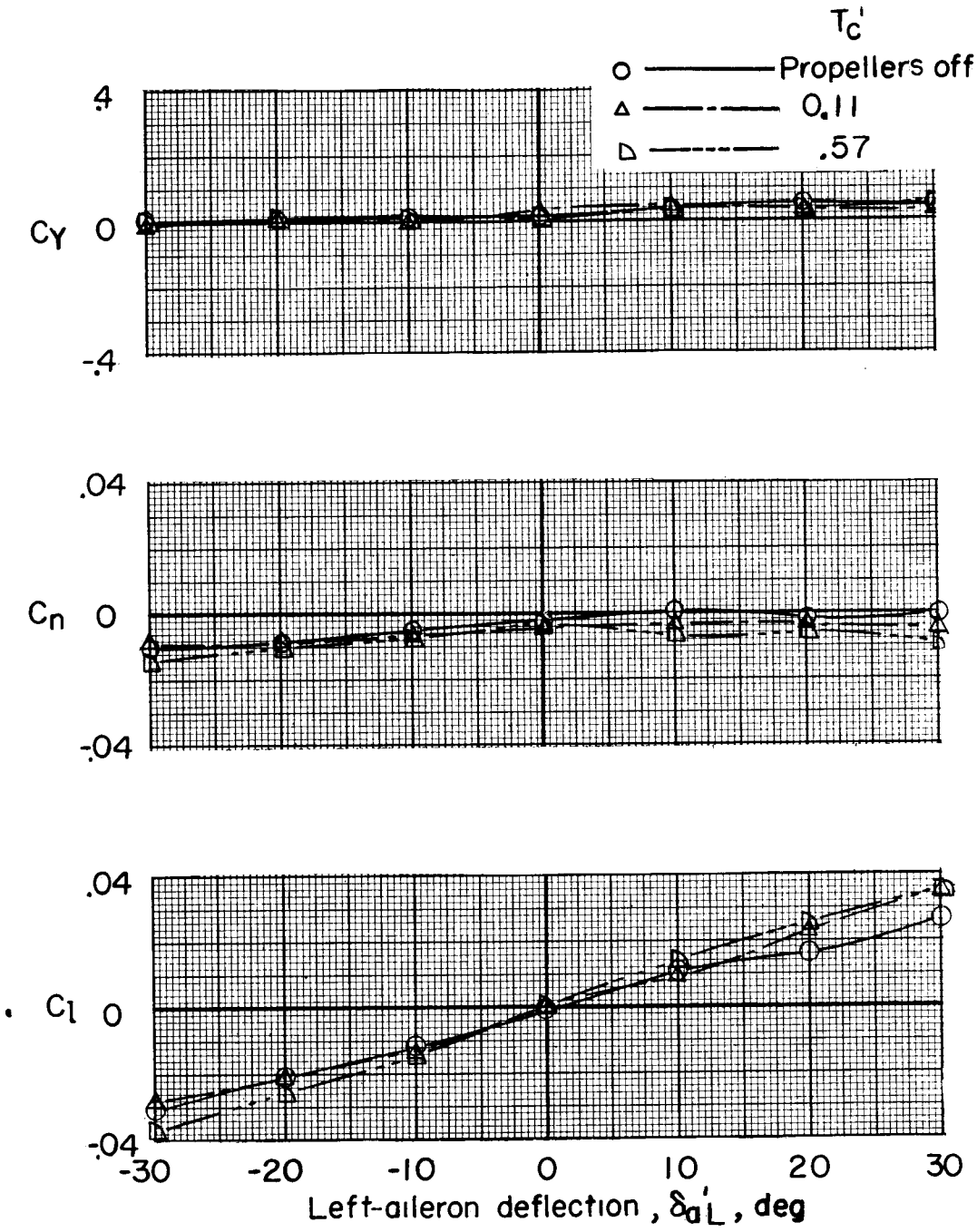

(a) $\delta_r = \alpha = 0^\circ$.

Figure 33.- Lateral control characteristics of long-wing configuration in normal forward flight. $i_w = 4.5^\circ$; $\delta_{a'R} = \beta = 0^\circ$; $\beta_F = 30^\circ$.

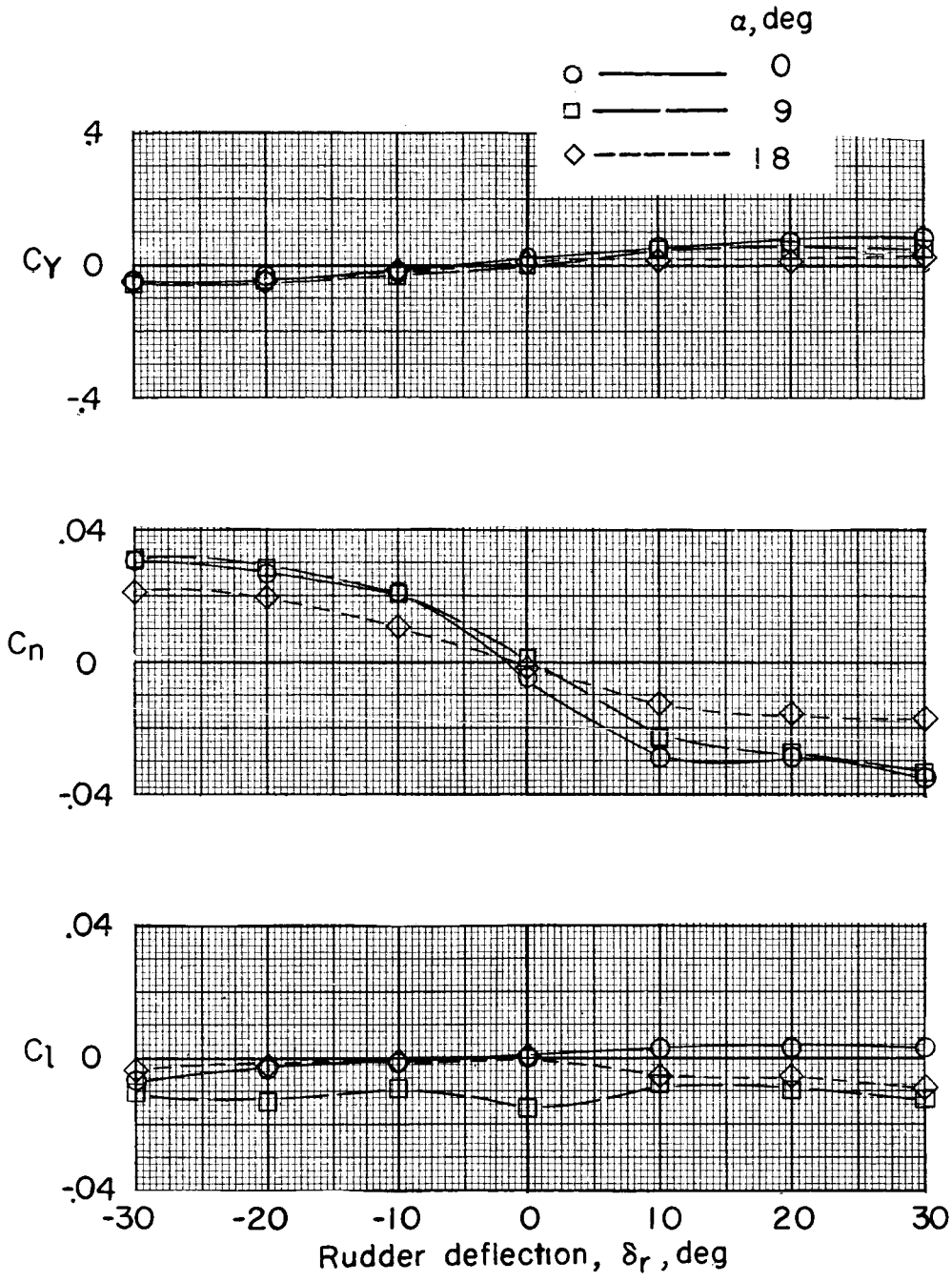

(b) $\delta_a'_L = 0^\circ$; $T_c' = -0.15$.

Figure 33.- Concluded.

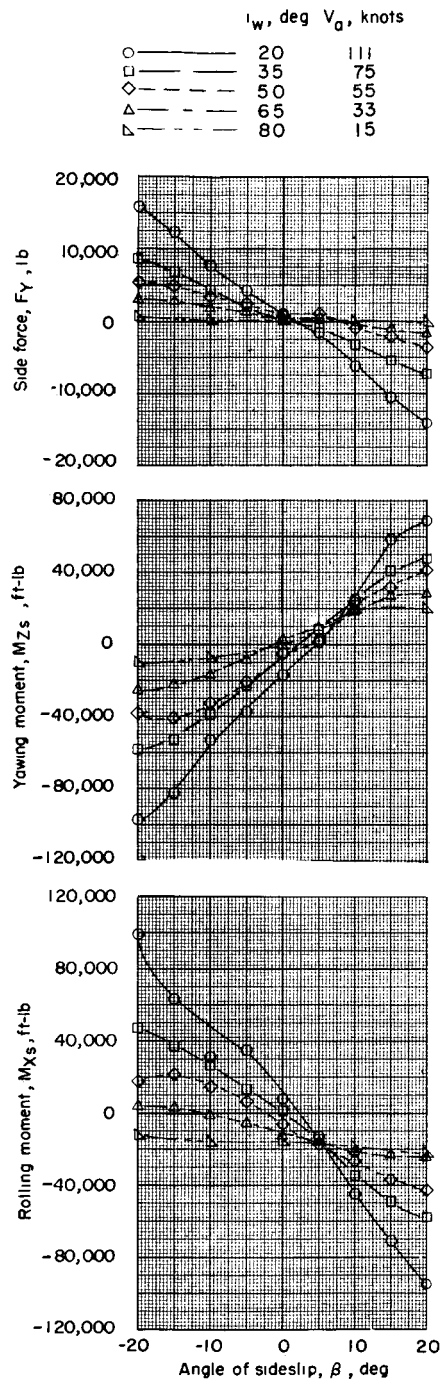

Figure 34.- Lateral stability characteristics in transition flight. Short wing; $\delta_a = \delta_r = \alpha = 0^\circ$; zero acceleration at $\beta = 0^\circ$; $\beta_F = 10^\circ$.

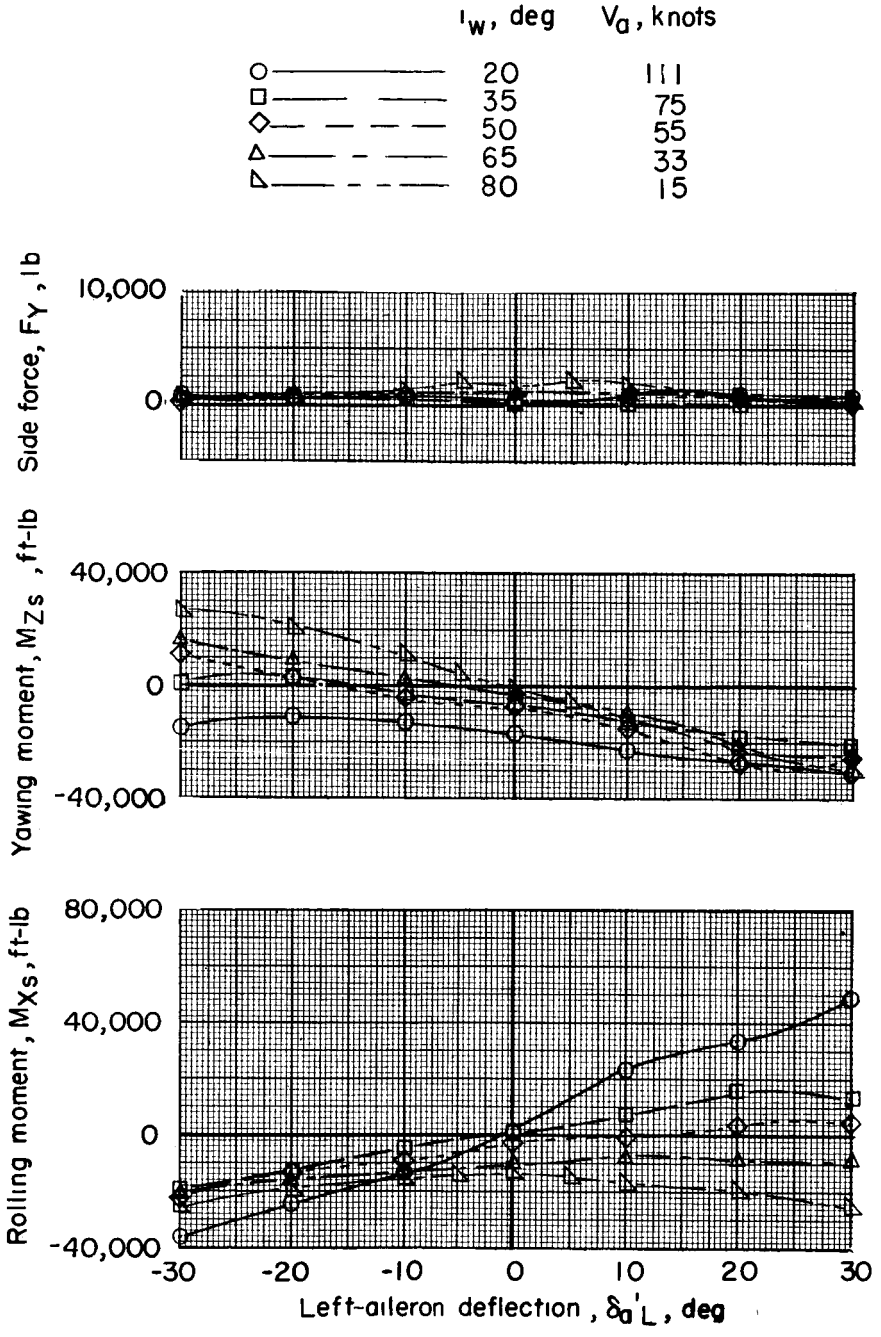

(a) $\delta_r = 0^\circ$; $\beta_F = 10^\circ$; zero acceleration at $\delta_a'_L = 0^\circ$.

Figure 35.- Lateral control characteristics in transition flight. Short wing; $\delta_a'_R = \beta = \alpha = 0^\circ$.

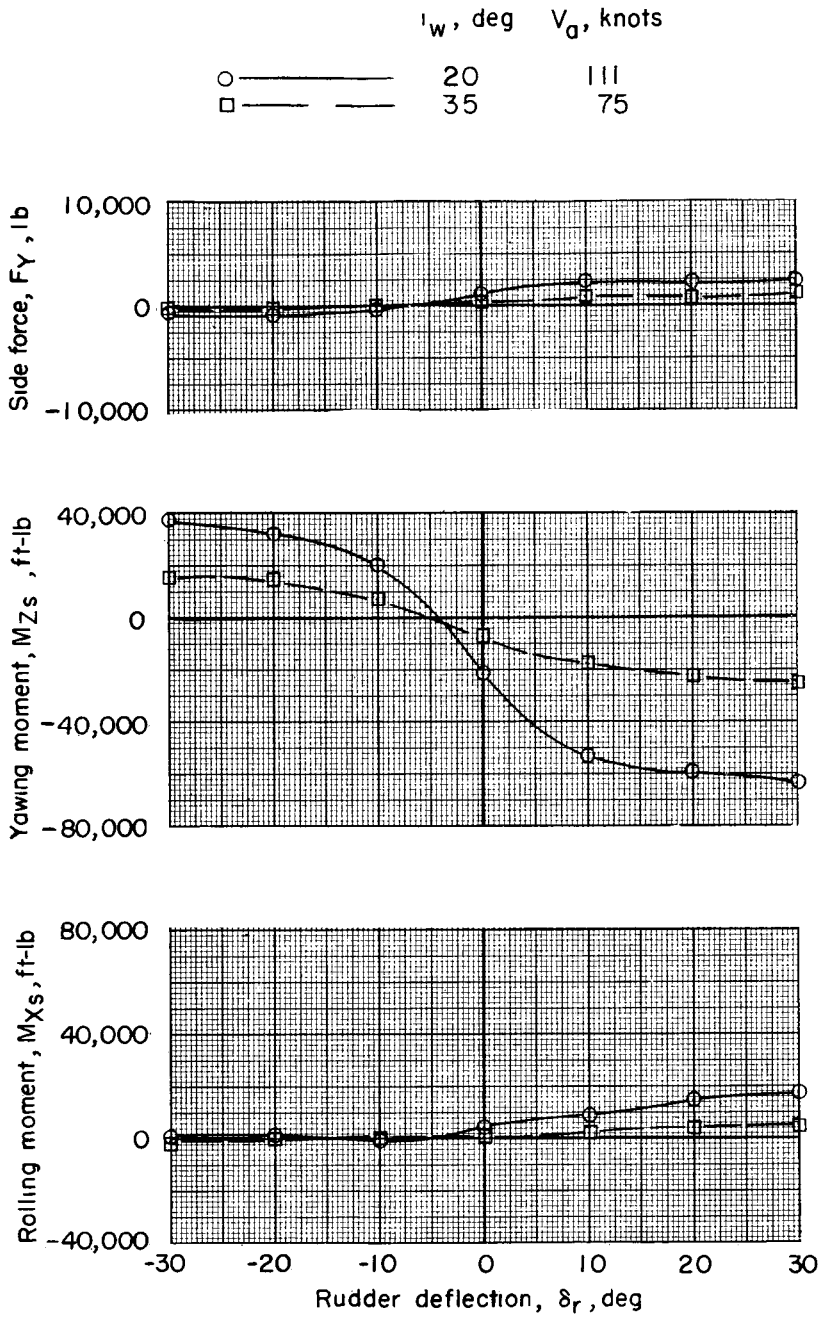

(b) $\delta_{a'L} = 0^\circ$; $\beta_F = 10^\circ$; zero acceleration at $\delta_r = 0^\circ$.

Figure 35.- Continued.

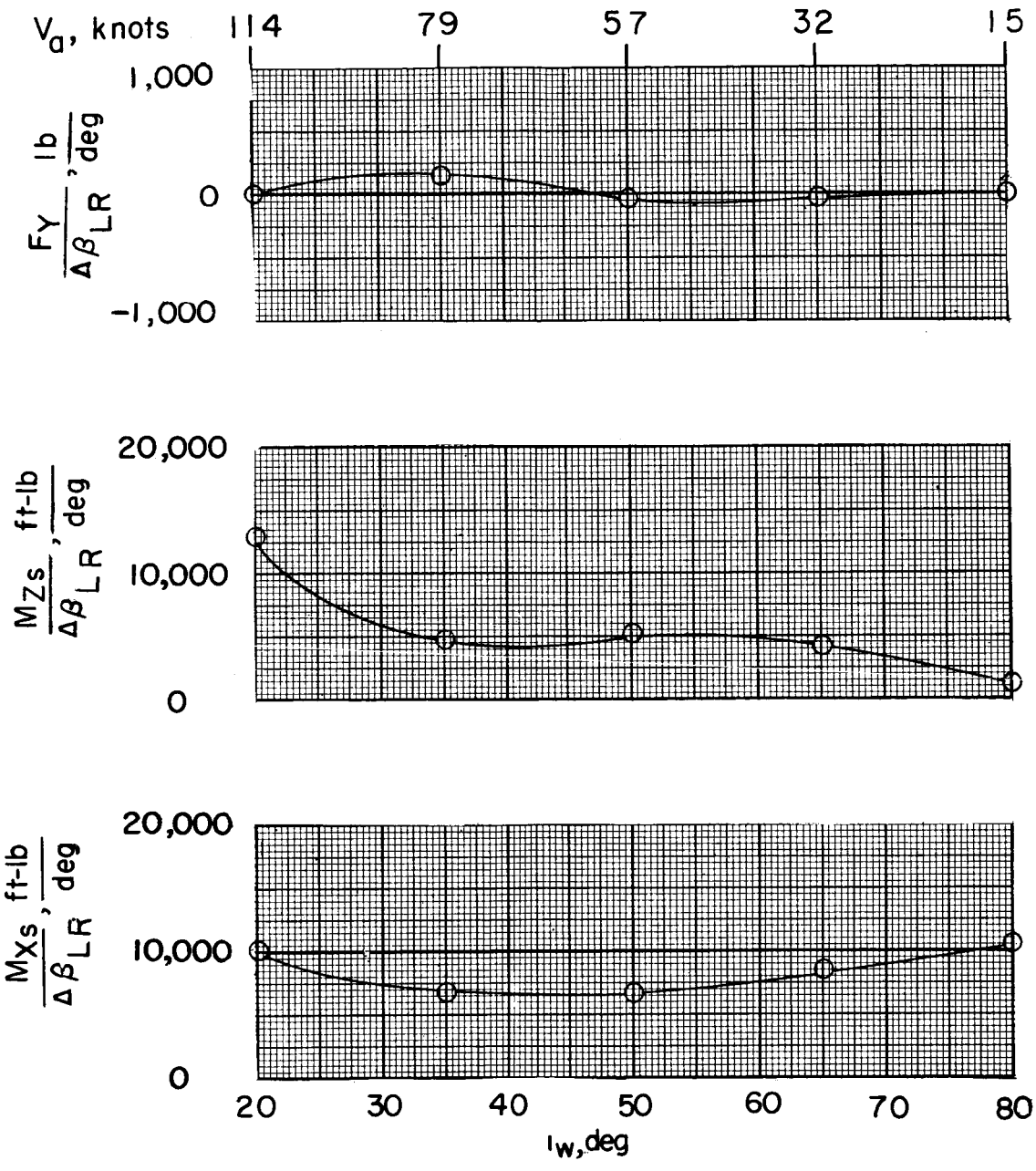

(c) $\delta_a{}'_L = \delta_r = 0^\circ$; $\beta_F = \beta_{RR} = 10^\circ$; β_{LR} varied between 9° and 12°; zero acceleration.

Figure 35.- Concluded.

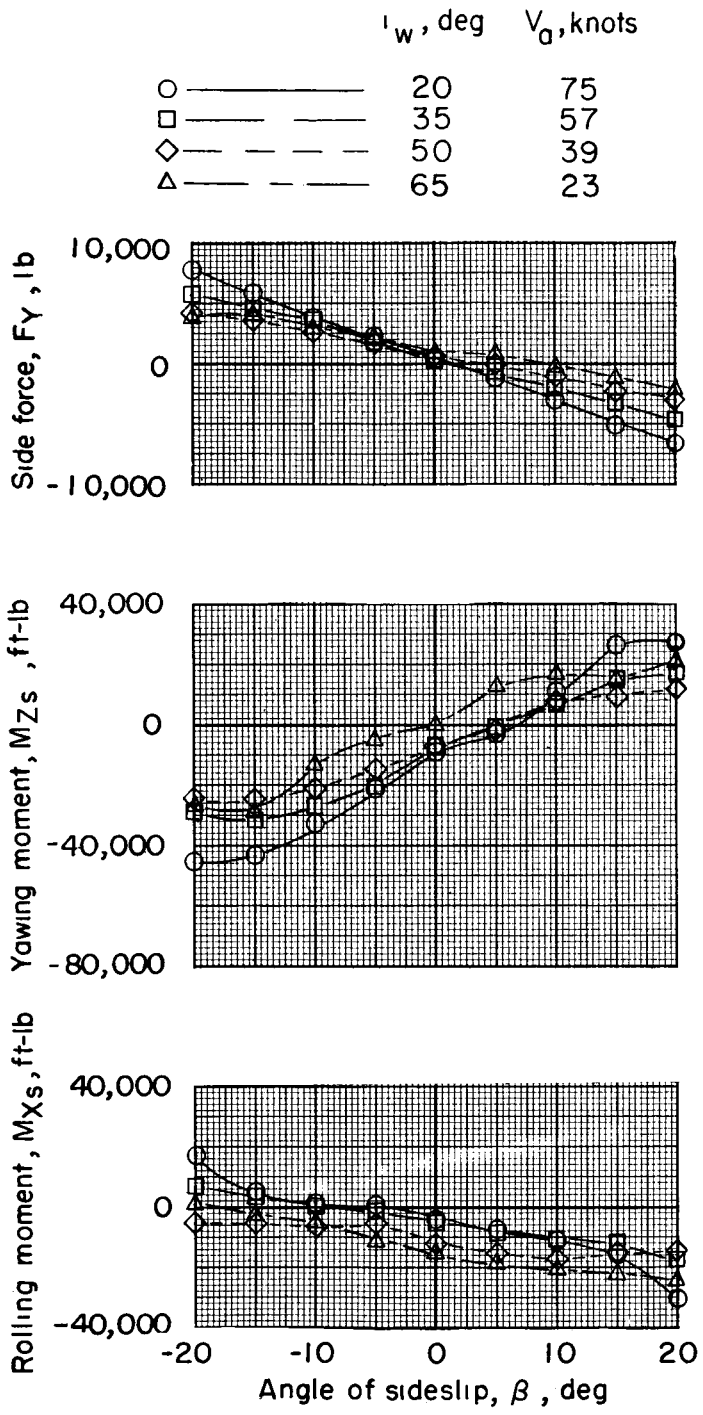

Figure 36.- Lateral stability characteristics of long-wing configuration in transition flight. $\delta_a = \delta_r = \alpha = 0^o$; zero acceleration at $\beta = 0^o$; $\beta_F = 10^o$.

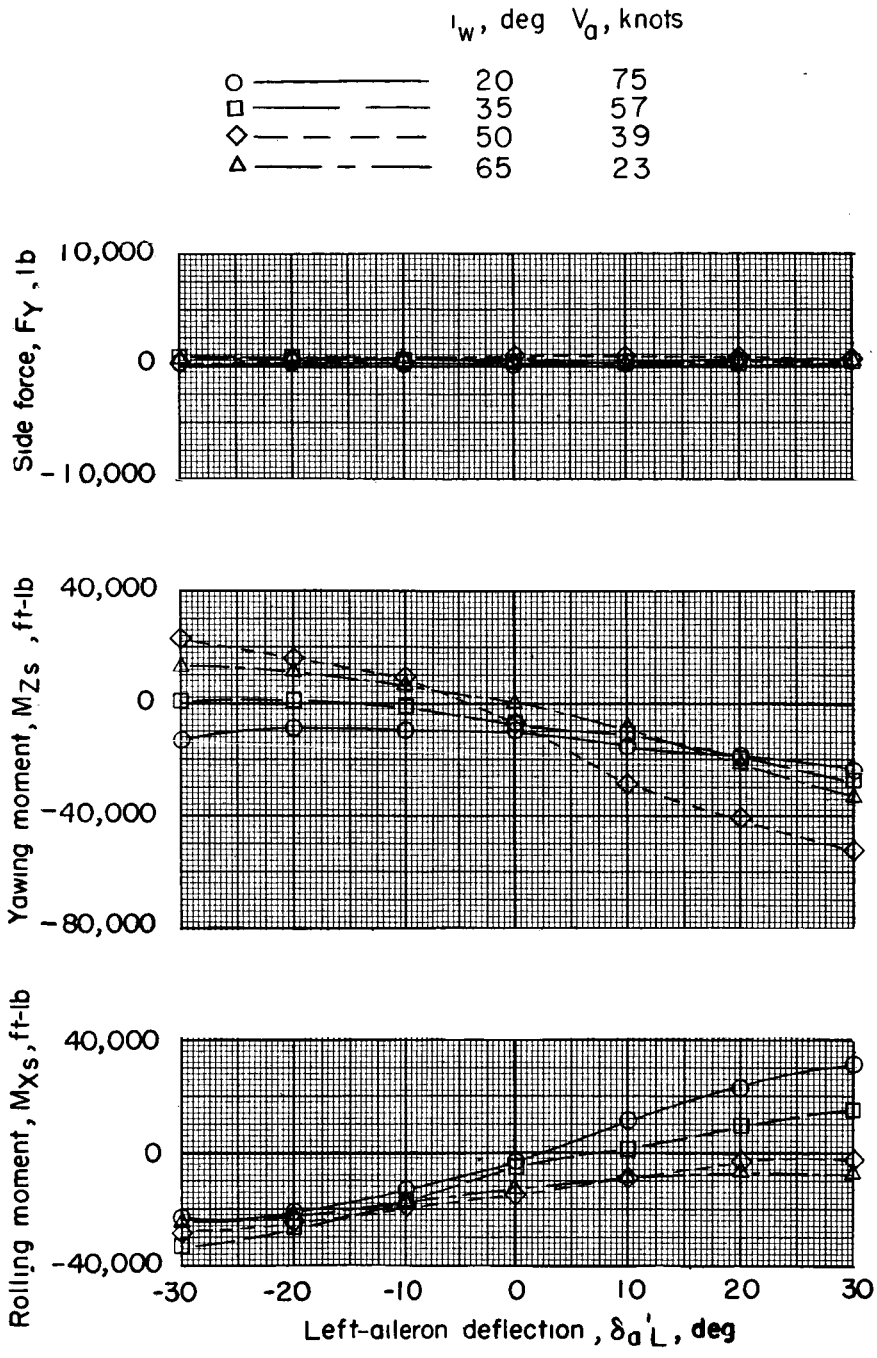

(a) $\delta_r = 0^\circ$; zero acceleration at $\delta_{a'L} = 0^\circ$.

Figure 37.- Lateral control characteristics of long-wing configuration in transition flight. $\delta_{a'R} = \beta = \alpha = 0^\circ$; $\beta_F = 10^\circ$.

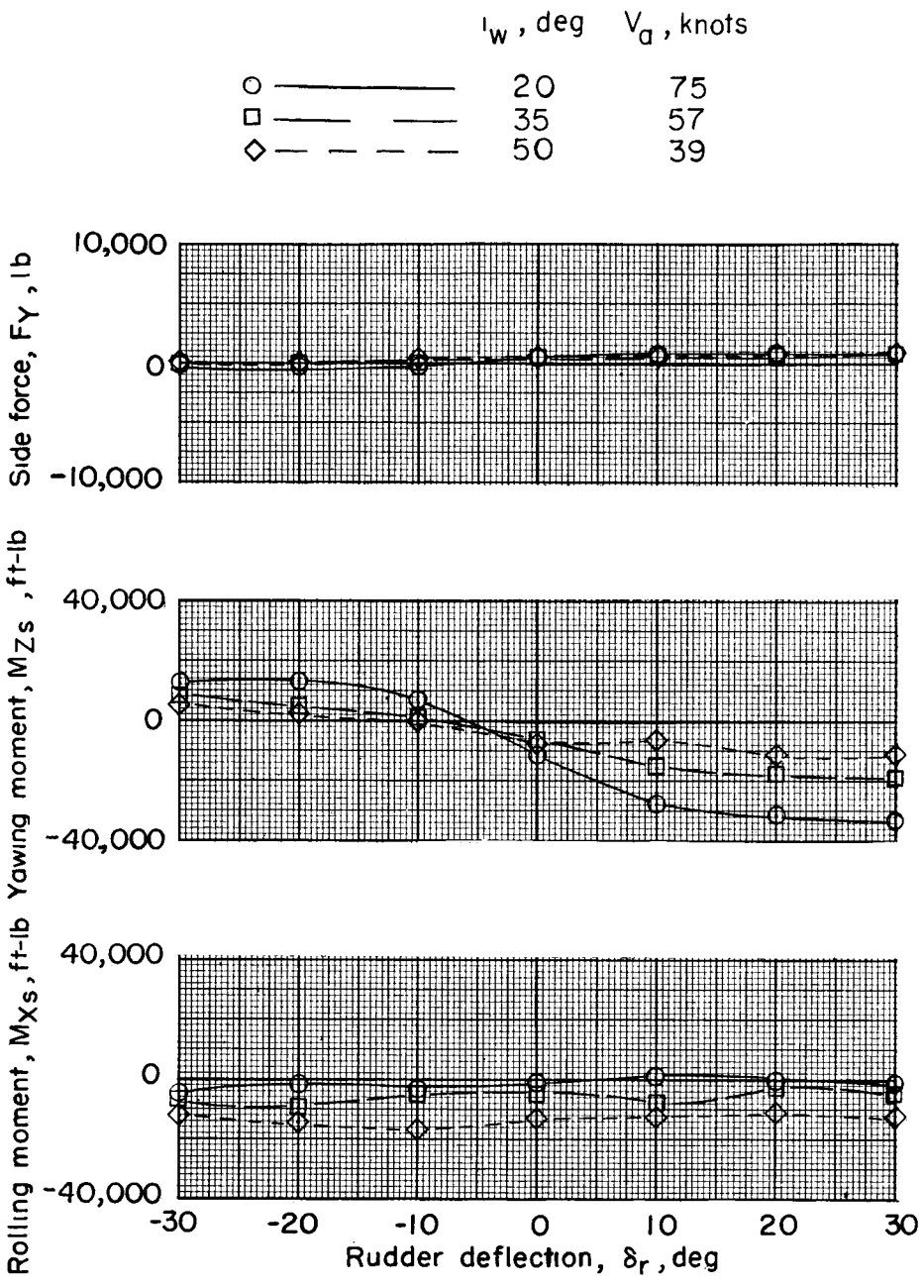

(b) δ_a'L = 0°; zero acceleration at δ_r = 0°.

Figure 37.- Concluded.

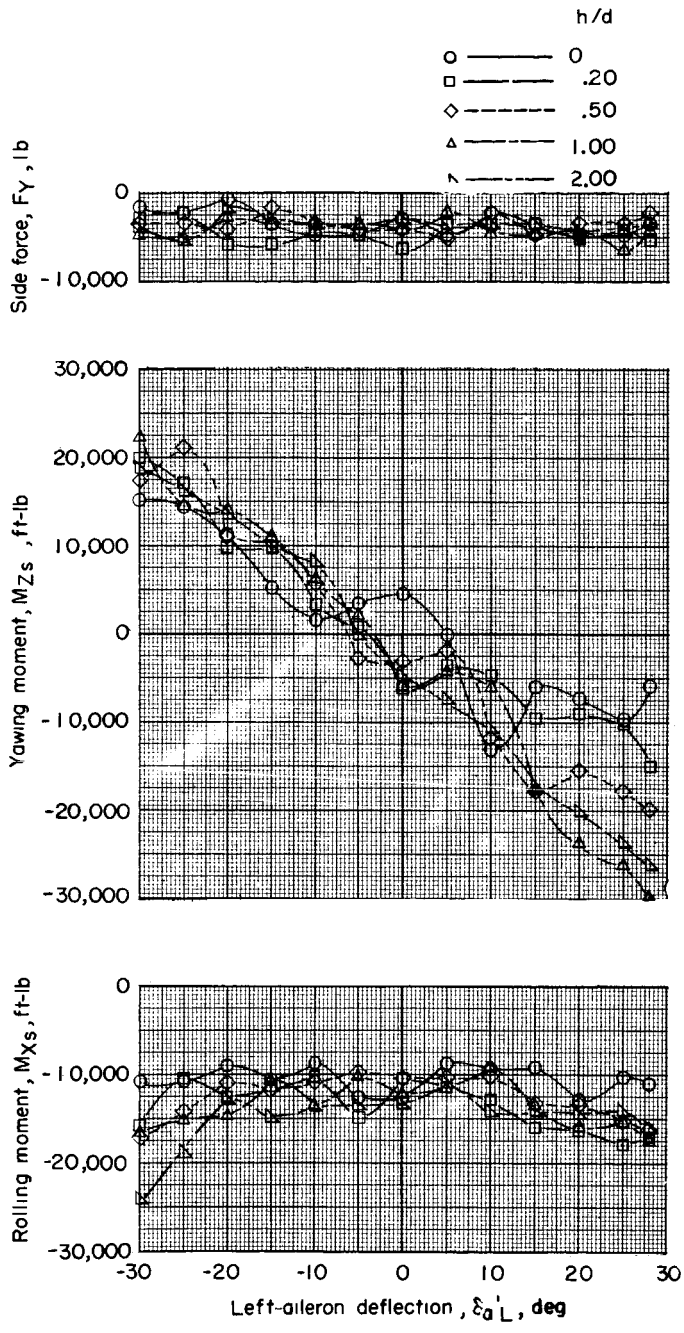

(a) $\beta_F = 16^\circ$; $\beta_{LR} = 14.5^\circ$.

Figure 38.- Lateral control characteristics when hovering in ground proximity. $i_w = 90^\circ$; short wing; $\delta_{a'R} = \delta_r = \beta = \alpha = 0^\circ$; $\beta_{RR} = 14.5^\circ$; $V_a = 0$.

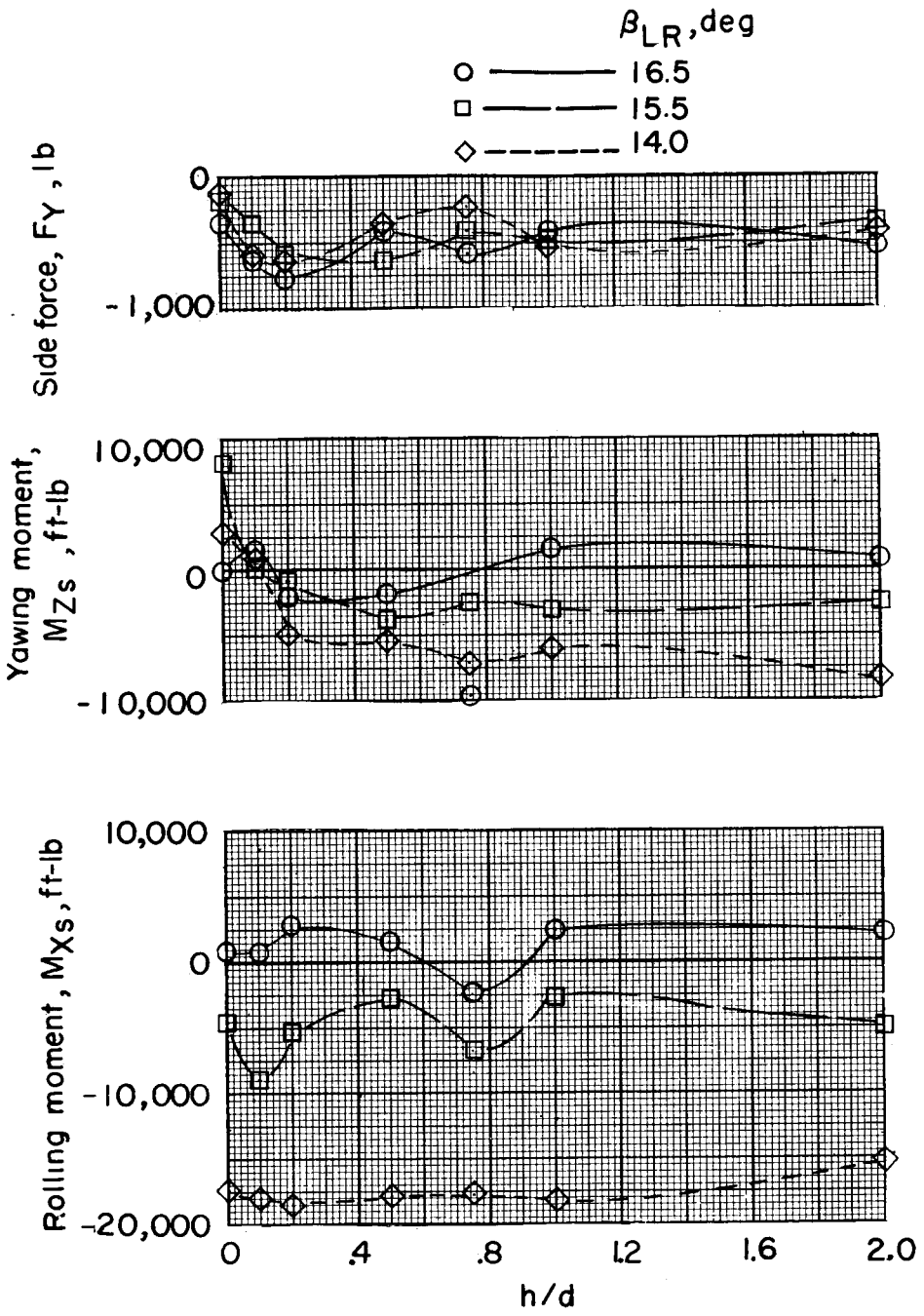

(b) $\delta_a{}'_L = 0^\circ$; $\beta_F = 16^\circ$.

Figure 38.- Concluded.

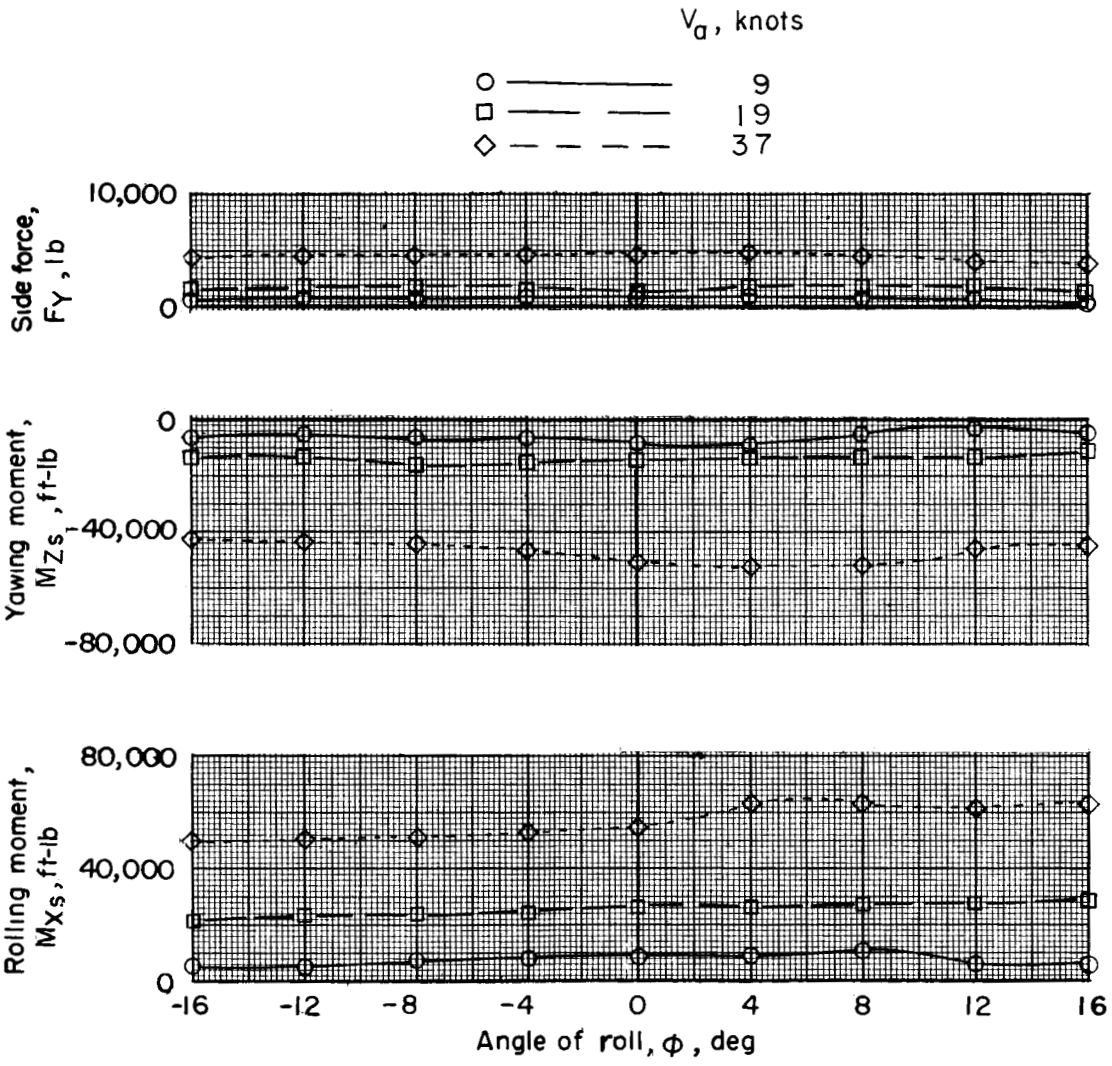

Figure 39.- Rolling stability characteristics in sidewise air flow when in hovering flight. $i_w = 94.5^\circ$; short wing; $\delta_a = \delta_r = \alpha = 0^\circ$; $\beta = 270^\circ$; $\beta_F = 10^\circ$.